Second Harmonic (SH) spectroscopic studies on the effect of curcumin-induced adsorption and transport characteristics of an organic cation across a lipid bilayer

By

Gopal Kishor Varshney

Enrolment No. CHEM03201104001

Raja Ramanna Centre for Advanced Technology,

Indore-452013, India

A thesis submitted to the

Board of Studies in Chemical Sciences

In partial fulfillment of requirements

for the Degree of

DOCTOR OF PHILOSOPHY

of

HOMI BHABHA NATIONAL INSTITUTE

August 2017

Homi Bhabha National Institute[1]

Recommendations of the Viva Voce Committee

As members of the Viva Voce Committee, we certify that we have read the dissertation prepared by **Gopal Kishor Varshney** entitled **"Second Harmonic (SH) spectroscopic studies on the effect of curcumin-induced adsorption and transport characteristics of an organic cation across a lipid bilayer"** and recommend that it may be accepted as fulfilling the thesis requirement for the award of Degree of Doctor of Philosophy.

Chairman – Dr. S. K. Dixit		**Date:** 11/4/18
Guide / Convener – Dr. Kaustuv Das		**Date:** 11/04/18
Examiner - Prof. Anindya Dutta, IIT Mumbai		**Date:** 11/04/2018
Member 1- Dr. M. P. Joshi		**Date:** 11/04/18
Member 2- Dr. S. N. Jha		**Date:**
Member 3- Dr. R. Makde		**Date:** 11/4/18
Member 4- Dr. A. K. Das, IIT Indore		**Date:** 11.4.2018
Member 5- Dr. D. Nayak, IIT Indore		**Date:** 11.4.2018
External Member - Dr. K. I. Priyadarshini, BARC		**Date:** 11.4.2018

Final approval and acceptance of this thesis is contingent upon the candidate's submission of the final copies of the thesis to HBNI.

I/We hereby certify that I/we have read this thesis prepared under my/our direction and recommend that it may be accepted as fulfilling the thesis requirement.

Date: 11/04/2018

Place: RRCAT, Indore

Dr. Kaustuv Das

(Guide)

[1] This page is to be included only for final submission after successful completion of viva voce.

STATEMENT BY AUTHOR

This dissertation has been submitted in partial fulfillment of requirements for an advanced degree at Homi Bhabha National Institute (HBNI) and is deposited in the Library to be made available to borrowers under rules of the HBNI.

Brief quotations from this dissertation are allowable without special permission, provided that accurate acknowledgement of source is made. Requests for permission for extended quotation from or reproduction of this manuscript in whole or in part may be granted by the Competent Authority of HBNI when in his or her judgment the proposed use of the material is in the interests of scholarship. In all other instances, however, permission must be obtained from the author.

Gopal Kishor Varshney

DECLARATION

I, hereby declare that the investigation presented in the thesis has been carried out by me. The work is original and has not been submitted earlier as a whole or in part for a degree / diploma at this or any other Institution / University.

Gopal Kishor Varshney

List of Publications arising from the thesis

In Journal:

1. Effect of Curcumin on the Diffusion Kinetics of a Hemicyanine Dye, LDS-698, across a Lipid Bilayer Probed by Second Harmonic spectroscopy.

   G. K. Varshney, R. K. Saini, P. K. Gupta, and K. Das

   Langmuir, **2013**, *29*, 2912-2918.

2. A comparative study on the effect of Curcumin and Chlorin-p6 on the transport of the LDS cation across a negatively charged POPG bilayers: Effect of pH.

   G. K. Varshney, S. R. Kintali, P. K. Gupta and K. Das

   Spectrochimica Acta Part A, **2017**, *173*, 132–138.

3. Effect of Bilayer Partitioning of Curcumin on the Adsorption and Transport of a Cationic Dye Across POPG Liposomes Probed by Second-Harmonic spectroscopy.

   G. K.Varshney, S. R. Kintali, P. K. Gupta and K. Das

   Langmuir, **2016**, *32*, 10415–10421.

4. Effect of Curcumin Addition on the Adsorption and Transport of a Cationic Dye across DPPG-POPG Liposomes Probed by Second Harmonic Spectroscopy.

   G. K. Varshney, S. R. Kintali, and K. Das

   Langmuir, **2017**, *33*, 8302-8310.

5. Deuterium Isotope Effect on Curcumin induced adsorption & transport properties of a cationic dye across POPG liposomes.

   G. K. Varshney, S. R. Kintali, and K. Das (To be submitted).

In conferences:

1. Diffusion Kinetics of a Hemicyanine Dye, LDS-698 Across a Lipid Bilayer Probed by Second Harmonic Spectroscopy.

   G. K. Varshney, R. K. Saini, P. K. Gupta, K. Das

   National Symposium on Radiation and Photochemistry (NSRP–2013), NEHU, Shillong, March 2013.

2. A comparative study on the effect of Curcumin & Chlorin-p6 on the transport of the LDS cation across a negatively charged POPG bilayer: Effect of pH.

   G. K. Varshney, S. R. Kintali, P. K. Gupta and K. Das

   National Symposium on Radiation & Photochemistry (NSRP-2015), IIT Kanpur, March 2015.

3. Effect of three pluronic polymers on the transport of an organic cation across an artificial membrane studied by Second Harmonic spectroscopy.

   S. R. Kintali, **G. K. Varshney** and K. Das

   National Laser Symposium (NLS-25), KIIT University, Bhubaneswar, December 2016.

4. Effect of Curcumin on the adsorption properties of a cationic dye across DPPG-POPG liposomes probed by Second Harmonic spectroscopy.

   G. K. Varshney, S. R. Kintali, and K. Das

   National Symposium on Radiation and Photochemistry (NSRP-2017) Manipal University, Karnataka, March 2017.

5. Effect of three bile salts on the transport of an organic cation across a negatively charged POPG membrane probed by Second Harmonic spectroscopy.

   S. R. Kintali, **G. K. Varshney**, and K. Das.

National Symposium on Radiation and Photochemistry (NSRP-2017) Manipal University, Karnataka, March 2017.

Other / Co-author Publications:

1. A comparative study on the effect of Curcumin and Chlorin-p6 on the diffusion of two organic cations across a negatively charged lipid bilayer probed by second harmonic spectroscopy.

   R. K. Saini, **G. K. Varshney**, A. Dube, P. K. Gupta, and K. Das.

   J. Mol. Struc. **2014**, *1074*, 22-26.

2. Hyper-Rayleigh scattering from gold nanoparticles: Effect of size and shape.

   K. Das, A. Uppal, **G. K. Varshney**, R. K. Saini, P. Mondal and P. K. Gupta.

   Spectrochim. Acta A, **2014**, *128*, 398-402.

3. Effect of three pluronic polymers on the transport of an organic cation across a POPG bilayer studied by second harmonic spectroscopy.

   S. R. Kintali, **G. K. Varshney** and K. Das.

   Chem. Phys. Lett. **2017**, *684*, 267-272.

Gopal Kishor Varshney

Dedicated to…

My Beloved Family

ACKNOWLEDGEMENTS

First and foremost, I would like to acknowledge and thank GOD Almighty for His blessings and providing me the strength and capabilities to proceed successfully. A major research work like this is never to be the work of anyone alone. The contributions of many different people, in their different way, have made this possible. On this occasion, it gives me an immense pleasure to express my gratitude to all those people who have helped me in various ways throughout my Ph.D. tenure. I have done my best in compiling the list of people all of whom made important contributions to my journey in obtaining PhD and I apologize for omissions, if any.

I wish to express my gratitude to my supervisor Prof. Kaustuv Das Scientific officer G, Laser Biomedical Applications Section, RRCAT, for his inspiring gratitude, invaluable suggestions and constant encouragement during this tenure. The completion of this project would not have been possible without his active involvement during all stages from the conception to the actual culmination of the project. I appreciate his vast knowledge and skills in many areas and his assistance in writing reports.

I am highly grateful to the members of doctoral committee, Dr. S. K. Dixit (Chairman), Dr. K. I. Priyadarsini (External expert member), Dr. M. P. Joshi (member) Dr. P. K. Gupta (former Chairman), Dr. D. K. Palit (former external expert member) and all other members for their critical review and suggestions during the annual reviews and pre-synopsis viva-voce. These valuable suggestions helped me a lot to improve the quality of the work presented in this thesis.

I also gratefully acknowledge the help rendered by Dr. S. K. Majumder, Head, LBAS and all the members of LBAS. I would specially like to express my appreciation and heartfelt thanks to Srinivasrao Kintali, Rajesh ji, Surya ji and Paromita for their support and unaccountable help at different stages of my Ph.D. I can never forget the light moments shared with them during tea break. I am highly grateful to Homi Bhabha National Institute, Department of Atomic Energy, RRCAT, Indore, for financial assistance during my research work. This research would not have been possible without this.

I convey my thanks to all my batch mates (55th batch BARC) especially Suman sir, Abhishek, Vipin, Diksha, Madhu and Mohsin. I also convey thanks to Shyam Sundar, Amol Singh, K.K. Da, Harish bhai, Ekta Mam, Yashveer, Dipankar, Smrtijit, Rahul, Ganga, Sudheer, Tufan, Chitradip, Aditya, Azam, Sahadev who have always been there to help and cheer me. I have spent some of the best moments of my life with these friends and can never forget the love, support and care that they have given during my stay in Ramanujan Hostel RRCAT. I would also like to acknowledge Dr. Bhuvnesh and Dr. Sanjit Debnath for their well wishes and support. It is not possible to mention every name here but they also have equal impact in my life.

Words fail to express my sentiments for my friends Aveshesh, Prakash, Guddan, Ziauddin, Akhil, Vivek, Pushpender, Amit, Lokesh, Akram, Shakeel, Sandeep, Hemant, Manish, Nipun, Praveen, Sudhanshu and Himanshu. Without their unconditional love, encouragement and continuous support, it would have been impossible for me to arrive where I am today.

I am forever indebted to my parents and my sisters Veenu jiji, Poonam jiji and Varsha for their unconditional love and encouragement throughout my entire life. I also owe special gratitude to my uncle, aunty, siblings Udit, Kirti and my in laws for their moral support.

Finally, I would like to thank my wife, Asmita, who has been my closet companion in all the ups and downs during this long journey. Words are not enough to express appreciation for her, whose love and care has taken the loads off my shoulder. Without her persuasion, I would not have finished this thesis. I take this opportunity to express my deepest gratitude to her.

Gopal

CONTENTS

SYNOPSIS

Surfaces and interfaces play a very important role in chemistry, physics and biology. Several dynamic processes, such as molecular adsorption and transport, transfer of energy, chemical reactions happen at a surface/interface. Among them, the most important interface is the biological interface, e.g. aqueous-membrane interface where events like adsorption and transport can trigger significant changes in the cellular functioning. Techniques to study surfaces and interfaces are therefore highly desirable. A powerful approach to study interfacial phenomena is based on the spectroscopic methods of second harmonic generation (SHG)[1-8.] Adsorption and transport kinetics of several organic ions across a lipid bilayer has been monitored by the SHG technique[2-3, 9-15].

Curcumin, a naturally occurring yellow-orange pigment derived from the rhizomes of *Curcuma longa* shows a wide variety of biological effects which include antioxidant, antiangiogenic, anticarcinogenic, and wound-healing capacities[16]. Curcumin has a great affinity for biological membranes at neutral pH and has been shown to alter their properties[17-21]. There are reports suggesting that many of its biological activities may arise from its effect on the membrane structure. Therefore, effect of curcumin on membrane bilayer is a subject of potential interest. The objective of the current thesis is to investigate the effect of curcumin on a negatively charged POPG bilayer using an organic cation as the probe. Using the ~800 nm quasi-CW output of a femtosecond (pulse width ~150 fs) Ti-Saphhire oscillator (Coherent Mira) the adsorption and transport kinetics of an organic cation in presence of curcumin and POPG liposomes were probed under different conditions using the interfacial selective SH spectroscopic technique[2-3, 9].

The organization of this thesis is as follows:

Chapter 1 provides an introduction to various interfacial spectroscopic techniques and describes in detail about the underlying principles of using SH spectroscopy to monitor real time molecular transport across a membrane bilayer. In addition, the potential of the lipophilic drug curcumin in altering the membrane properties is also discussed.

Chapter 2 describes the experimental setup used to monitor the real time molecular transport across a membrane bilayer. Preparation and characterization of lipid bilayers as well as other supplementary experimental techniques (fluorescence and light scattering spectroscopy) are also described. Finally, the spectroscopic characterization of the SH probe (LDS-698 cation: LDS^+; a hemicyanine dye) used in this study is also described here.

From **Chapter 3** the experimental results are presented. In Chapter 3, effect of curcumin on the transport characteristics of the LDS^+, across a model POPG membrane have been investigated. The transport of LDS^+ across POPG bilayer was observed to be faster by ~56 times in the presence of curcumin (curcumin (C):lipid (L)); C/L mole ratio ~0.2) at 25 °C. Further, it was observed that under similar C/L ratio, increasing the bilayer rigidity by using cholesterol and lowering the temperature (2 °C) the observed transport of the LDS-698 increased marginally (~4 times) demonstrating that the effect of curcumin is more dominant than the effect of increasing bilayer rigidity. Control experiments with other lipophilic molecules like Diphenylhexatriene (DPH) and Nile Red showed that the effect of liposomal curcumin is superior in making the POPG membrane more permeable to LDS^+. Consistent with the previous reports of curcumin affecting the bilayer organization, this study additionally demonstrates increased permeability of liposomal curcumin, in particular against organic cations. It is speculated that origin of this enhanced membrane permeability by lipophilic molecules may depend upon the interaction of the molecule with the polar head group region of the lipid which, in turn, is expected to depend on the chemical structure of the molecule.

Chapter 4 describes an attempt to compare the membrane (POPG) permeability property of curcumin with another lipophilic molecule chlorin-*p6* (C*p6*). Studies carried out in the pH range 4.0-8.0 showed that while C*p6* significantly enhanced the transport of LDS^+ at pH 4.0, for curcumin, the transport of the cation was seen to increase with increasing pH, with maximum effect at pH 7.4. The pH dependent bilayer localization of both the drugs was investigated by conducting steady state fluorescence resonance energy transfer (FRET) studies using DPH labeled lipids as donors and either curcumin or C*p6* as acceptor. The FRET results, combined with the relative population of the various ionic/ non-ionic species of the drugs at different pH suggest that distance dependent interaction between the various ionic species of the drugs and polar head groups of the lipid is responsible for the observed pH dependence enhancement of the drug induced membrane permeability.

In **Chapter 5,** the effect of curcumin partitioning into a POPG bilayer on the adsorption and transport properties of LDS^+ has been investigated. The intensity of SH electric field ($E_{2\omega}$) arising due to LDS^+ adsorbed on the outer bilayer of the POPG liposome was observed to increase instantaneously (< 1 second) following addition of curcumin. The fractional increase in the SH electric field ($E^f_{2\omega}$) and the bilayer transport rates (k_T) of LDS^+ were studied with respect to the pH of the solution and also with the curcumin content in the lipid bilayer. Results obtained indicate that compared to the anionic form of the drug, its neutral form is more conducive for increasing the $E^f_{2\omega}$ of LDS^+. With increasing curcumin content in the lipid bilayer two distinct regimes could be observed in terms of $E^f_{2\omega}$ and k_T values of LDS^+. For C/L ratio ≤ 0.02 the $E^f_{2\omega}$ of LDS^+ increased rapidly while k_T remained unchanged; and for C/L ratio ≥ 0.02; the $E^f_{2\omega}$ values remained more or less constant while there was a significant (~40 times) increase followed by a modest increase in the k_T values of LDS^+. The observed results support an earlier two-state binding model of curcumin with the POPG bilayer[20]. In addition, it is further proposed that at low C/L ratio curcumin binds to the surface

of the bilayer replacing the counter ions (Na^+) bound to the lipid head groups which changes the bilayer surface charge density thereby causing more LDS^+ cations to adsorb on the bilayer surface. At high C/L ratio curcumin intercalates within the hydrophobic domain of the bilayer altering its hydrophobicity inducing enhanced transport of the LDS^+ cation. Results presented in this work provide further insights about how curcumin alters bilayer properties when it partitions from the aqueous to the bilayer phase.

Chapter 6, which is a further extension of the work done in Chapter 5, describes the effect of bilayer rigidity on the curcumin induced changes in the adsorption and transport characteristics of LDS^+. Bilayer rigidity is manipulated by using POPG and DPPG lipids. Curcumin induced changes in the SH electric field signal of the LDS^+ ions [$E_{2\omega}(LDS^+)$] were observed to depend critically on the bilayer acyl chain saturation/ unsaturation ratio (S/ U). Following our earlier work, (Chapter 5) the increase in the $E_{2\omega}(LDS^+)$ signal is attributed to the release of the Na^+ counter-ions present in the head-group region of the bilayer by curcumin and the decay of the $E_{2\omega}(LDS^+)$signal is attributed to the bilayer intercalated state of curcumin. While the changes observed in the $E_{2\omega}(LDS^+)$ signal in presence of POPG liposomes were consistent with our earlier study (Chapter 5), they were significantly different for DPPG liposomes, following curcumin addition. While the increase in the $E_{2\omega}(LDS^+)$ signal in presence of POPG liposomes, is marginal (~10-20 %) and instantaneous (<1 second) followed by a rapid decay (completed within ~100 second), in presence of DPPG liposomes it was observed to increase slowly and at saturation shows a substantial increase (100-200 %), following curcumin addition. The observed kinetic trends of the $E_{2\omega}(LDS^+)$ signal following curcumin addition is explained on the basis of the relative strength of the Na^+-POPG and Na^+-DPPG interaction. Higher ordering of the lipid acyl chain region in DPPG liposome makes the Na^+-DPPG interaction much stronger than the Na^+-POPG interaction. When liposomes constituted from POPG and DPPG lipids are used, curcumin induced kinetic

characteristics of the $E_{2\omega}$ (LDS^+) signal showed a mixture of the individual kinetic characteristics observed for the liposomes made from pure POPG and pure DPPG lipids. It is proposed that in liposomes made from POPG and DPPG lipids, individual domains of POPG and DPPG lipids exist at low temperature as suggested by the observed temperature dependent kinetic characteristics of the $E_{2\omega}$ (LDS^+) signal following curcumin addition. These domains are dependent on the S/U ratio and phase state of the bilayer. The gel phase was observed to be more conducive for individual domain formation. Results presented in this work not only supports the notion that biological activity of curcumin is associated with its bilayer altering properties but more interestingly it provides a qualitative insight about how bilayer phase separation can be achieved by modulating the hydrophobic interactions between the lipid acyl chains.

Studies carried out so far have emphasized only on the counter-ion lipid head group interactions. However, the role of interfacial water molecules must be also acknowledged and investigated. In order to investigate the role of interfacial water on the curcumin induced disordering in the PG bilayer, experiments were conducted with liposomes suspended in water and in deuterated water (D_2O). The effect of replacing water by D_2O on the curcumin induced changes in the adsorption and transport characteristics of LDS-698 is described in **Chapter 7**. The isotope effect experiments are designed such as to investigate separately the "deuterium isotope effect" (i.e. where there is H/D exchange) and "solvent isotope effect" (where H_2O is replaced by D_2O). Results obtained showed a significant isotope effect on the adsorption and transport properties of LDS^+ while curcumin is partitioning into a POPG bilayer. This is largely due to the solvent isotope effect and is attributed to the D_2O induced modification of bilayer properties.

Finally, in **Chapter 8** a summary of the major observations is presented. A brief outline of future investigations that may evolve from the thesis is also provided.

References

1. Corn, R. M.; Higgins, D. A. *Chem. Rev.* **1994**, *94*, 107125.
2. Eisenthal, K. B. *Chem. Rev*. **1996**, *96*, 1343−1360.
3. Eisenthal, K. B. *Chem. Rev*. **2006**, *106*, 1462−1477.
4. Bredenbeck, J.; Ghosh, A.; Nienhuys, H.-K. Bonn, M. *Acc. Chem. Res*. **2009**, *42*, 1332−1342.
5. Yan, E. C. Y.; Fu, L.; Wang, Z.; Liu, W. *Chem. Rev*. **2014**, *114*, 8471−8498.
6. Roy, S.; Covert, P. A.; Fitz Gerald, W. R.; Hore, D. K. *Chem. Rev*. **2014**, *114*, 8388−8415.
7. Johnson, C. M.; Baldelli, S. *Chem. Rev.* **2014**, *114*, 8416−8446.
8. Nihonyanagi, S.; Yamaguchi, S.; Tahara, T. *Chem. Rev*. **2017**, *117*, 10665−10693.
9. Srivastava, A.; Eisenthal, K. B. *Chem. Phys. Lett*. **1998**, *292*, 345−351.
10. Liu, Y.; Yan, E. C. Y.; Eisenthal, K. B. *Biophys. J*. **2001**, *80*, 1004−1012.
11. Liu, J.; Subir, M.; Nguyen, K.; Eisenthal, K. B. *J. Phys. Chem. B* **2008**, *112*, 15263−15266.
12. Gh., M. S.; Wilhelm, M. J.; Dai, H-L. *J. Phys. Chem. Lett*. **2016**, *7,* 3406-3411.
13. Wilhelm, M. J.; Sheffield, J. B.; Gh., M. S.; Wu, Y.; Spahr, C.; Gonella, G.; Xu, B.; Dai, H-L. *ACS Chem. Biol*. **2015**, *10*, 1711−1717.
14. Zeng. J.; Eckenrode, H. M.; Dounce, S. M.; Dai, H-L. *Biophys. J*. **2013**, *104*, 139−145.
15. Kim, J. H.; Yim, S-Y.; Oh, M-K.; Phanb, M. D.; Shin, K. *Soft Matter* **2012**, *8*, 6504−6511.
16. Aggarwal, B. B.; Sundaram, C.; Malini, N.; Ichikawa, H. In. *Molecular Targets and Therapeutic Uses of Curcumin in Health and Disease*; Aggarwal, B. B., Surth, Y. J., Eds.; Springer: New York, **2007**.

17. Ingolfsson, H. I.; Koeppe, R. E.; Andersen, O. S. *Biochemistry* **2007**, *46*, 10384–10391.

18. Jaruga, E.; Salvioli, S.; Dobrucki, J.; Chrul, S.; Bandorowicz-Pikuła, J.; Sikora, E.; Franceschi, C.; Cossarizza A.; Bartosz, G. *FEBS Lett*. **1998**, *433*, 287−293.

19. Jarugaa, E.; Sokala, A.; Chrulb, S.; Bartosza, G. *Exp. Cell Res*. **1998**, *245*, 303.

20. Hung, W. C.; Chen, F. Y.; Lee, C. C.; Sun, Y.; Lee, M. T.; Huang, H. W. *Biophys. J.* **2008**, *94*, 4331−4338.

21. Barry, J.; Fritz, M.; Brender, J. R.; Smith, P. E.; Lee, D. K.; Ramamoorthy, A. *J. Am. Chem. Soc.* **2009,** *131*, 4490−4498.

LIST OF FIGURES

LIST OF TABLES

LIST OF ABBREVIATION

SHG	Second harmonic generation
SFG	Sum frequency generation
HRS	Hyper-Rayleigh scattering
MG	Malachite green
IHT	Intramolecular hydrogen atom transfer
ESIHT or ESIPT	Excited - State Intramolecular hydrogen atom (or proton) transfer
TCSPC	Time correlated single photon counting system
FRET	Fluorescence resonance energy transfer
LDS-698	2-[4-[4-(dimethylamino)phenyl]-1,3-butadienyl]-1-ethylpyridinium monoperchlorate
DPH	Di-phenyl hexatriene
Cp_6	Chlorin-p_6
POPC	1-palmitoyl-2-oleoyl--sn-glycero-3-phosphocholine
POPG	1-palmitoyl-2-oleoyl-sn-glycero-3-phospho-(1'-rac-glycerol) sodium salt
POPS	L-α Phodphatidyl l-Serine
DPPG	2-(3-(diphenylhexatrienyl) propanoyl)-1-hexadecanoyl-sn-glycero-3-phosphocoline
DPH	Di-phenyl hexatriene
D_2O	Deuterated water

Chapter 1

In this chapter an introduction to various interfacial spectroscopic techniques are presented followed by a description of the underlying principles of using second harmonic spectroscopy to monitor the real time molecular transport across a membrane bilayer. The chapter is concluded after a discussion on the membrane altering properties of the lipophilic drug curcumin.

1.1 Interfaces

Surfaces and interfaces play a very important role in chemistry, physics and biology. The interface, which is typically a few molecular or atomic layers thick, separates the two phase states of matter where the transfer of chemical species, charges, and energy between the two phases takes place. The special properties of interfaces arise due to the asymmetrical environment experienced by atomic/molecular/ionic/charge species that exist there. Due to this interfacial asymmetry, which is absent in the bulk media, the chemical, physical, and biological properties of an interface are different from the bulk media that surrounds it. As a result many bulk properties such as molecular association (static as well as dynamic), chemical changes, charge and energy relaxation etc are significantly altered at the interface. Therefore understanding the properties of interfaces are highly relevant due to its fundamental scientific value as well as its importance in the technological, environmental, and medical field [1,2]. Techniques to study interfaces are therefore highly desirable. The use of traditional optical spectroscopic techniques such as absorption and emission spectroscopy as well as vibrational infrared and Raman spectroscopy to investigate the properties of interfaces at the atomic/molecular level is often difficult due to the fact that they cannot differentiate optical signals originating from the interface against that coming from the bulk

medium. For example, if the species of interest is present in the bulk as well as at the interface then the optical signal coming from that species is expected to be dominated by the contribution coming from the bulk medium since its concentration is significantly larger in the bulk medium. With the advent of pulsed, high-power tunable lasers, nonlinear laser spectroscopic techniques whose underlying principles allows them to be interface selective can be used to avoid the dominating signals coming from the bulk media. The nonlinear spectroscopic techniques which have this interface selectivity are second harmonic and sum frequency generation (SHG & SFG) [2-22]. A scematic energy level diagram illustrating the SHG and SFG process are illustrated in Figure 1.1. The interface selectivity of SHG and SHG arises from the fact that these second-order nonlinear processes are electric dipole forbidden in centrosymmetric media. Therefore bulk media which is centrosymmetric in nature will be not conducive for SHG or SFG in second order. However, at an interface, where there is no centrosymmetry, it is possible for the interface species to generate second harmonic (light wave at twice the frequency) or sum frequency light (the sum of the frequencies of the light waves that are incident on the sample).

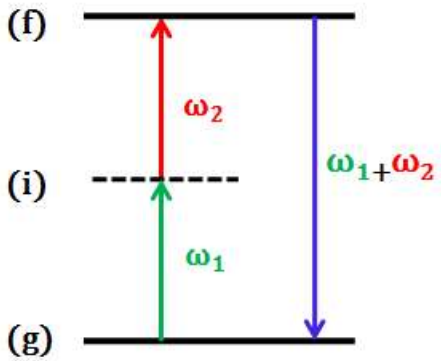

Figure 1.1*: Energy-level diagram illustrating the SHG & SFG process. The electronic energy states (g) and (f) corresponds to the ground and excited state and (i) corresponds to the virtual state. For SHG,* $\omega_1 = \omega_2$.

1.2 SHG & SHG from biological interfaces

1.2.1 The role of symmetry

The origin of the interface specificity of these second order nonlinear processes is the intrinsically noncentrosymmetric nature of the interfaces [2, 23]. In order to understand how symmetry plays a crucial role we consider the following.

The interaction of light with matter is dominated by linear process when the strength of the light field is weak. In this case, the induced polarization P(t), linearly depends upon the electric field strength.

$$P(t) = \chi^{(1)} E_{\omega}(t) \tag{1.1}$$

where $\chi^{(1)}$ is the linear susceptibility and E_{ω}(t) is the incident electric field of the light.

However when the light field becomes very intense (for e.g. lasers) the optical response can be described by expressing the polarization P(t) as a power series in the field strength E_{ω}(t) as [24]:

$$P(t) = \chi^{(1)} E_{\omega}(t) + \chi^{(2)} E_{\omega}(t)\, E_{\omega}(t) + \chi^{(3)} E_{\omega}(t)\, E_{\omega}(t)\, E_{\omega}(t) + \ldots \tag{1.2}$$

$$P(t) = P^{(1)}(t) + P^{(2)}(t) + P^{(3)}(t) + \ldots \tag{1.3}$$

where $\chi^{(2)}$ and $\chi^{(3)}$ is known as the second and third-order nonlinear susceptibility respectively. The induced second order polarization $P^{(2)}$(t) can be expressed as [25-28],

$$P^{(2)}(t) = \chi^{(2)} E_{\omega}(t)\, E_{\omega}(t) \tag{1.4}$$

Where E_{ω}(t) is incident electric field and $\chi^{(2)}$ is the second order nonlinear susceptibility of the medium. A rigorous expression for eq. (1.4) where $P^{(2)}$(t) and E_{ω}(t) are expressed as vectors and $\chi^{(2)}$ as a tensor is

$$P_i^{(2)}(t) = \sum_{j,k} \chi_{i,j,k}^{(2)}\, E_{\omega}^{j}(t)\, E_{\omega}^{k}(t) \tag{1.5}$$

Where *i, j, k* are the three normal coordinates of laboratory system. For a medium having inversion symmetry, the reflection along that plane will not change the sign or magnitude of $\chi^{(2)}$. However, an inversion operation on the electric field $E_\omega(t)$ will reverse the sign of the electric field as well as the second order polarization $P^{(2)}(t)$.

In this case, Eq. 1.4 is transformed as:

$$-P^{(2)}(t) = \chi^{(2)}\left(-E_\omega(t)\right)\left(-E_\omega(t)\right) \tag{1.6}$$

Combining Eq. 1.4 with Eq. 1.6, gives $P^{(2)}(t) = -P^{(2)}(t)$, and therefore, $P^{(2)}(t)$ must be zero. Therefore, the solution for $\chi^{(2)}$ must be zero. This means that SHG/SFG is not allowed in a centrosymmetric medium. However, at an interface, where inversion symmetry is no longer conserved, $P^{(2)}(t)$ is not necessarily equal to $-P^{(2)}(t)$ on performing an inversion operation. Therefore $\chi^{(2)}$ at interface is not necessarily to be zero, suggesting that SHG & SFG from interfaces is allowed.

Thus bulk centrosymmetric systems do not radiate coherent SHG/SFG because of symmetry reasons. From a molecular picture if we consider a bulk media, for every molecule oriented in one direction, it is very likely that there will be another neighbor molecule oriented in the opposite direction. The nonlinear polarizations induced in these oppositely oriented molecules by the incident light will be of opposite phase with respect to each other as their distance is much less compared to the coherence length of the process and thus will cancel each other. Therefore the net second-order polarization is zero, and there is no coherent SHG or SFG radiated from the bulk. Although coherent SHG and SFG is not allowed in bulk centrosymmetric media due to the reasons discussed above, it is pertinent to note that the fluctuations in molecular density and molecular orientation in isotropic bulk solutions can disrupt the phase cancellation and generate incoherent second-order light scattering, which is

also referred as hyper-Rayleigh scattering (HRS). Indeed, HRS has been observed in bulk centrosymmetric media [29-30].

1.2.2 SHG & SFG from centrosymmetric structures

Although SHG/SFG is forbidden in centrosymmetric media, microscopic centrosymmetric particles suspended in a liquid medium can generate SHG/SFG [31]. This can be explained by considering a bare microsphere of diameter L (Figure 1.2). Since the opposite positions of the microscopic particle surface has oppositely oriented surface structures the generated second harmonic (SH) electric field will have opposite phases. The total SH field arising due to a pair of oppositely oriented surface structures is:

$$E_{2\omega} \propto \beta^{(2)} \mathrm{E}_{\omega} \mathrm{E}_{\omega} \left(1 - \mathrm{e}^{-\mathrm{i}\Delta\vec{\mathrm{k}}.\vec{\mathrm{L}}}\right) \tag{1.7}$$

where $\beta^{(2)}$ is the second-order polarizability of the microsphere and $\Delta\vec{\mathrm{k}}$ is scattering vector given by:

$$\Delta\vec{k} = \vec{k}_{2\omega} - 2\vec{k}_{\omega} \tag{1.8}$$

where $\vec{k}_{2\omega}$ and $\vec{k}_{\omega}$ are the light propagation vectors for the second harmonic light at 2ω and the fundamental light ω respectively. The amplitude of the scattering vector is defined as:

$$\Delta k = \frac{4\pi(n_{\omega} - n_{2\omega})}{\lambda_{\omega}} = \frac{4\pi\Delta n}{\lambda_{\omega}} \tag{1.9}$$

Therefore it follows that if the separation length L between the oppositely oriented surface structures is much less than wavelength of fundamental light (case a; Figure 1.2), then $\Delta\vec{\mathrm{k}}.\vec{\mathrm{L}} \ll \lambda$ and consequently $\mathrm{E}_{2\omega} = 0$. On the other hand, if separation length L is comparable to the wavelength of fundamental light (case b; Figure 1.2), then $\mathrm{E}_{2\omega} \neq 0$. Therefore, although the particle is centrosymmetric depending upon its diameter and wavelength of incident radiation it can generate SHG/SFG. $\mathrm{E}_{2\omega}$ will be maximum when $\Delta\vec{\mathrm{k}}.\vec{\mathrm{L}} \sim \pi$.

Individual large noncentrosymmetric entities suspended in bulk solution can also generate SHG which has been observed in randomly oriented suspensions in solution [32]. This was attributed to the noncentrosymmetric interior region of the individual microscopic particles. In addition, semiconductor quantum dots and metallic crystals also give rise to SHG, which has been attributed to their noncentrosymmetric structure [33].

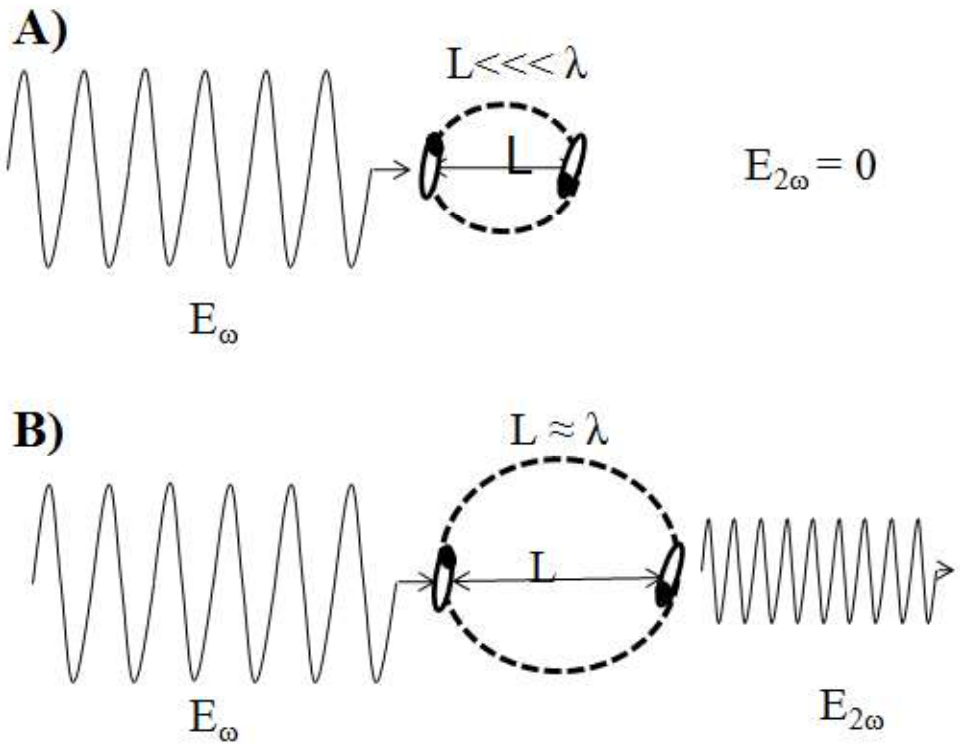

Figure 1.2: *A schematic diagram explaining the principles of SHG originating from a micro particle surface.*

1.2.3 Electronic Second Harmonic Generation Spectroscopy

The changes in the dipole moment of a molecule induced by an external electric field may be quantified as:

$$\mu_l = \alpha_{lm}^{(1)} E_m + \frac{1}{2}\alpha_{lmn}^{(2)} E_m E_n + \frac{1}{6}\alpha_{lmno}^{(3)} E_m E_n E_o + \ldots\ldots\ldots + \frac{1}{n!}\ \alpha^{(n)} E^n \qquad (1.10)$$

where $\alpha^{(n)}$ is the n^{th} order polarizability and *l, m, n*, ... are any of the molecule-fixed Cartesian coordinates. For large ensembles of molecules lying in the focus of laser beams (~ several microns diameter), the polarization, P (dipole moment per unit volume) is:

$$P_i = \varepsilon_0 \left(\chi_{ij}^{(1)} E_j + \frac{1}{2}\chi_{ijk}^{(2)} E_j E_k + \frac{1}{6}\chi_{ijkl}^{(3)} E_j E_k E_l + \cdots + \frac{1}{n!}\ \chi^{(n)} E^n \right) \qquad (1.11)$$

where $\chi^{(n)}$ is the n^{th} order susceptibility, ε_0 is the vacuum permittivity, and *i, j, k*, ... represents the laboratory-frame Cartesian coordinates. SHG originates from second order contribution to the polarization:

$$P_i(2\omega) = \varepsilon_0 \frac{1}{2}\chi_{ijj}^{(2)} E_j(\omega) E_j(\omega) \qquad (1.12)$$

This phenomenon which is also known as frequency doubling is commonly implemented experimentally by directing a single beam to the solid−liquid interface of interest. The fundamental frequency is removed by means of optical filters (band-pass and/or notch filters), and the second-harmonic (SH) light is detected. A schematic of the experimental configuration is illustrated in Figure 1.3 (a). As indicated in eq 1.12, both input beams are j polarized, and the *i*-component of the SH intensity is sent to the detector. The intensity of the SH electric field is proportional to the magnitude squared of the effective susceptibility, $|\chi_{\text{eff}}{}^{(2)}|^2$, and the intensity squared of the pump beam, I^2 as:

$$I_i(2\omega) \propto \left| \chi_{\text{eff},ijj}^{(2)} \right|^2 I_j^2(\omega) \qquad (1.13)$$

Thus the *ijj*-element of $\chi_{eff}^{(2)}$ couples two *j*-polarized input beams at frequency ω to the detected *i*-polarized beam at 2ω.

The input beam can also be separated into two paths, so as to approach the interface from different directions/angles. In this configuration, the SH light which is generated along the momentum-conserving direction, is not collinear with the transmitted/reflected input beams, and therefore may be spatially filtered from the intense input light sources. Such a configuration also allows the two pump beams to be polarized independently along j and k directions (eq 1.14). The second-order susceptibility, $\chi^{(2)}$ which is a 27-element rank-3 tensor couples the input fields E_j and E_k to the *i*-th component of the induced polarization. Elements of the effective susceptibility are related to the actual $\chi^{(2)}$ tensor elements as:

$$\chi_{\mathrm{eff},ijk}^{(2)} = [L_{ii}(2\omega).\hat{\mathrm{e}}_i(2\omega)]\chi_{ijk}^{(2)}[L_{jj}(\omega).\hat{\mathrm{e}}_j(\omega)][L_{kk}(\omega).\hat{\mathrm{e}}_k(\omega)] \qquad (1.14)$$

where L are the local field corrections and $\hat{e}$ are the unit polarization vectors. Once the $\chi^{(2)}$ elements have been extracted from the measured elements of $\chi_{eff}^{(2)}$ with the help of above equation the orientational information of the molecules at the interface could be obtained by using the realtion between $\chi^{(2)}$ and the molecular hyperpolarizability $\alpha^{(2)}$ [16, 34-35].

Till now the interface is assumed to be uncharged. If the interface is charged there is an extra surface-bound electric field E_0 whose strength is reflected in the magnitude of a third-order component of the induced polarization [36, 37]. Since E_0 is static in nature, the third-order response (due to E_0) is detected simultaneously with the second-order response as:

$$P_i(2\omega) = \varepsilon_0 \frac{1}{2}\chi_{ijj}^{(2)}E_j(\omega)E_j(\omega) + \varepsilon_0 \frac{1}{6}\chi_{ijj0}^{(3)}E_j(\omega)E_j(\omega)E_0 \qquad (1.15)$$

This process, known as electric field induced second harmonic (EFISH) generation, has been used to determine the pK_a values of protonation sites at an oxide water interface [38], measure the isoelectric point [37] and estimate the cation−DNA binding energies [39].

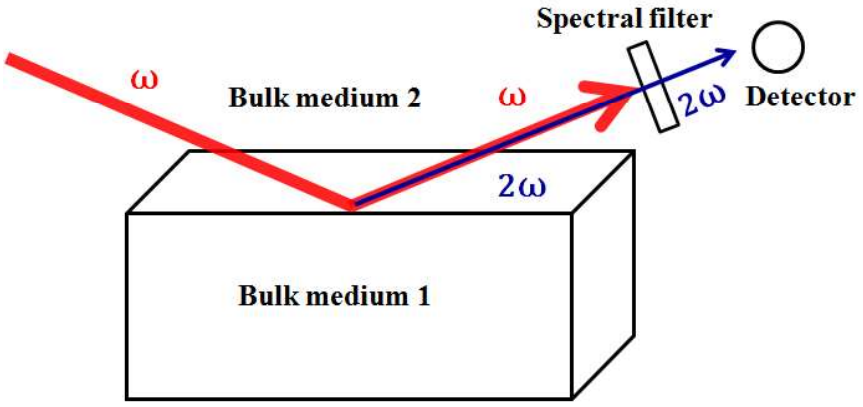

(a)

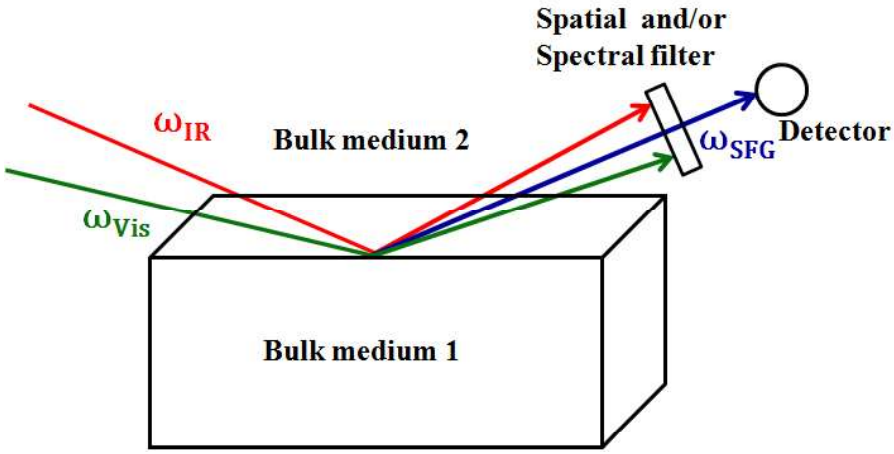

(b)

Figure 1.3: *Typical experimental configurations illustrating (a) SHG from an interface (gas/liquid or solid/liquid) using a collinear geometry (b) visible-infrared SFG from an interface (gas/liquid or solid/liquid) using a noncollinear geometry. Both SHG & SFG experiments may also be performed in either geometry.*

1.2.4 Electronic Sum Frequency Generation Spectroscopy

Sum-frequency generation (SFG) which is the non-degenerate analog of SHG is performed with two lasers of different frequencies, ω_1 and ω_2. Figure 1.3 (b) illustrates a general schematic of a noncollinear geometry where the phase-matching direction of the reflected SFG beam is spatially separated from the two pump beams. Generally for probing biomolecules at a solid−liquid or air-water interface, the popular choice is to have one of the lasers (ω_1) in the visible region (e.g. 532 or 800 nm, which is typically far from any electronic resonance), and the other laser (ω_2) being either broadband or tunable throughout the mid-infrared region (1000−4000 cm^{-1}). In this combination, resonance enhancement is observed as the probe frequency $\omega_2 = \omega_{IR}$ approaches one of the q^{th} vibrational modes at ω_q. The frequency-dependent molecular hyperpolarizability then can be expressed as:

$$\alpha^{(2)}_{lmn}(\omega_{\mathrm{IR}}) = \alpha^{(2)}_{\mathrm{NR},lmn} + \sum_{q} \frac{\langle 0|\bar{\alpha}_{lm}|1\rangle\langle 1|\,\bar{\mu}_{n}|0\rangle}{\omega_{\mathrm{q}} - \omega_{\mathrm{IR}} - i\Gamma_{q}} \tag{1.16}$$

where $\alpha_{NR}^{(2)}$ is the non-resonant contribution and Γ_q is the Lorentzian line width (*l, m, n* are the molecule-fixed Cartesian coordinates). By taking $|0\rangle$ and $|1\rangle$ as the vibrational ground and excited state respectively, $\bar{\alpha}_{lm}$ and $\bar{\mu}_{n}$ as the polarizability and the dipole moment operator respectively, it comes out that the SFG response is a product of the Raman transition polarizability and IR transition dipole moment. Therefore vibrational SFG spectra provide information similar to IR and Raman spectra, but only from molecules residing at the interface. In a traditional (homodyne) SFG experiment, the measured intensity is proportional to the magnitude squared of the effective susceptibility

$$I_i(\omega_{\mathrm{vis}} + \omega_{\mathrm{IR}}) \propto \left|\chi^{(2)}_{\mathrm{eff},ijk}\right|^2 I_j(\omega_{\mathrm{vis}}) I_k(\omega_{\mathrm{IR}}) \tag{1.17}$$

In comparison to the SHG expression (eq. 1.13) we note that in SFG, since the pump beams have different frequencies, it is more convenient to have different polarization states (e.g. *j*-

polarized visible, and *k*-polarized infrared) for them, which can therefore access additional elements of $\chi_{eff}^{(2)}$. Additionally, since the vibrational signature of interfacial molecules is desired, it is common practice to plot the sum-frequency intensity as a function of the changing ω_{IR}.

1.3 SHG: A spectroscopic tool to monitor bilayer transport of molecules

1.3.1 Membrane transport

Several dynamic processes, such as molecular adsorption and transport, transfer of energy, chemical reactions happen at a surface/interface. Among them, the most important interface is the biological interface, e.g. aqueous-membrane interface where events like adsorption and transport can trigger significant changes in the cellular functioning. The basic structure of a bio-membrane is a bilayer made up of amphiphiles called as lipids, which self-assemble into a spherical structure with an enclosed aqueous compartment. The two monolayers comprising the bilayer have the hydrophobic alkane chains of the lipid molecules facing each other with the polar headgroups of the lipid molecules projecting into the internal as well as into the external aqueous region. Liposomes which are widely used as bio-membrane mimetic structures are by themselves centrosymmetric.

The adsorption and transport of molecules across lipid bilayers have been probed by a variety of spectroscopic techniques like NMR [40-44], EPR [45], absorption [46-47] and fluorescence spectroscopy [48-56]. It is pertinent to note that in order to monitor molecular adsorption and transport across the bilayer, molecules adsorbed on the surface of the liposomes must show different spectroscopic signature than those in bulk solution which is often difficult to realize.

1.3.2 SHG for membrane transport: Principles

One of the most interesting applications of SHG is that it can be used to observe molecular transport across a bilayer. This was first demonstrated by Eisenthal and co-workers by monitoring the time dependent SH signal of a cation, malachite green (MG) across a negatively charged phosphatidylglycerol bilayer [57]. The principle of this method is based on the fact that molecules adsorbed on the outer surface of a liposome are oriented in a preferred way, and by symmetry, when they are adsorbed on the inner surface of the liposome they would have the opposite orientation. The detailed principle of how SHG can be used to monitor the bilayer trasnport of molecules is described below.

First of all, the molecule of interest should have a reasonable hyperpolarizability at the wavelength of the fundamental radiation. Generally the 800-850 nm output of a femtosecond Ti-Saphhire oscillator is used for excitation purpose. For this, the dipole moment should increase significantly while going from the ground to the excited state. This is generally the case for dye molecules having extended electronic de-localizations. Additionally, the molecule should have sufficient absorption at the second harmonic wavelength of the incident radiation for resonance enhancement of the SHG process. Lastly, in order to cross the lipid bilayer it is preferable that the molecule should also have a significant amphiphilic character which helps it to distribute itself at the aqeous-bilayer interface.

Sperical liposomes whose size is of the order of the wavelength of the fundamental (~ 800 nm) radiation are used as models to probe the bilayer trasnport. Following a rapid mixing of the molecules and liposomes, the SH electric field generated from the molecules adsorbed on the outer lipid bilayer will be in phase and will add coherently to generate a non-zero SH electric field (Figure 1.4). In contrast, due to their random orientation molecules present in the bulk water will not generate coherent SH but they can still generate incoherent SH by HRS as discussed before. It is pertient to note that due to its coherent nature SH generated

from molecules adsorbed on the outer surface of the liposome will be significantly higher than the incoherent HRS generated from molecules present in the bulk medium. When the molecules transport across the lipid bilayer, and get absorbed to the inner surface of the liposome, the adsorbed molecules on the inner and outer surface of the lipid bilayer are oppositely oriented. Since the oppositely oriented molecules are separated by the bilayer thickness (~ 5 nm) which is much less than the coherence length of the SHG process (typically 1.0 μM for 800 nm excitation), the SH electric field generated from the oppositely oriented molecules will be out of phase and cancel each other. Thus the resulting SH field generated from the molecules adsorbed on the liposome surface at any time t will be proportional to the population difference of the molecules between the outer and inner surface at that time. Therefore, the transport process can be monitored in real time by monitoring the SHG signal subsequent to the addition of molecules to the liposomes. The second harmonic electric field $E_{2\omega}$ generated by the light field E_{ω}, incident on a liposome is proportional to the second order susceptibility χ^2, which contains information of the adsorbate population. From the measured SHG signal, $I_{2\omega}$, the second harmonic field, $E_{2\omega}$, is calculated as follows:

$$E_{2\omega}(t) = \sqrt{I_{dye+liposome}(t) - I_{background}} \tag{1.18}$$

where $I_{dye+liposome}(t)$ is the SHG signal detected at 2ω at time t and $I_{background}$ represents the background SH signal due to the dye molecules presnt in the bulk (HRS) and also due to the weak SH light generated by the liposomes and water. After adding the liposome solution to the dye solution (or, vice-versa), the second harmonic field $E_{2\omega}$ is proportional to the difference in the populations of the dye molecules located on the outer surface, $N_0(t)$, and the inner surface, $N_i(t)$, of the liposomes at a time t as:

$$E_{2\omega} \propto [N_0(t) - N_i(t)] E_{\omega} E_{\omega} \tag{1.19}$$

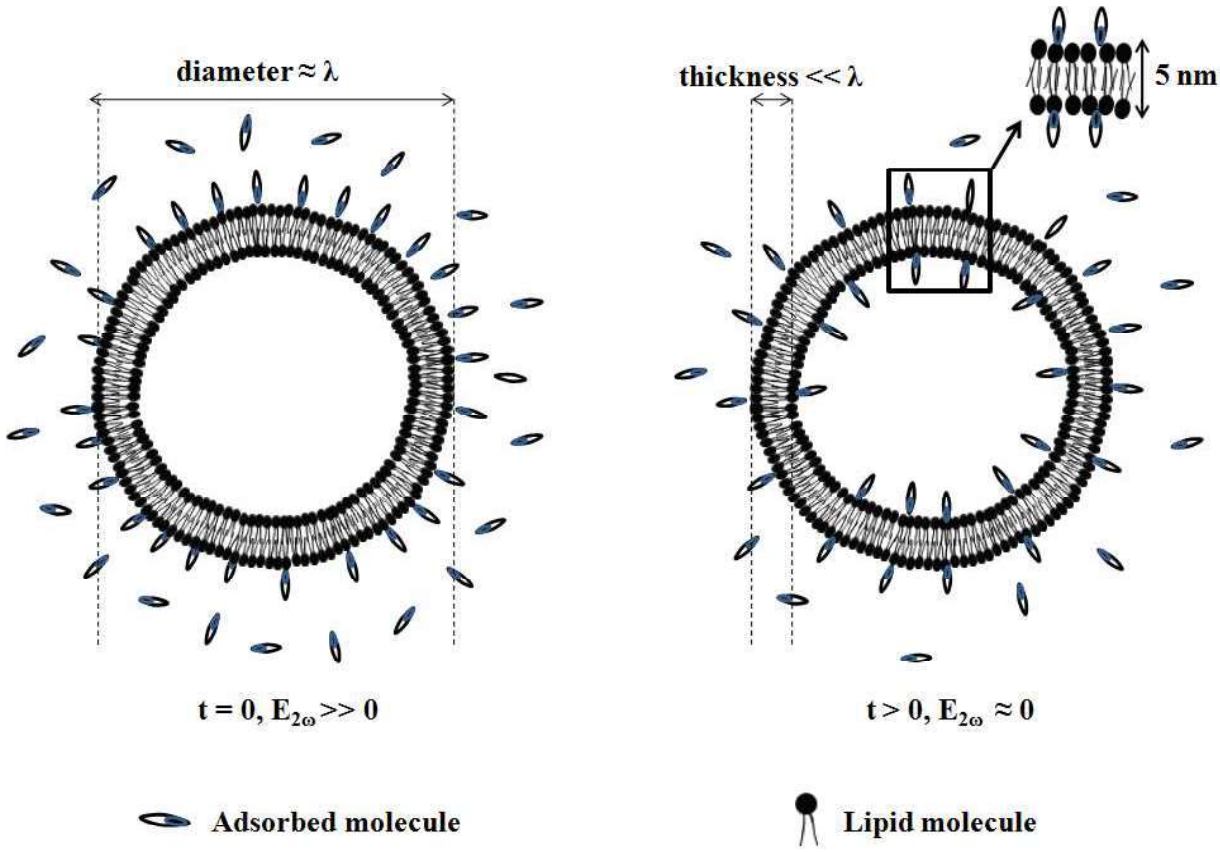

Figure 1.4: *Schematic illustration of the principle of using SHG to monitor molecular transport across a bilayer. At t = 0, the adsorption of SH active molecules on the outer surface generates a non-zero coherent SH signal. At times t > 0, molecular transport across the bilayer reduces the SH signal due to phase cancellation of the molecules adsorbed on the outer and inner surfaces of the bilayer.*

Generally the observed decays of the SH electric field can be fitted to exponential decay functions of the following form:

$$E_{2\omega}(t) = A_0 + \sum a_i \exp(-t/\tau_i) \quad (1.20)$$

It is pertinent to note that at equilibrium conditions, i.e. when the transport is completed, the SH electric field $E_{2\omega}$ is significantly greater than zero (corresponding to the term A_0 in eqn. 1.20). This has been attributed to the finite population difference in the dye molecules adsorbed on the outer (N_{out}) and inner (N_{in}) surface of the liposome and the term $1\text{-}A_0$ represents the N_{in}/ N_{out} ratio.

1.3.3 SHG for membrane transport: Applications

Following the first study where it was demonstrated that SHG technique can be used to monitor the bilayer trasnport of MG [57] several other works have been carried out by Eisenthal and co-workers. The effect of bilayer rigidity (by adding cholesterol; 0–50 mol %) on the transport of MG across an unilamellar dioleolyphosphatidylglycerol (DOPG) liposome bilayers was studied. Results obtained indicated that cholesterol retards the rate of transport of MG (six times for 50 mol % cholesterol content) across liposome bilayers. This is consistent with the expectation that increasing the bilayer rigidity will result in slower transport [58]. SHG can also be used to measure the surface potential of charged liposomes. Using negatively charged DOPG liposomes the surface potential was found to be in the range of 20 to 100 mV depending on the electrolyte (NaCl or $MgSO_4$) present in the solution. The charge density was found to be ~1.3×10^{14} per cm^2, which corresponds to ~70 $Å^2$/charge, comparable to the area per phospholipid headgroup [59]. The effect of bilayer surface charge density on the adsorption and transport properties of MG was also studied using the SHG technique. Using liposomes of different lipid compositions it was observed that MG adsorption and transport rate increased linearly with the fraction of negatively charged lipids

in the bilayer which demonstrates that adsorption of the MG cation on the outer surface of the bilayer is initiated by electrostatic attraction and the subsequent transport is driven by an assyemtry generated in the potential between the outer and inner bilayer [60]. The effect of different counterions on the transport rate of MG was also studied using DOPG liposomes. It was observed that at higher counterion concentration the transport rate of MG depends on the species of the counterion used but at lower (> 1 mM) counterion concentration the transport rate of MG is independent of the species of the counterion used [61]. Eisenthal's group has also studied the effect of other lipophilic molecules on the transport kinetics of MG. In particular they have studied the effect of the antibiotic valinomycin, (which can transport alkali ions across a phospholipid bilayer), gramicidin A (which forms an ion channel across which alkali and hydronium ions can be transported) and carbonyl cyanide-m-chlorophenylhydrazone (a weak acid which works as a proton trasnporter). The effects of these ionophores on the transport of MG and the percentage of MG ions transported from the outer to the inner bilayer were found to be different based on their individual ionophoretic property [62-63].

One of the most interesting applications of this technique was done by Dai and co-workers who have studied the adsorption and transport of the MG ion across the *Escherichia coli* membrane. They have fitted the SH kinetics of the MG ion using a multiprocess kinetic model which revealed that compared to the the cytoplasmic membrane, the transport of MG ion through the outer membrane is much faster [64]. In a further extension of their work they have combined optical transmission microscopy (TM) with second-harmonic light scattering (SHS), to independently measure the uptake and transport of MG ions across *Escherichia coli* bacteria. A combination of TM and SHS allows a fully complementary and quantitative characterization of MG ion uptake. While, TM permits the detection of the changing bulk MG ion concentrations within the bacteria, SHS was shown to provide sequential

differentiation of MG ion density at membrane surfaces. Further, simultaneous global analysis of the TM and SHS observations yielded the MG ion transport rate constants for all traversed cellular barriers [65]. They have also studied the adsorption and transport characteristics of MG ion and a neutral molecule, bromocresol purple (BCP), against pre- and post-DMSO induced differentiated murine erythroleukemia (MEL) cells by time and wavelength-resolved SHG. It was observed that only MG cation adsorbs onto the surface of the MEL cell due to electrostatic interaction between the opposite charges of the MG cation and the MEL cell. By varying pH and cell morphology, it was established that the interaction between MG ion and MEL cells is predominantly through sialic acid carboxyl groups of the MEL cells. However, in contrast to synthetic liposomes and bacterial membranes, the surface adsorbed MG cations are unable to traverse the MEL cell membrane [66]. In an interesting study, the real-time and membrane specific quantitative characterization of the bacterial uptake of crystal-violet (CV), the dye used in Gram's protocol was investigated using the SHS and TM techniques. Observed results contradict the currently accepted mechanism that, for both Gram-negative and Gram-positive bacteria, CV readily traverses the peptidoglycan mesh (PM) and cytoplasmic membrane (CM) before equilibrating within the cytosol. Based on their observations they suggest that not only is CV unable to traverse the CM but, on the time-scale of the Gram-stain procedure, CV is kinetically trapped within the PM [67]. They have also studied chemically induced enhancements in membrane permeability. They have observed that the transport rate of MG cation increases by nearly an order of magnitude following addition of 0.1 mM ATPe to *Escherichia coli*. Due to the absence of an ATPe-enhanced permeability in liposomes this effect is attributed to protein-mediated enhanced permeability of *Escherichia coli* [68]. Finally they have also addressed the important issue of how to determine the transport rates of molecules which are SHG inactive. They have monitored the SHG produced from an SHG-active reference molecule (MG), in the presence

of an SHG-inactive target molecule-of-interest as both molecules compete to cross a membrane. Using a weakly SHG-active dication, propidium, they have measured the transport of MG cation across the outer-membrane protein channels in living bacteria and shown that the SHG-inactive Pro transport rate can be deduced as a perturbation in the measured transport rate of MG cation [69].

This thesis deals with the effect of the curcumin on the transport rate of an SH active cation across negatively charged phosphatidylglycerol model membrane. In the following section the importance of drug-lipid interaction will be discussed which will be followed by a discussion on curcumin and its biological effects.

1.4 Drug-lipid interactions

Understanding drug-lipid interactions at a molecular level is crucial for pharmacological science because they are very important to predict the pharmacokinetic properties of the drugs such as it's transport, biodistribution and accumulation and hence efficacy [70]. In majority of the cases, drugs have to cross the membrane to show their pharmacological activitiy since they have intracellular targets [71]. However, during their adsorption and transport they can modulate the physical properties of the membranes by changing membrane permeability, membrane potential, microviscosity, membrane fluidity, membrane order, membrane elasticity etc. Since biological membranes have a very balanced environment, therefore, any change in its structure may affect its proper functioning. However biological membranes are a complex and highly diverse system which makes them difficult to undertstand correctly how a drug affects the membrane proeprties. Therefore simplified artificial membrane systems have been used to gain a primary insight into the drug-membrane interactions. Liposomes are one of such simplified system which mimics the fundamental structure of the natural membrane.

1.4.1 Curcumin

Plant based medicines has gained a lot of public attention and led to extensive research owing to the potential of natural organic substances of which they are composed of. These natural organic compounds have a pronounced effect on human health and the prevention and treatment of several chronic diseases [72]. In this context, polyphenols have been most promising natural organic compounds because of their health promoting properties such as antioxidant, wound healing, immune modulator actions, anti fungal, antiviral, antibacterial, anti-ageing, anticancer etc. [73]. They are secondary metabolites of the plants which contain one or more benzene rings with one or more hydroxyl substituents [74, 75] and generally derived from several components of the human food such as tomatoes, grapes, berries, ginger, chilly and turmeric etc. Curcumin is currently one of the most studied polyphenolic substance derived from the rhizomes of turmeric (Curcuma longa) [76], a rich source of polyphenols and used as a spice, herbal medicine, coloring agent in food and textile industries [77, 78]. It has also been used as ayurvedic medicine to cure cough, fever, skin diseases, diabetic wounds, hepatic disorders, inflammation and liver diseases etc [79]. In addition, reduction in the certain type of cancers (10-50 %) has also been suggested by epidemiological studies among people who consumed the spice regularly [80, 81]. The yellow color of the turmeric is majorly due to tumerin (rhizomes of turmeric plants) which is a water soluble peptide, essential oil and major chemical curcuminoids [82]. The three major components of curcuminoids are curcumin (77%), demethoxycurcumin (17%), and bisdemethoxycurcumin (3%) (Figure 1.5) which usually constitute approximately 2-8% of turmeric [83]. Recent studies also showed the presence of trace amount of the fourth component known as cyclocurcumin in addition to these three components [84]. The biological properties of curcumin have been reported as early as in the 1970s [73, 77, 85]. The ability of curcumin to

act as an anticancer agent was demonstrated in mid 1990 [79] and thereafter interest in the biological activity of the pigment has increased significantly.

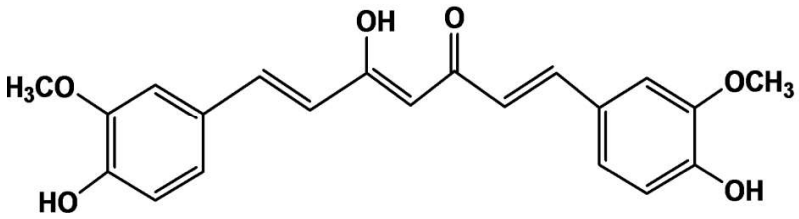

A: Enol form of curcumin

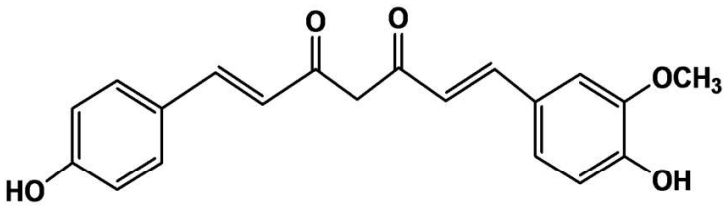

B: Demethoxycurcumin

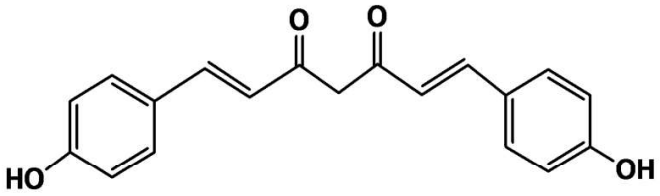

C: Bisdemethoxycurcumin

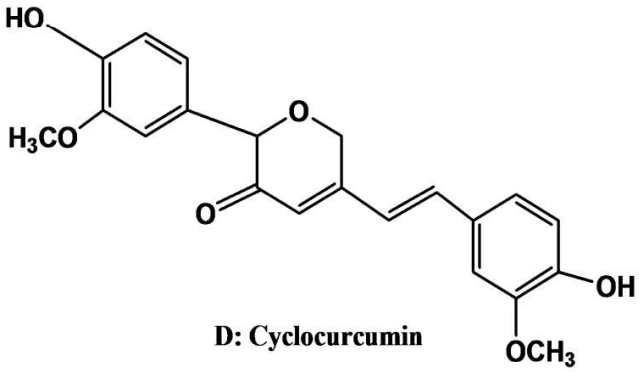

D: Cyclocurcumin

Figure 1.5*: Structutre of curcuminoids*

1.4.1.1. General properties

Curcumin was first discovered from the rhizomes of C. longa by Vogel and extracted in impure form in 1815. Its purified form was obtained in 1842 [86]. It is a low molecular weight molecule consists of two phenolic hydroxyl groups, two methoxyl groups and β-diketone moieties. The IUPAC name of the curcumin is (1E,6E)-1,7-bis(4-hydroxy-3-methoxyphenyl)-1,6-heptadiene-3,5-dione. The physicochemical properties of curcumin are listed in table 1.1.

Table 1.1: *Physiochemical properties of curcumin*

Curcumin	Properties
Appearance	Yellow orange crystalline powder
Molecular Formula	$C_{21}H_{20}O_6$
Molecular Weight	368.38 g/mol
Melting point	179-183 °C
Solubility	Insoluble in water at neutral pH

Curcumin is not soluble in non-polar solvents such as diethyl ether, mineral oil and some vegetable oils and sparingly soluble in water but highly soluble in some polar solvents such as methanol, acetone, ethyl acetate, dimethyl sulfoxide (DMSO), acetonitrile and acetone [87]. The solubility of curcuminoid powder in organic solvents ranges from 0.4-11 mg/ml [88]. Curcuminoid compounds have been reported to be more soluble in alkaline conditions as compared to acidic conditions in their aqueous solutions [89]. Wang et al. have reported the octanol-water partition coefficients (log P) of curcuminoids. They reported the log P values for curcumin, demethoxycurcumin and bismethoxycurcumin as 2.92, 3.08 and 3.32 respectively [90]. High log P value of a compound indicates that it is lipophilic in character. The upper limit of log P value is considered to be 5. Therefore, the result reported by Wang et

al. suggests that curcumin compounds are lipophilic. The aqueous solubility of curcumin however may be increased substantially by its incorporation in several organized assemblies like micelles, polyethylene glycol, polysaccharides, cyclodextrins, liposomes etc [89, 91].

1.4.1.2. Structural properties

Using various spectroscopic techniques several studies have been performed to understand the structural properties of curcumin and its derivatives in different solvents, [92-97]. The diketo group present in the curcumin is responsible for keto-enol tautomerism and depending upon the environmental conditions such as temperature, substituents on the aromatic rings and the polarity of the solvents, these tautomeric forms (Figure 1.6) can also exist in different types of cis and trans isomers [92, 93]. Among all the possible isomers only three of them can be considered as the candidates for the ground state of curcumin.

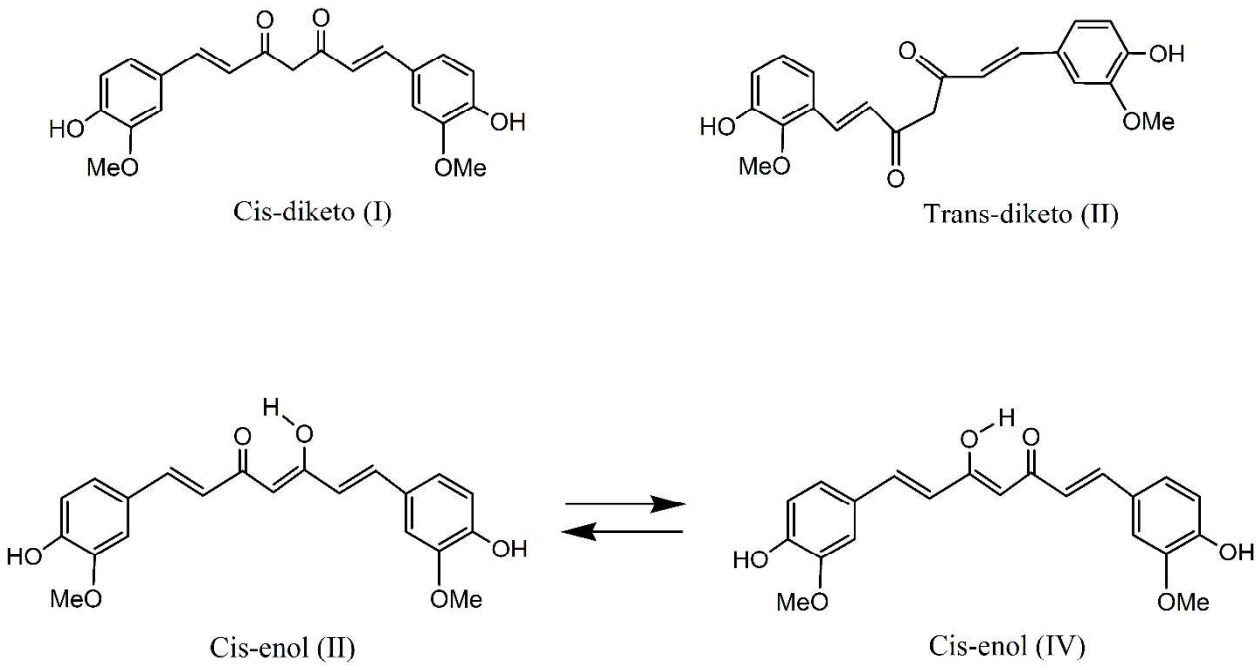

Figure 1.6: *Chemical structures of the cis-diketo, trans-diketo and keto-enol tautomeric forms of curcumin.*

It has been suggested by ab-initio computation study that trans-diketo form (II) is the more stable isomer of curcumin as compared to cis-diketo form (I) [95] because of the less electrostatic repulsion between the two carbonyl groups present in curcumin. However, results from several spectroscopic studies suggested that cis-diketo form of curcumin converts into enol form (III) by transfer of a hydrogen from the $–CH_2$ group and is the major conformer of curcumin in a variety of solvents [94-100]. Keto-enol tautomers of curcumin have also been observed in water/acetonitrile solution by Kawano et al. Results obtained from liquid chromatography/mass spectrometry suggest that enol is a major form of curcumin in this solution [101]. In addition, structural properties of curcumin have been investigated in polar (DMSO), protic (D_2O-DMSO) and in nonpolar ($CDCl_3$) solvents by ^{1}H and ^{13}C NMR spectroscopy [97]. Results obtained revealed that curcumin predominantly exists in the enol form in most of the organic solvents. Keto form may also exist in equilibrium with enol form under some special conditions like in acidic pH. Results obtained from the DFT studies on the calculation of fully optimized geometry of enolic curcumin, both in the vacuum as well as in solution phase indicate that cis enol form has a larger dipole moment (10.8 Debye in solution and 7.7 Debye in the gas phase) which leads to the formation of an intramolecular hydrogen bond between the phenolic OH and the keto group. Also, enol form having a dihedral angle of 180° is more stable than keto form due to the perfect resonance between two phenolic rings which results in the distribution of electron density over the entire molecule [95, 102-108]. Curcumin exists in keto form predominantly in acidic and aqueous solution as well as in cell membranes [91] whereas enol form of curcumin predominates in alkaline solutions [109]. In the pH range of 3-7, the keto form of curcumin has a highly activated carbon atom because of the heptadienone linkage between two methoxyphenol rings and due to the delocalization of the unpaired electrons on the neighboring oxygen atoms, the C-H bonds attached to this activated carbon become very weak. Therefore, curcumin in

keto form acts as a powerful hydrogen atom donor [110] whereas at pH 8 and above, the enol form of the curcumin dominates and behaves as an electron donor. Curcumin has three ionizable protons, one from enolic hydroxyl group and two from phenolic hydroxyl groups. Depending upon the pH of the solution, curcumin can exist in different ionized forms [Figure 1.7]

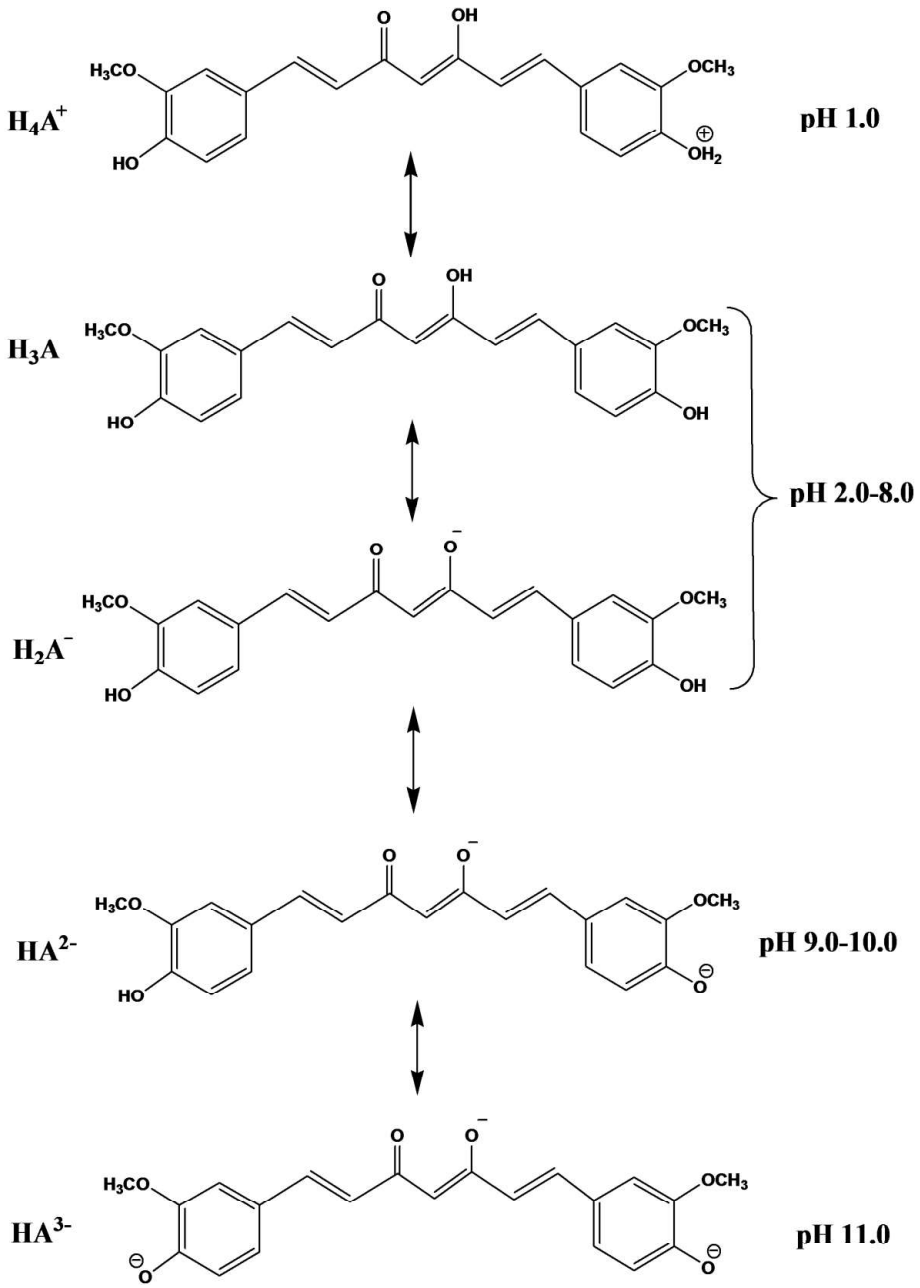

Figure 1.7: *Different ionic forms of curcumin at different pH values*

The pK_a values of curcumin have been investigated by performing several in-depth studies [111-117]. The results suggest that the pK_a values curcumin depends upon the solvent used. The pH dependence of curcumin decomposition has been studied in the pH range of 3 to 10. Results suggested that the decomposition of curcumin is pH dependent and found to be more at basic pH [91]. The pH dependent hydrolytic degradation of the curcumin has been investigated by Tønnesen et al. The authors suggested three pK_a values of 7.75, 8.55 and 9.05 for the dissociation of the hydrogen from the enolic and for the two phenolic groups respectively [111]. Different pK_a values of curcumin have also been reported in studies using potentiometric titrations [112, 113]. In another study, Tang et al have proposed the pK_a values of curcumin to be 8.1 and 10.15 due to the enolic and phenolic protons [114]. The result of DFT study suggests that enolic group of curcumin has lowest pK_a value. Attempts have been made to investigate the dissociation of the enolic proton independently by potentiometric titrations and spectrophotometric studies of curcumin derivatives in which phenolic groups were blocked by substitution [115, 117]. The range of pK_a values for the dissociation of the enolic proton was observed to lie in between pH 8.8 to 9.4.

1.4.1.3 Excited state photophysical properties

Spectroscopic characterization of the excited state of curcumin is a subject of immense interest for researchers due to its photosensitizing effect [118, 119]. Upon optical excitation, curcumin induces the formation of radicals causing cellular damage and apoptosis [120]. The results obtained from several studies on the excited state properties of curcumin showed that excited-state intramolecular hydrogen atom (or proton) transfer (ESIHT or ESIPT) process and dipolar solvation are the two major photophysical process for the relaxation of curcumin excited state [117, 121-131]. Photoexcitation of curcumin from the ground electronic (S_0) state to the first excited singlet (S_1) is accompanied with a significant change in the dipole

moment ($\Delta\mu \sim 6.1$ D) [80] and therefore solvation is expected from to play an important role in the excited-state relaxation dynamics of curcumin. Several studies [121, 125-127] have also predicted that the ESIHT process in the hydrogen-bonded chelate ring of the cis-enol form (Structures III & IV, Figure 1.6) plays an important role in the efficient non-radiative deactivation process of the excited state. The excited-state photophysics of curcumin in surfactant micelles as well as in alcoholic solutions was studied by Adhikary et al. using subpicosecond fluorescence upconversion spectroscopy [127, 128]. The result suggested the presence of two decay components in the excited-state kinetics with the lifetimes of about 12-20 and 100 ps in methanol and ethylene glycol (EG). Shorter lifetime component was insensitive to deuteration of the acidic hydrogens of curcumin but it significantly affected the longer lifetime component. Therefore, the shorter lifetime component was attributed to solvation of the S_1 state and the longer lifetime to the ESIHT process. ESIHT of curcumin has been investigated in sodium dodecyl sulfate (SDS), dodecyl trimethyl ammonium bromide (CTAB) and Triton X-100 (TX-100) by fluorescence upconversion spectroscopy. It has been demonstrated that micelle aggregates enhance the stability and solubility of the curcumin in aqueous solution [128-129]. Result suggests that time constant of ESIHT of curcumin ranges from 50 -80 ps in these micelles. Triton X-100 (TX-100) has a lower ESIHT rate as compare to other two micelles. Intermolecular hydrogen bonding was suggested for this effect. The dynamics of the S_1 state in different solvents using time-resolved absorption and fluorescence spectroscopic techniques with subpicosecond time resolution has been studied by Ghosh et al. [132]. According to them, solvation is the major process contributing to the relaxation dynamics of the S_1 state. Specific hydrogen-bonding interaction between curcumin and the solvent has also a great influence on solvation dynamics. In polar solvents, the deactivation occurs as a result of stretching vibration in the intermolecular hydrogen bonds formed by the hydrogen-bonding (both donating and accepting) solvents. However, the

non-radiative deactivation of the S_1 state in non-polar solvents occurs via ultrafast excited-state intramolecular hydrogen transfer (ESIHT) reaction in the six-membered hydrogen-bonded chelate ring of curcumin. Erez et al. have investigated ESIHT reaction between excited curcumin, a photoacid and acetate, a mild base, by monitoring the fluorescence property of curcumin in methanol and ethanol solutions [133]. They observed that in presence of 1.8 M acetate ions, the steady-state emission intensity, as well as the average fluorescence decay time was reduced by a factor of 5. It was concluded that the large reduction in the fluorescence intensity was due to the excited-state proton transfer from the acidic groups of curcumin to the acetate anion.

1.4.1.4 Biological effects

Curcumin has been extensively studied because of its pharmaceutical properties such as anti oxidant [134], anti-inflammatory [135,136], cardioprotective [137], hepatoprotective [138], anti-infectious properties [139] and much more. Ongoing research on the therapeutic application of curcumin shows that it suppresses initiation, progression, and metastasis of the variety of tumors [140-143].These activities of the curcumin are based on its chemical features and interaction with multiple signaling molecules. Several biological molecules including growth factors, growth factor receptors, transcription factors, cytokines, and enzymes have been identified as targets of curcumin [134-152]. The drug is also quite efficient to modulate phototoxicity to bacterial systems, which is mediated through the excited states of curcumin and their subsequent reactions with oxygen [153].

1.4.1.5 Interaction with biological membranes

The interaction of curcumin with biological membranes is an area of potential research interest. Several studies have been reported which show that curcumin has a great affinity for biological membranes and can change their properties to a greater extent [152-161]. It has been proposed from an earlier study that curcumin regulates the expression and function of several unrelated proteins such as transcription factor, membrane proteins and antiapoptotic proteins indirectly by changing the physical properties of the membrane rather than directly binding to them. [153-157]. A report from Jarugaa et. al. says that membrane permeability of rat thymocyte cells increases after being treated with curcumin [153]. Curcumin also significantly affects the bilayer properties in erythrocyte membranes [154]. Subsequently several model bilayers have been utilized for carrying out studies to investigate the effect of curcumin on their properties [155-158]. Ingolfsoon *et al* have studied the curcumin induced changes in the physical properties of bilayer by monitoring the lifetime and the appearance rates of the gramicidin channels in the bilayer. They suggested that curcumin decreases the energetic cost of bilayer deformation by increasing the lifetime and the appearance rates of the gramicidin channels [152]. Results obtained from ITC and X-ray lamellar diffraction studies after the interaction of curcumin with a model bilayer consisting of DOPC lipid suggest that it causes thinning of the bilayer as well as weakens its elastic moduli [155]. In another study, curcumin induced changes in the membrane thickness and membrane area of giant DOPC unilamellar vesicles have been investigated by Sun et al. Binding of the curcumin with the DOPC unilamellar vesicles was found to be a two-step process. At lower concentration, curcumin first binds to the aqueous-membrane interface and then gradually partitions into the hydrocarbon region of the bilayer at higher concentrations. The physical properties of the lipid bilayer are greatly altered in the presence of curcumin that includes a decrease of the hydrocarbon thickness and softening of its elastic rigidity [156]. Effect of

curcumin was also seen on model multilamellar DPPC and DEPE membranes and it has been suggested that the drug is oriented in the bilayer with its main axis parallel to the acyl chains and interacts with the polar head groups of the lipid in such a way that favors negative curvature of the membrane [157]. Curcumin has also shown a strong effect on model membrane structure consisting of DMPC, DHPC and DPPC lipids as revealed from solid-state NMR and DSC experiments . The drug inserts deep into the membrane in a trans-bilayer orientation, anchored by hydrogen bonding to the phosphate group of lipids. In addition, curcumin also forms higher order oligomeric structures in the membrane that span and thin the bilayer [158]. In another study, function and mode of action of curcumin in modulating the formation of lipid raft domain using model membranes have been studied by total internal reflection fluorescence microscopic technique. It was observed that curcumin induces fusion of lipid raft domains at low concentrations by changing the boundary between the ordered and disordered phases [159]. Interaction of the curcumin with DPPC and DMPG bilayer has also been investigated by atomistic MD simulations. Result obtained suggests extra stabilization for curcumin in head group interface and its perpendicular orientation with respect to the bilayer maximizes favorable contact with polar groups of the lipid and water molecules. Curcumin affinity was found to be higher for DMPG lipids as compare to the DPPC lipids and this was explained on the basis of hydrogen bonding between curcumin and glycerol group of the DMPG bilayers [160]. Interactions of the curcumin with SPC, HSPC and DPPC liposomes have been investigated by absorption and fluorescence spectroscopy . Interaction of curcumin with lipid bilayers depends upon the bilayer rigidity and this has been shown to be higher (two times) for un-saturated PC liposomes compared to saturated PC liposomes [161].

1.5. Objective and scope of the present thesis

The medicinal pigment curcumin shows a wide variety of biological effects and also has a great affinity for biological membranes [152-161]. The effect of curcumin on membrane bilayer is a subject of potential research interest. There are several reports which suggest that curcumin alter the properties of the membranes [153-157]. Therefore, it is tempting to speculate that the biological activity of curcumin may arise from its effect on the membrane structure. A powerful approach to study interfacial phenomena is SHG spectroscopy. Since SHG, by symmetry restriction, probes only the interfacial region, it is possible to use this technique to study the adsorption and transport kinetics of molecules across a lipid bilayer [16-17, 57]. The objective of the current thesis is to investigate the effect of curcumin on a negatively charged PG bilayer using an organic cation as the probe utilizing the interfacial selective SHG spectroscopic technique. Using the ~800 nm quasi-CW output of a femtosecond Ti-Saphhire oscillator the adsorption and transport kinetics of a SH active organic cation in presence of curcumin and liposomes having PG head groups were probed under different conditions to understand how the drug affects the bilayer permeability.

The organization of the remaining chapters of this thesis is as follows:

Chapter 2 describes in detail about the experimental techniques used with a particular emphasis on the experimental setup used to monitor the real time molecular transport across a membrane bilayer. In addition, the spectroscopic characterization of the SH probe used in this study is also described here.

In Chapter 3, the effect of curcumin on the transport characteristics of the SH probe, LDS^+ ions, across a model POPG membrane is described.

Chapter 4 compares the effect curcumin with another lipophilic molecule chlorin-p6 (cp6) on the POPG membrane permeability against LDS^+ ions.

In Chapter 5 the effect of curcumin partitioning into a POPG bilayer on the adsorption and transport properties of LDS^+ ions is described.

Chapter 6, which is a further extension of the work done in Chapter 5, describes the effect of bilayer rigidity on the curcumin induced changes in the adsorption and transport characteristics of LDS^+ ions. Bilayer rigidity is manipulated by using POPG and DPPG lipids. The effect of replacing water by D_2O on the curcumin induced changes in the adsorption and transport characteristics of LDS^+ ions across a POPG bilayer is described in Chapter 7.

Finally in Chapter 8 a summary of the major observations is presented. A brief outline of future investigations that may evolve from the thesis is also provided.

References

1. Aamson, A. W. *Physical Chemistry of Surfaces*, 4th ed.; Wiley: New York, **1982**.
2. Bloembergen, N. *Nonlinear Optics*; Wiley: New York, **1965**.
3. Williams, D. J. Ed. *Nonlinear Optical Properties of Organic and Polymeric Materials*; ACS Symposium Series 233; American Chemical Society: Washington, DC, **1985**.
4. Richmond, G. L.; Robinson, J. M.; Shannon, V. L. *Prog. Surf. Sci*. **1988**, *28*, 1−70.
5. Shen, Y. R. *Annu. Rev. Phys. Chem*. **1989**, *40*, 327−350.
6. Heinz, T. F. *In Nonlinear Surface Electromagnetic Phenomena*; Ponath, H. E., Stegeman, G. I., Eds.; North-Holland: Amsterdam, **1991**, 353−416.
7. Eisenthal, K. B. *Annu. Rev. Phys. Chem*. **1992**, *43*, 627−661.
8. Corn, R. M.; Higgins, D. A. *Chem. Rev*. **1994**, *94*, 107−125.
9. Dick, B. *Chem. Phys*. **1985**, *96*, 199−215.
10. Mizrahi, V.; Sipe, J. E. *J. Opt. Soc. Am. B* **1988**, *5*, 660−667.
11. Tamburello Luca, A. A.; He´bert, P.; Brevet, P. F.; Girault, H. H. *J. Chem. Soc., Faraday Trans.* **1995**, *91*, 1763−1768.
12. Dick, B.; Gierulski, A.; Marowsky, G. *Appl. Phys. B* **1985**, *38*, 107−116.
13. Felderhof, B. V.; Marowsky, G. *Appl. Phys. B* **1987**, *44*, 11−17.
14. Bain, C. D. *J. Chem. Soc., Faraday Trans*. **1995**, *91*, 1281−1296.
15. Marlow, F.; Weruer, L.; Hill, W. *Surf. Sci*. **1991**, *249*, 365−372.
16. Eisenthal, K. B. *Chem. Rev.* **1996**, *96*, 1343−1360.
17. Eisenthal, K. B. *Chem. Rev.* **2006**, *106*, 1462−1477.
18. Bredenbeck, J.; Ghosh, A.; Nienhuys, H. K. Bonn, M. *Acc. Chem. Res*. **2009**, *42*, 1332−1342.
19. Yan, E. C. Y.; Fu, L.; Wang, Z.; Liu, W. *Chem. Rev.* **2014**, *114*, 8471−8498.
20. Roy, S.; Covert, P. A.; Fitz Gerald, W. R.; Hore, D. K. *Chem. Rev.* **2014**, *114*, 8388−8415.

21. Johnson, C. M.; Baldelli, S. *Chem. Rev*. **2014**, *114*, 8416−8446.

22. Nihonyanagi, S.; Yamaguchi, S.; Tahara, T. *Chem. Rev*. **2017,** *117*, 10665−10693.

23. Giordinaine, J. A. *Phys. Rev. A* **1963**, *138*, 1559.

24. Shen, Y. R. *Nature* **1989**, *337*, 519−525.

25. Shen, Y. R.; Martini, F. de. in: V. M. Agronovich and D. L. Mills (Eds.), *Surface Polaritons,* North-Holland, **1982** pp. 629.

26. Heinz, T. F. *Ph.D Dissertation*, University of California, Berkeley, **1982**.

27. Sipe, J. E.; Stegman, G. I. in: V. M. Agronovich and D. L. Mills (Eds), *Surface Polaritons*, North-Holland, **1982** pp. 661.

28. Fukui, M.; Stegman, G. I. in: A. D. Boardman (Eds), *Electromagnetic Surface Modes*, John Wiley & Sons, **1982** pp. 725.

29. Clays, K.; Persoons, A. *Phys. Rev. Lett*. **1991**, *66*, 2980−2983.

30. Terhune, R. W.; Maker, P. D.; Savage, C. M. *Phys. Rev. Lett*. **1965**, *14*, 681−684.

31. Wang, H.; Yan, E. C. Y.; Borguet, E.; Eisenthal, K. B. *Chem. Phys. Lett.* **1996**, *259*, 15−20.

32. Song, Q.; Wan, C. Z.; Johnson, C. K. *J. Phys. Chem*. **1994**, *98*, 1999−2001.

33. Aktsipetrov, O. A.; Elyutin, P. V.; Nikulin, A. A.; Ostrovskaya, E. A. *Phys. Rev. B* **1995**, *51*, 17591−17599.

34. Hicks, J. M.; Kemnitz, K.; Heinz, T. F.; Eisenthal, K. B. *J. Phys. Chem*. **1986**, *90*, 560−562.

35. Higgins, D. A.; Abrams, M. B.; Byerly, S. K.; Corn, R. M. *Langmuir* **1992**, *8*, 1994−2000.

36. Lee, C. H.; Chang, R. K.; Bloembergen, N. *Phys. Rev. Lett.* **1967**, *18*, 167−170.

37. Yeganeh, M. S.; Dougal, S. M.; Pink, H. S. *Phys. Rev. Lett*. **1999**, *83*, 1179−1182.

38. Ong, S.; Zhao, X.; Eisenthal, K. B. *Chem. Phys. Lett*. **1992**, *191*, 327−335.

39. Holland, J. G.; Geiger, F. M. *J. Phys. Chem. B* **2013**, *117*, 825−832.

40. Buster, D. C.; Hinton, J. F.; Millett, F. S.; Shungu, D. C. *Biophys. J.* **1988**, *50*, 145−152.

41. Xiang, T. X.; Anderson, B. D. *Biophys. J.* **1997**, *72*, 223−237.

42. Cruciani, O.; Mannina, L.; Sobolev, A. P.; Cametti, C.; Segre, A. L. *Molecules* **2006**, *11*, 334−344.

43. Mel'nikov, S. M.; Seijen ten Hoorn, J. W. M.; Eijkelenboom, A. P. A. M. *Chem. Phys. Lipids* **2004**, *127*, 121−141.

44. Vermathen, M.; Vermathen, P.; Simonis, U.; Bigler, P. *Langmuir* **2008**, *24*, 12521−12533; Vermathen, M.; Marzorat, M.; Vermathen, P.; Bigler, P. *Langmuir* **2010**, *26*, 11085−11094.

45. Cafiso, D. *Methods Enzymol*. **1989**, *172*, 331–345; Cafiso, D. S.; Hubbell W. L. *Biophys. J*. **1983**, *44*, 49−57.

46. Kaiser, S.; Hoffmann, H. J. *Coll. Interfac. Sci*. **1996**, *184*, 1−10.

47. Voelker, D.; Smejtek, P. *Biophys. J*. **1996**, *70*, 818−830.

48. Terce, F.; Tocanne, J. F.; Laneelle, G. *Eur. J. Biochem*. **1982**, *125*, 203-207.

49. Aubard, J.; Lejoyeux, P.; Schwaller, M. A.; Dodin, G. *J. Phys. Chem*. **1990**, *94*, 1706-1711.

50. Eidelman, O.; Cabantchik, Z. I. *Biochim. Biophys. Acta* **1989**, *988*, 310−334.

51. Casals, C.; Miguel, E.; Perez-Gil, J. *Biochem. J.* **1993**, *296*, 585−593.

52. Kuzelova, K.; Brault, D. *Biochemistry* **1994**, *33*, 9447−9459.

53. Kuzelova, K.; Brault, D. *Biochemistry* **1995**, *34*, 11245−11255.

54. Maman, N.; Brault, D. *Biochim. Biophys. Acta* **1998**, *1414*, 31−42.

55. Bonneau, S.; Maman, N.; Brault, D. *Biochim. Biophys. Acta* **2004**, *1661*, 87−96.

56. Maman, N.; Dhami, S.; Phillips, D.; Brault, D. *Biochim. Biophys. Acta.* **1999**, *1420*, 168−178.

57. Srivastava, A.; Eisenthal, K. B. *Chem. Phys. Lett*. **1998**, *292*, 345−351.

58. Yan, E. C. Y.; Eisenthal, K. B. *Biophys. J.* **2000**, *79*, 898−903.

59. Liu, Y.; Yan, E. C. Y.; Zhao, X. L.; Eisenthal, K. B. *Langmuir* **2001**, *17*, 2063−2066.

60. Y. Liu, Yan, E. C. Y.; Eisenthal, K. B. *Biophys. J.* **2001**, *80*, 1004−1012.

61. Shang, X. M.; Liu, Y.; Yan, E.; Eisenthal, K. B. *J. Phys. Chem. B* **2001**, *105*, 12816−22.

62. Liu, J.; Subir, M.; Nguyen, K.; Eisenthal, K. B. *J. Phys. Chem. B* **2008**, *112*, 15263−66.

63. Liu, J.; Shang, X. M.; Pompano, R.; Eisenthal, K. B. *Faraday Discussions* **2005**, *129*, 291−299.

64. Zeng, J.; Eckenrode, H. M.; Dounce, S.; Dai, H. L. *Biophys. J.* **2013**, *10*, 139−145.

65. Wilhelm, M. J.; Sheffield, J. B.; Gonella, G.; Wu, Y.; Spahr, C.; Zeng, J.; Xu, B.; Dai, H. L. *Chem. Phys. Lett.* **2014**, *158*, 605−606.

66. Zeng, J.; Eckenrode, H. M.; Dai, H. L.; Wilhelm, M. J. *Colloids Surf B Biointerfaces* **2015**, *127*, 122−129.

67. Wilhelm, M. J.; Sheffield, J. B.; Sharifian Gh., M.; Wu, Y.; Spahr, C.; Gonella, G.; Xu, B.; Dai, H. L. *ACS Chem Biol.* **2015**, *10*, 1711−1717.

68. Wilhelm, M. J.; Sharifian Gh., M.; Dai, H. L. *J. Biochem*. **2015**, *54*, 4427−4430.

69. Sharifian Gh., M.; Wilhelm, M. J.; Dai, H. L. *J. Phys. Chem. Lett.* **2016**, *7***,** 3406−3411.

70. Seydel, J. K.; Wiese, M. *Drug-Membrane Interactions*, Wiley VCH, Weinheim, **2002**.

71. Yildirim, M. A.; Goh, K. I.; Cusick, M. E.; Barabàsi, A. L.; Vidal, M. *Nat. Biotechnol*. **2007**, *25*, 1119−1126.

72. Schmidt, B. M.; Ribnicky, D. M.; Lipsky, P. E.; Raskin, I. *Nature Chemical Biology* **2007**, *3*, 360−366.

73. Paszkiewicz, M.; Budzynska, A.; Rozalska, B.; Sadowska, B. *Postepy hig med dosw* **2012**, *66*, 637−646.

74. Randhir, R.; Lin, Y. T.; Shetty, K. *Process Biochem.* **2004**, *39*, 637−646.

75. Velderrain-Rodriguez, G. R.; Palafox-Carlos, H.; Wall-Medrano, A.; Ayala-Zavala, J. F.; Chen, C-Y. O.; Robles-Sanchez, M.; Astiazaran-García, H.; Alvarez-Parrilla, E.; González-Aguilar, G. A. *Food Funct.* **2014**, *5*, 189−197.

76. Aggarwal, B. B.; Surh, Y. J.; Shishodia, S. *Advances in Experimental Medicine and Biology* **2007**, Springer, New York, 595.

77. Srimal, R. C.; Dhawan, B. N. *J. Pharm Pharmacol* **1973**, *25*, 447−452.

78. Srinivasan, K. R. *Current Science* **1952**, *21*, 311−312.

79. de Boer, H. J.; Contingting, C. *J. Ethnopharmacol* **2014**, *151*, 747−67.

80. Carter, A. *JNCI News* **2008**, *100*, 616−617.

81. Aggarwal, B. B.; Sung, B. *Trends Pharmacol. Sci.* **2008**, *30,* 85−94.

82. Chattopadhyay, I.; Biswas, K.; Bandhopadhyay, U.; Banerjee, R. K. *Curr. Sci.* **2004**, *87*, 44−53.

83. Strimpakos, A. S.; Sharma, R. A. *Antioxidants Redox Signaling* **2008**, *10*, 512−534.

84. Harada, T.; Giorgio, L.; Harris, T. J.; Pharm, D. T.; Ngo, H. T.; Need, E. F.; Coventry, B. J.; Lincoln, S. F.; Easton, C. J.; Buchanan, G.; Kee, T. W. *Mol. Pharmaceutics* **2013**, *10*, 4481−4490.

85. Lemos, M. A.; Hungerford, G. *Photochem Photobiol* **2013**, *89*, 1071−1078.

86. Prasad, S.; Gupta, S. C.; Tyagi, A. K.; Aggarwal, B. B. *Biotechnol. Adv.* **2014**, *32*, 1053−64.

87. Smith, J.; Hong-Shum, L. *Food additives Data Book* (pp. 228). UK: Blackwell Science.

88. Quitschke, W. W. *Bioavailability and metabolism of curcuminoids*. In M. Diederich & K. Noworyta, Natural compounds as inducers of cell death. Netherlands: *Springer*. pp. 95-124

89. Tønnesen, H. H. *Die Pharmazie* **2012**, *57*, 820−824.

90. Wang, X.; Kim, R. J.; Lee, S. B.; Kim, Y. J.; Jung, M. Y.; Kwon, H. W.; Ahn, Y. J. *BMC Complement Altern Med* **2014**, 14−88.

91. Wang, J. Y.; Pan, M. H.; Cheng, A. L.; Lin, L. I.; Ho, Y. S.; Hsieh, C. Y.; Lin, J. K. *J. Pharma. Biomed. Anal.* **1997**, *15*, 1867−1876.

92. Wright, J. S. *J. Mol. Struct. Theochem.* **2002**, *591*, 207−217.

93. Corango, P; Claramunt, R. M.; Bouissane, L.; Alkorta, I.; Elguero, J. *Tetrahaedron* **2008**, *64*, 8089−8094.

94. Sun, Y. M.; Wang, R. X.; Yuan, S. L.; Lin, X. J.; Liu, C. B. *Chinese J. Chem.* **2004**, *22*, 827−830.

95. Balasubramanian, K. J. *Agric. Food Chem.* **2006**, *54*, 3512−3520.

96. Barclay, L. R.; Vinquist, M. R.; Mukai, K.; Goto, H; Hashimoto, Y.; Tokunaga, A.; Uno, H. *Org. Lett*. **2000**, *2*, 2841−2843.

97. Payton, F.; Sandusky, P.; Alworth, W. L. *J. Nat. Prod*. **2007**, *70,* 143−146.

98. Roughley, J.; Whiting, D. A. *J. Chem. Soc., Perkin Trans.1* **1973**, *20*, 2379−2381.

99. Matthes, H. W. D.; Luu, B.; Ourisson, G. *Photochemistry* **1980**, *170*, 425−428.

100. Pedersen, U.; Rasmussen, P. B.; Lawesson, S. O.; *Liebigs Ann. Chem.* **1985**, *8*, 1557−69.

101. Kawano, S. I.; Inohana, Y.; Hanshi, Y.; Lin, J. M. *Chin. Chem. Lett*. **2013**, *24*, 685−687.

102. Shen, L.; Ji, H. F.; *Spectrochim. Acta Part A* **2007**, *67*, 619−623.

103. Shen, L.; Ji, H. F.; Zhang, H. Y. *Chem. Phys. Lett.* **2005**, *409*, 300−303.

104. Shen, L.; Zhang, H. Y.; Ji, H. F. *Org. Lett*. **2005**, *7*, 243−246.

105. Kong, L.; Priyadarsini, K. I.; Zhang, H. Y. *J. Mol. Struct. Theochem*. **2004**, *688*, 111−116.

106. Sun, Y. M.; Zhang, H. Y.; Chen, D. Z.; Liu, C. B. *Org. Lett*. **2002**, *4*, 2902−2911.

107. Galasso, V.; Kovac, B.; Modelli, A.; Ottaviani, M. F.; Pichierri, F. *J. Phys. Chem. A* **2008**, *112*, 2331−2338.

108. Murakami, Y.; Ishi, H.; Takada, N.; Takada, S.; Machino, M.; Ito, S.; Fujisawa, S. *Anticancer Res.* **2008**, *28*, 699−707.

109. Sharma, R. A.; Gescher, A. J.; Steward, W. P. *Eur. J. Cancer,* **2005**, *41*, 1955−1968.

110. Jovanovic, S. V.; Steenken, S.; Boone, C. W.; Simic, M. G. *J. Am. Chem. Soc.* **1999**, *121*, 9677−9681.

111. Tonnesen, H. H.; Karlsen, J.; Lebensm, Z. *Unters. Forsch*. **1985**, *180*, 402−404.

112. Dietze, F.; Arrieta, A. F.; Zimmer, U. *Pharmazie* **1997**, *52*, 302−306.

113. Borsari, M., Ferrari, E.; Grandi, R.; Saladini, M. *Inorg. Chim. Acta* **2002**, *328*, 61−68.

114. Tang, B.; Ma, L.; Wang, H.; Zhang, G. *J. Agric. Food Chem*. **2002**, *50*, 1355−1361.

115. Bernabe-Pineda, M.; Ramirez-Silva, M. T.; Romer-Romo, M.; Gonazalez Vergara, E.; Rojas-Hernandez, A. *Spectrochim. Acta A* **2004**, *60*, 1091−1097.

116. Zhao, et al. *Nat. Prod. Commun.* **2008**, *3*, 229−232.

117. Priyadarsini, K. I.; Maithy, D. K.; Naik, G. H.; Sudheer M. K.; Unnikrishnan, M. K.; Satav, J. G.; Mohan, H. *Free Radic. Biol. Med*. **2003**, *35*, 475−484.

118. Hagg, A. B.; Bruzell, E.; Kristensen, S.; Tønnesen, H. *Eur. J. Pharm. Sci.* **2012**, *47*, 65−74.

119. Park, K.; Lee, J. H. *Oncol. Rep.* **2001**, *17*, 537−540.

120. Detty, M. R.; Gibson, S. L.; Wagner, S. J. *J. Med. Chem.* **2004**, *47*, 3897−3915.

121. Khopde, S. M.; Priyadarsini, K. I.; Palit, D. K.; Mukherjee, T. *Photochem. Photobiol*. **2000**, *72,* 625−631.

122. Priyadarshini, K. I. *Free Rad. Biol. Med.* **1997**, *23*, 838−843.

123. Barik, A.; Priyadarsini, K. I.; Mohan, H. *Orient. J. Chem*. **2002**, *18*, 427−432.

124. Priyadarsini, K. I. *J. Photochem. Photobiol. C*. **2009**, *10*, 81−95.

125. Nardo, L.; Paderno, R.; Andreoni, A.; Masson, M.; Haukvik, T.; Tonnesen, H. H. *Spectroscopy* **2008**, *22*, 187−198.

126. Nardo, L.; Andreoni, A.; Bondani, M.; Masson, M.; Tonnesen, H. H. *J. Photochem. Photobiol. B: Biol.* **2009**, *97*, 77-86.

127. Caselli, M.; Ferrari, E.; Imbriano, C.; Pignedoli, F.; Saladini, M.; Ponterini, G. *J. Photochem. Photobiol. A: Chem.* **2010**, *210*, 115−124.

128. Adhikary, R.; Mukherjee, P.; Kee, T. W.; Petrich, J. W. *J. Phys. Chem. B* **2009**, *113*, 5255−5261.

129. Adhikary, R.; Carlson, P. J.; Kee, T. W.; Petrich, J. W. *J. Phys. Chem. B* **2010**, *114,* 2997−3004.

130. Dahl, T. A.; Bilski, P.; Reszka, K. J.; Chignell, C. F. *Photochem. Photobiol.* **1994**, *59*, 290−294.

131. Chignell, C. F.; Bilski, P.; Reszka, K. J.; Motten, A. G.; Sik, R. H.; Dahl, T. A. *Photochem. Photobiol.* **1994**, *59*, 295−302.

132. Ghosh, R.; Mondal, J. A.; Palit, D. K. *J. Phys. Chem. B* **2010**, *114*, 12129−12143.

133. Erez, Y.; Presiado, I.; Gepshtein, R., Huppert, D. *J. Phys. Chem. A* **2011**, *115*, 10962−10971.

134. Sreejayan; Rao, M. N. *J. Pharm. Pharmacol*. **1997**, *49,* 105−107.

135. Brouet, I.; Oshima*,* H.; *Biochem. Biophys. Res. Commun.* **1995**, *206*, 533−540.

136. Dikshit, M.; Rastogi, L.; Shukla, R.; Srimal, R. C. *Indian J. Med. Res.* **1995**, *101*, 31−35.

137. Venkatesan, N. *Br. J. Pharmacol.* **1998**, *124,* 425−427.

138. Kiso, Y.; Suzuki, Y.; Watanabe, N.; Oshima, Y.; Hikino, H. *Planta Med.* **1983**, *49*, 185−187.

139. Chan, M. M.; Adapala, N. S.; Fong, D. *Parasitol Res*. **2005**, *96*, 49−56.

140. Anand, P.; Sundaram, C.; Jhurani, S.; Kunnumakkara, A. B.; Aggarawal, B. B. *Cancer Lett.* **2008**, *267*, 133−164.

141. Aggarwal, B. B.; Gehlot, P. *Curr. Opin. Pharmacal.* **2009**, *9*, 351−369.

142. Aggarwal, B. B.; Shishodia, S.; Sandur, S. K.; Pandey, M. K.; Sethi, G. *Biochem. Pharmacol.* **2006**, *72*, 1605−1621.

143. Gupta, S. C.; Prasad, S.; Kim, J. H.; Patchva, S.; Webb, L. J.; Priyadarsini, I. K. *Nat. Prod. Rep.* **2011**, *28*, 1937−1955.

144. Cheng, A. L.; Hsu, C. H.; Lin, J. K.; Hsu, M. M.; Ho, Y. F.; Shen, T. S.; Ko, J. Y.; Lin, J. T.; Lin, B. R.; Wu, M. S.; Yu, H. S.; Jee, S. H.; Chen, G. S.; Chen, T. M.; Chen, C. A.; Lai, M. K.; Pu, Y. S.; Pan, M. H.; Wang, Y. J.; Tsai, C. C.; Hsieh, C. Y. *Anticancer Res.* **2001**, *21*, 2895−2900.

145. Hatcher, H.; Planalp, R.; Cho, J.; Torti, F. M.; Torti, S. V. *Cell. Mol. Life Sci.* **2008**, *65*, 1631−1652.

146. Pari, L.; Tewas, D.; Eckel, J. *Physiol. Biochem.* **2008**, *114,* 127−149.

147. Mecocci, P.; Mariani, E.; Polidori, M. C.; Hensley, K.; Butterfield, D. A. *Cent. Nerv. Syst. Agents Med. Chem.* **2008**, *8*, 48−63.

148. Kaludercic, N.; Lindsey, M. L.; Tavazzi, B.; Lazzrin, G.; Palocci, N. *Card. Vasc. Drug Rev.* **2008**, *26,* 24.

149. Goel, A.; Kunnamakkara, A. B.; Aggarwal, B. B. *Biochem. Pharmacol.* **2008**, *75*, 787−809.

150. Khan, N.; Afaq, F.; Mukhtar, H. *Antioxid. Redox Signal.* **2008**, *10*, 475−510.

151. Bilmen, J. G.; Khan, S. Z.; Javed, M. U. H.; Michelangeli, F. *Eur. J. Biochem*. **2001**, *268*, 6318−6327.

152. Ingolfsson, H. I.; Koeppe, R. E.; Andersen, O. S. *Biochemistry* **2007**, *46*, 10384−10391.

153. Jaruga, E.; Salvioli, S.; Dobrucki, J.; Chrul, S.; Bandorowicz-Pikuła, J.; Sikora, E.; Franceschi, C.; Cossarizza, A.; Bartosz, G. *FEBS Lett.* **1998**, *433*, 287−293.

154. Jaruga, E.; Sokala, A.; Chrulb, S.; Bartosza, G. *Exp. Cell Res.* **1998**, *245*, 303−312.

155. Hung, W. C.; Chen, F. Y.; Lee, C. C.; Sun, Y.; Lee, M. T.; Huang, H. W. *Biophys. J.* **2008**, *94*, 4331−4338.

156. Sun, Y.; Lee, C. C.; Hung, W. C.; Chen, F. Y.; Lee, M. T.; Huang, H. W. *Biophys. J.* **2008**, *95*, 2318−2324.

157. Perez-Lara, A.; Ausili, A.; Aranda, F. J.; Godos, A.; Torrecillas, A.; Corbalan-Garcia, S.; Gomez-Fernandez, J. C. *J. Phys. Chem. B* **2010**, *114*, 9778−9786.

158. Barry, J.; Fritz, M.; Brender, J. R.; Smith, P. E.; Lee, D. K.; Ramamoorthy, A. *J. Am. Chem. Soc.* **2009**, *131*, 4490−4498.

159. Tsukamotao, M.; Kuroda, K.; Ramamoorthy, A.; Yasuhara, K. *Chem. Commun.* **2014**, *50*, 3427−3430.

160. Jalili, S.; Saeedi, M. *Journal of Biomolecular Structure and Dynamics* **2015**, 327−340.

161. Bhattarai, R.; Roy, B.; Guha, P.; Bista, A.; Bhadra, A.; Karmakar, G.; Nahak, P.; Chettri, P.; Panda, A. K. *J. Surface Sci. Technol*. **2015**, *31*, 77−85.

Chapter 2

Instrumentations and Methods

This chapter describes the chemicals used, preparation and characterization of liposomes as well as other supplementary experimental techniques (absorption, fluorescence and light scattering spectroscopy) used in the dissertation. The experimental setup used to monitor the real time molecular transport across lipid bilayer is described in detail. Finally, the spectroscopic characterization of the SH probe (LDS^+ ion) used in this thesis is also described here.

2.1 Chemicals used

LDS-698 (from Exciton) was a gift from Prof. N. Sarkar and was used as received. Cp_6, a kind gift from Dr. A. Dube was used as received. Curcumin (Sigma Product No. C7727) was further purified by TLC according to a reported method [1]. Heavy water (D_2O > 95% pure) from Heavy water division, BARC, Mumbai, India was used as received. Deuterated methanol (> 99%) from Sigma was used as received. For the experiments conducted in chapter 7, the enolic hydrogen of curcumin was deuterated by following an earlier report [2]. Briefly, curcumin dissolved in deuterated methanol was allowed to equilibrate for 48 hours which results in the replacement of the enolic hydrogen by deuterium. For the preparation of liposomes, several lipids like POPC, POPG, POPS, DPPG & Cholesterol were purchased from Sigma and Avanti polar lipids and were used as received. DPH-POPC from Molecular Probes was used as received. For the preparation of DPH labeled POPG lioposomes, a concentrated stock solution of DPH-POPC lipid was mixed with a concentrated stock solution of POPG lipid so that the ratio of DPH-POPC: POPG was 1:150. The chemical structures of the different phospholipids used for the preparation of different liposomes in this thesis are shown in Figure 2.1.

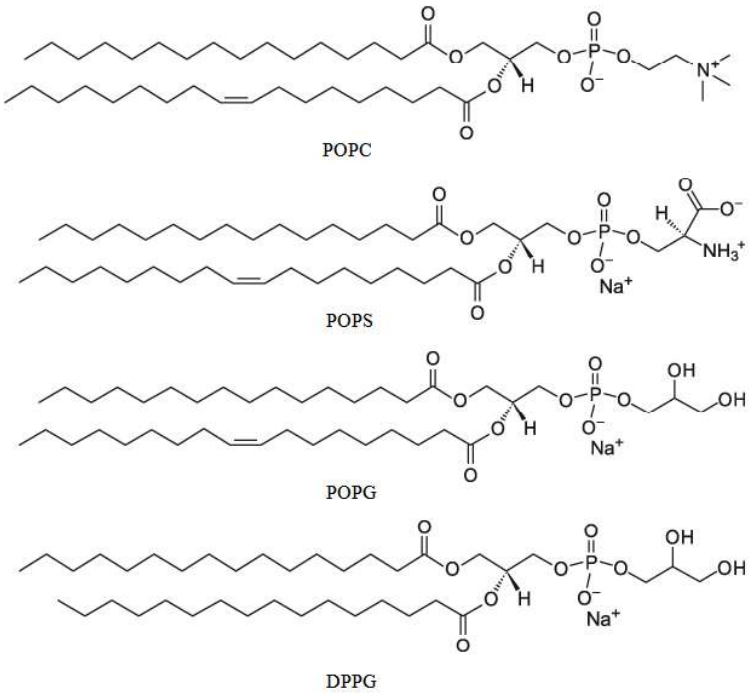

Figure 2.1: *Chemical structures of the different lipids used.*

2.2 Preparation & characterization of unilamellar liposomes

Liposomes were prepared by two methods in our studies. These methods are given below.

2.2.1 Rotary evaporation method

In this method, a 20 μL stock solution of the phospholipid (0.1M) in chloroform was added to a clean and dry 50 ml round bottom flask followed by addition of 980 μL of chloroform and 200 μL of methanol. All mixing the contents 7 ml of phosphate buffer solution was added carefully by a pipette along the wall of round bottom flask so that the organic and aqueous phase remains separate. To remove the organic solvent, the flask was slowly attached to a rotary evaporator and rotated at 40 rpm under vacuum for approximately 3 min. The removal of organic solvent was validated by the lack of the bubble formation in the solution. After complete evaporation of the organic solvent, 6.5 mL of an opalescent fluid containing liposomes was obtained [3]. The final concentration of the lipid was ~ 0.3mM.

2.2.2 Thin film method

In this method, 200 μL of 0.1M stock solution of phospholipid (in chloroform) was taken in a round bottom flask. In the case of mixed liposomes, an appropriate amount of stock solution of different phospholipids was mixed according to the desired mole ratio. To make a thin film of lipid, the organic solvent was evaporated overnight at 40 rpm under reduced pressure using a rotary evaporator. After that, the dried film was hydrated with 10 ml of 10 mM phosphate buffer solution and vortexed for 10 minutes to produced unilamellar liposomes [4]. To reduce the polydispersity in the liposome size, the lipid solution was passed several times through cellulose-acetate membranes (pore size 450 nm and 200 nm). The prepared samples were then transferred to glass bottles and stored in the refrigerator at 4 °C. These liposomes were observed to be stable for more than one week. The final lipid concentration in the liposomes prepared in this way was 2 mM.

2.2.3 Characterization of liposomes

Prior to the SHG experiments, liposomes prepared from the different phospholipids and their combinations were characterized for their size and zeta potential using a Brookhaven 90 Plus size and zeta potential analyzer. This instrument can measure particle size ranging from ~1 nm to ~6 μM with an accuracy of ± 5%, and zeta potential from -150 mV to + 150 mV with an accuracy of ± 2%.

2.2.3.1 Size Measurement of the liposomes

Hydrodynamic radius and polydispersity of the liposomes were determined by dynamic light scattering method. Liposome solution was illuminated with a 635 nM diode laser light and scattered signal was collected at the right angle to that of the incident light. Dynamic light scattering (DLS) technique, also known as photon correlation spectroscopy (PCS), measures

the translational diffusion coefficient of the liposomes, due to Brownian motion of the liposomes in suspension, through analysis of the time dependent fluctuations in the intensity of the scattered light [5]. Bigger liposomes diffuse more slowly as compare to the smaller liposomes in the solution, and the fluctuations in the scattering light intensity changes accordingly. The translational diffusion coefficient is related to the radius of the liposome by the Stokes-Einstein equation:

$$D_T = \frac{k_B\, T}{6\pi\eta\, R_H} \tag{2.1}$$

where D_T is the translational diffusion coefficient, k_B is the Boltzmann constant, T is absolute temperature in Kelvin, η is the viscosity of the solvent and R_H is the hydrodynamics radius of the liposome.

2.2.3.2 Zeta potential measurement of the liposomes

Zeta potential is related to the overall charge of a microparticle suspended in a particular medium. Higher value of the zeta potential implies greater stability of the microparticles. Zeta potential is measured from the electrophoretic mobility of the microparticles moving under an applied field [6]. For the measurement of the zeta potential of the prepared liposome solutions, an electric field is applied to the liposome solution. Liposomes having charge move towards the oppositely charge electrode. The direction of their movement represents the kind of charge on them and the velocity with which they moves towards the oppositely charge electrode is directly propositional to the magnitude of the charge on them. Under some approximations, zeta potential can be measured from the electrophoretic mobility by the Henry's equation:

$$U_E = \frac{2\,\varepsilon\, z\, f(ka)}{3\eta} \tag{2.2}$$

where, U_E is the electrophoretic mobility, z is the zeta potential, ε dielectric constant, η is the viscosity and $f(ka)$ is the Henry's function [7].

For experiments conducted in Chapter 4, the size and zeta potential of the liposomes at different pH and with/without drugs are provided in table 2.1

Table 2.1: *Size and zeta potential parameters for POPG liposomes under different experimental conditions (lipid 50 µM; Curcumin 3 µM).*

System	Zeta potential (mV)	Diameter(nm)	polydispersity
pH 5.0			
POPG liposome	-85.92	190.1	0.137
+Curcumin at 0Hr	-89.55	186.8	0.142
+ Curcumin at 1Hr	-80.08	183.1	0.131
+Curcumin at 2Hr	-86.62	184.3	0.125
+Curcumin at 3Hr	-86.55	183.4	0.130
+Curcumin at 4Hr	-80.18	186.4	0.148
+ Curcumin overnight	-95.45	183.5	0.120
pH 7.4			
POPG liposome	-90.17	188.7	0.142
+Curcumin at 0Hr	-89.18	189.0	0.110
+ Curcumin at 1Hr	-95.49	186.8	0.135
+Curcumin at 2Hr	-87.96	189.1	0.114
+Curcumin at 3Hr	-88.91	190.0	0.149
+Curcumin at 4Hr	-83.09	190.3	0.120
+ Curcumin overnight	-96.60	182.8	0.138
pH 8.0			
POPG liposome	-89.07	190.8	0.164
+Curcumin at 0Hr	-95.41	196.7	0.162
+ Curcumin at 1Hr	-80.81	195.5	0.175
+Curcumin at 2Hr	-94.61	194.7	0.163
+Curcumin at 3Hr	-90.60	200.9	0.148
+Curcumin at 4Hr	-86.03	198.0	0.172
+ Curcumin overnight	-95.23	194.7	0.157

For experiments conducted in Chapter 5, unilamellar POPG liposomes were suspended in 20 mM phosphate buffer solution. The size and zeta potential of the liposomes at different pH are provided in Table 2.2.

Table 2.2: *Size and zeta potential parameters for POPG liposomes under different experimental conditions*

POPG liposome at	Zeta potential (mV)	Diameter (nm)	polydispersity
pH 5.0	-83.92 ± 7.0	192.1 ± 17.0	0.151 ± 0.04
pH 6.0	-87.02 ± 12.0	196.4 ± 25.0	0.143 ± 0.06
pH 7.4	-91.17 ± 9.0	188.7 ± 11.0	0.140 ± 0.08
pH 8.0	-86.07 ± 11.0	190.8 ± 14.0	0.161 ± 0.05
pH 8.5	-91.87 ± 8.5	185.9 ± 21.0	0.153 ± 0.04

For experiments conducted in Chapter 6, unilamellar liposomes made from different mole-ratio of POPG and DPPG lipid were suspended in 20 mM phosphate buffer solution. The size and zeta potential of the liposomes are provided in Table 2.3.

Table 2.3: *Size and zeta potential of POPG-DPPG liposomes.*

Liposome composition	Size (nm)	Zeta-potential (mV)	Poly-dispersity
DPPG	186 ± 19	-110 ± 12	0.098 ± 0.006
DPPG:POPG(5:1)	180 ± 14	-102 ± 14	0.110 ± 0.009
DPPG:POPG(3:1)	173 ± 22	-104 ± 11	0.085 ± 0.005
DPPG:POPG(1:1)	183 ± 16	-108 ± 16	0.091 ± 0.007
DPPG:POPG(1:3)	179 ± 11	-113 ± 14	0.076 ± 0.006
POPG	183 ± 20	-105 ± 13	0.093 ± 0.006

For experiments conducted in Chapter 7, Unilamellar POPG liposomes were prepared in 20 mM pH 5.0 (or pD 5.0) citrate buffer solution using either H_2O or D_2O as the solvent. The size and zeta potential of the liposomes suspended in H_2O or D_2O were observed to be similar (200 ± 10 nm and -79 ± 10 mV).

2.3.1 UV-Visible spectroscopy

UV-Visible spectroscopy is a very basic but widely used spectroscopic technique to obtain information about the ground state absorption characteristics of an absorbing species. This

technique provides useful information regarding the nature of the interaction between the ground state of the absorbing molecule and its surrounding environment [8-11]. The Beer-Lambert's law governs the absorption of energy by a molecule**.** According to this law, the fraction of the incident light absorbed by the sample solution is proportional to concentration of absorbing species and its specific molar extinction coefficient ε at a defined wavelength λ.

$$\log_{10}\left(I_0/I\right) = A = \varepsilon cl \qquad (2.3)$$

where I_0 = intensity of the incident light, I = intensity of transmitted light, A = Absorbance, **ε** = Molar absorbance or absorption coefficient (in dm^3 mol^{-1} cm^{-1} units), c = concentration of the compound in the solution (in mol dm^{-3} units), and l = path length of light in the sample (in cm units).

The quantity $\log_{10}(I_0/I)$ is commonly known as the optical density or absorbance of the material. The steady state absorption spectra were carried out using a UV-Visible absorption spectrometer model Cintra 20 (GBC Scientific Equipment Ltd.). It is a dual beam direct ratio recording system having Czerny-Turner style monochromators with holographic grating and variable slit widths and the detector is a photomultiplier tube. The wavelength range covered by the spectrometer is 190 to 900 nm with spectral band pass from 0.2 to 5 nm variable in the step of 0.1 nm having a wavelength accuracy of ± 0.2 nm. As the light source, the spectrometer uses a 35 W tungsten-halogen lamp for the 900 to 350 nm region and another 30 W deuterium lamp for covering the 350-190 nm region which changes automatically at selected wavelength. Photometric linearity is better than 1% up to an absorbance value of 3.0 and lowest absorbance measurable is ~ 0.005. For absorbance measurements, the sample was kept in a quartz cuvette having a path length of 1 cm.

2.3.2 Fluorescence spectroscopy

Fluorescence spectroscopy is an important investigational tool in many areas of biological science and analytical science due to its higher sensitivity and selectivity. In this process, first the molecule in its ground electronic state absorbs a photon of appropriate energy within 10^{-15} second and goes to a higher excited state. After reaching there, the molecule can come back to the ground state either through radiative or through various non-radiative pathways that are shown in the Jablonski diagram (Figure 2.2). Radiative pathway includes the emission of photon where as non-radiative pathways include energy transfer, collision quenching etc. [8,9,12].

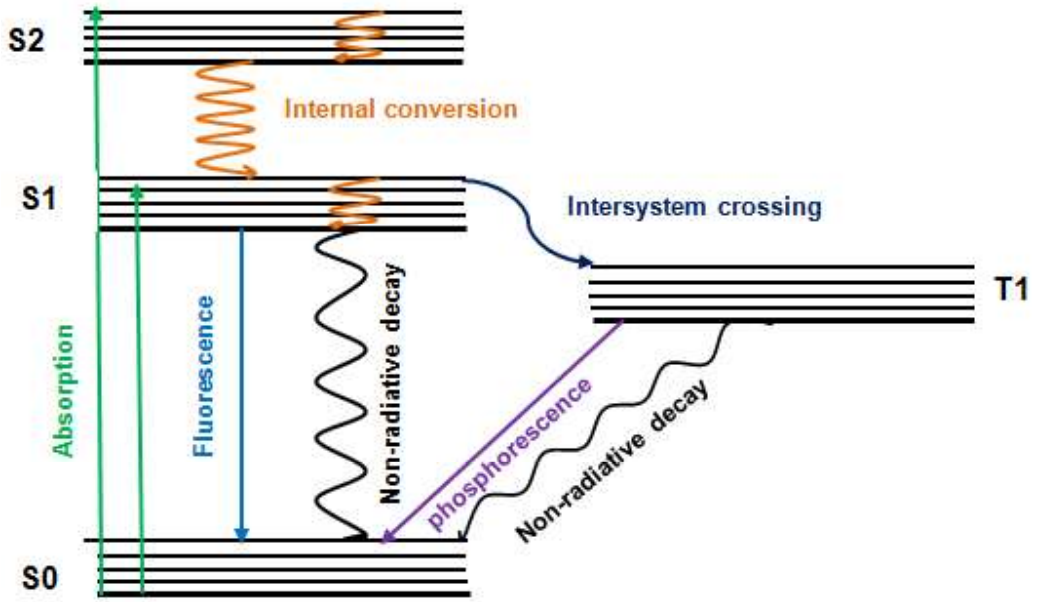

Figure 2.2: *Jablonski diagram showing the different process occurring after the interaction of light with a molecule.*

The steady state emission measurements were recorded using a Spex Fluorolog 2 fluorimeter. It consists of a 450 W Xenon lamp that generates a continuum of visible and UV light, an excitation monochromator to select the desired wavelength for excitation, a sample compartment and emission monochromator attached with photomultiplier tube (PMT) to analyze the fluorescence signal. Intensity and wavelength spread of the light was controlled

by the entrance and the exit slits placed before each monochromator. Excitation light from the Xenon lamp passed through an excitation monocromator which selectively passes a narrow band of the excitation light that strike the sample in sample holder. The emission from the sample was collected by the emission monochromator which is placed at right angle with respect to the excitation beam in order to minimize the risk of detection of stray light by the photomultiplier tube. The emission after passing through the emission monochromator is detected by the PMT which has a sensitivity ranging from 250 to 850 nm. An emission spectrum of a sample is recorded by scanning the emission monochromator for a constant excitation wavelength (λ_{ex}). Similarly, an excitation spectrum was recorded by scanning the excitation monochromator at a fixed emission wavelength (λ_{em}).

2.3.2.1 Time-resolved fluorescence measurements

Time resolved fluorescence measurements were carried out using the time-correlated single photon counting (TCSPC) technique. It is a most widely used technique to record the time dependent fluorescence of a sample with single photon detection sensitivity in the nanosecond to picosecond time scale. The basic principle of the TCSPC relies on the fact that after excitation of the sample with short pulse from a laser, time-dependent probability distribution of the single photon emission from the sample is equivalent to time dependent changes in the fluorescence intensity in the sample following its short pulse excitation [9,13]. Figure 2.3 describes a schematic block diagram of a TCSPC system. The excitation light pulse from the excitation source is split into two parts. One part is used to excite the sample and another part is directed to trigger a photodiode. The optical signal generated by the photodiode generates an electrical START signal which is routed through a constant-fraction-discriminator (CFD) and reaches to the time-to-amplitude converter (TAC) module. After

receiving the start pulse, a timing capacitor in the TAC starts to charge linearly. Meanwhile, the sample after optical excitation starts to generate emission photons. These emitted photons

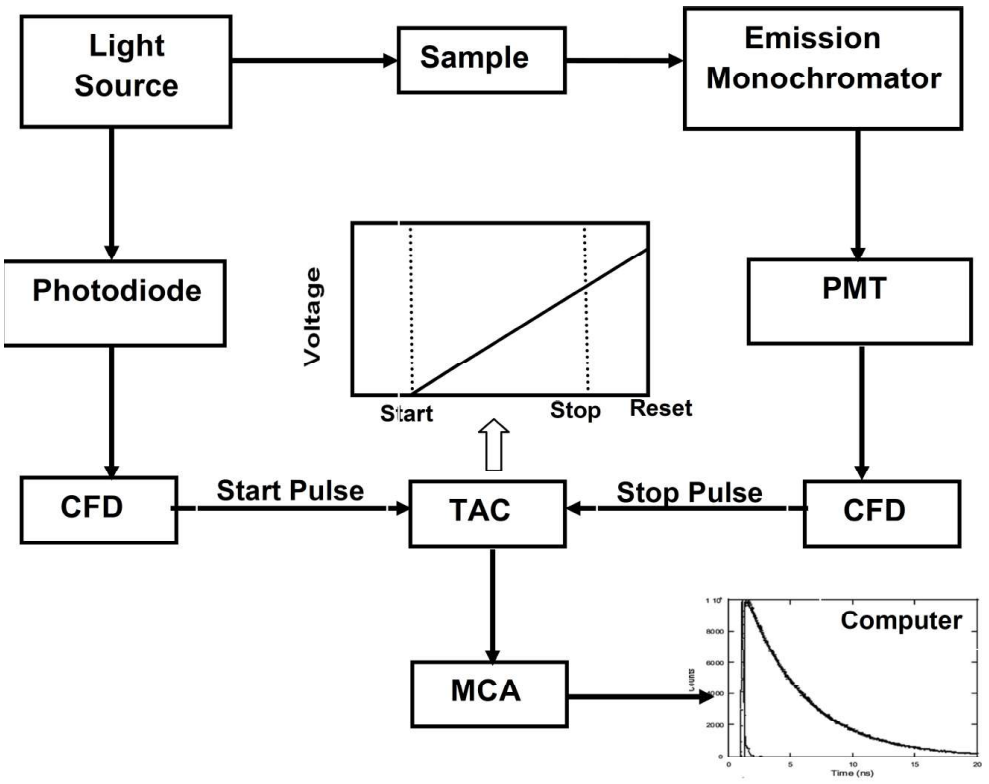

***Figure 2.3**: Typical block diagram of a TCSPC instrument.*

are detected one by one by the PMT to generate electrical STOP pulses for each of the individual emission photon received. These electrical pulses which are also routed through another CFD reaches to the same TAC unit. On receiving the first electrical STOP pulse, TAC stops the charging of the capacitor and delivers a voltage output which is directly prepositional to the delay time (Δt) between the start and stop pulses reaching the TAC unit. The ADC module converts this voltage to a numerical value which is then fed into the input of a multi channel analyzer (MCA) and selects the particular channel in the MCA where a single count is added up. A histogram of the counts is generated in the MCA after repetition of this cycle (from excitation to data storage in the MCA) again and again. This distribution of the counts against the channel number in MCA represents the fluorescence decay curve of

the sample which is convoluted with instrument response function (IRF) of the TCSPC system. IRF is the dead time of the TCSPC and limits its time resolution. IRF is collected in a similar way just by replacing the sample by a non fluorescent scattering sample. Using an iterative method, the intrinsic emission decay kinetics is deconvoluted from the IRF. To avoid the pulse pile-up error, the collection rate of the emission photons by the stop PMT is kept low, around 2% or less, compared to the repetition rate of the excitation pulses. Low pulse energy and low sample concentration are also recommended to ignore this effect.

For the measurements carried out in this thesis, a TCSPC system called Lifespec-RED from Edinburgh Instruments is used. Second harmonic output of a tunable femto second laser (Cohrent Model Verdi pumped by Cohrent Model Mira) was used as the excitation source having pulses of ~ 150 fs. A pulse picker (Coherent model 9200) was used to select pulses at 3.8 MHz repetition rate. Fluorescence from the sample was collected at the right angle to the excitation. An emission polarizer was used before the collection optics and fluorescence is recorded at magic angle (54.7 °C) polarization with respect to excitation light. To avoid the scattered excitation light, proper emission filters were used. Fluorescence signal was detected by a thermoelectric cooled Hamamatsu microchannel plate PMT (R3809U-50) and the IRF of this instrument was ~ 50 ps. The fluorescence decays were deconvoluted from the IRF using iterative software based on global least squares analysis algorithm provided by the manufacture and fit to either single or multi exponential function as described in the equation:

$$I(t) = \sum_{i}^{n} a_i \; e^{-\left(\frac{t}{\tau_i}\right)} \tag{2.4}$$

Where τ_i is the fluorescence lifetime, a_i is the pre-exponential factor of the ith component of the sample. The goodness of the fit was judged by visual inspection of the plots of weighted residuals which was randomly distributed around zero line and reduced chi-square value close to 1.0 [13].

2.3.2.2 Resonance Energy Transfer (RET)

Resonance energy transfer is an additional possible relaxation pathway for an excited molecule, which occurs only in certain conditions. In this non-radiative process, an excited state molecule (donor) can return to its ground state by transferring the excited state energy to another molecule (acceptor) via long rang dipole–dipole interactions. RET is also known as fluorescence resonance energy transfer when the donor molecule is fluorescent and acceptor molecule may or may not be fluorescent. There are certain conditions, which should be satisfied for this relaxation pathway to occur such as the donor to acceptor distance must be within 10-100 Aº of each other. Second, for effective transfer over the range from 10 Aº to 100 Aº, emission spectrum of donor molecule must overlap with the absorption spectrum of acceptor molecule adequately, so that several vibronic transitions in the donor molecule have practically the same energy as the corresponding transitions in the acceptor. Third is emission dipole moment of the donor must be appropriately oriented with respect to the excitation dipole moment of acceptor. In addition, the last condition is that the excited state lifetime of the donor molecule must be of sufficient duration to allow energy transfer. Because FRET is a non-radiative process, signature of this process is quenching of the donor emission while increase in the emission of acceptor. Förster first proposed the mechanism of FRET in 1946. He developed a non-radiative transfer rate equation which relates to the inter-chromospheres distance and the spectroscopic properties of the chromospheres and they showed that FRET efficiency decreases with the sixth power of the distance between the donor and acceptor [14]. This theory, critically verified by Stryer et. al. in 1967, cited FRET as “Spectroscopic ruler” because of its distance dependency [15].

The rate of energy transfer from donor to acceptor is given by

$$k_T(r) = \frac{Q_D\,\kappa^2}{\tau_D r^6}\left(\frac{9000(\ln 10)}{128\pi^5 N n^4}\right)\int_0^\infty F_D(\lambda)\varepsilon_A(\lambda)\lambda^4 d\lambda \qquad (2.5)$$

where Q_D is the quantum yield of the donor in the absence of acceptor, n refractive index of the medium, N is the Avogadro's number, r is the distance between the donor and acceptor and τ_D is the lifetime of the donor in the absence of acceptor, $F_D(\lambda)$ is the corrected fluorescence intensity of the donor in the wavelength range λ to $\lambda + \Delta\lambda$ with the total intensity (area under the curve) normalized to unity. ε_A is the extinction coefficient of the acceptor at excitation wavelength. *J(λ)* is called the overlap integral which is given (in nanometers) by:

$$J(\lambda) = \int_0^\infty F_D(\lambda)\varepsilon_A(\lambda)\lambda^4 d\lambda \tag{2.6}$$

κ is known as orientation factor which depends upon the relative orientation of the donor emission dipole moment with the acceptor excitation dipole moment and can have the value of 0 to 4. Orientation factor can be expressed as:

$$k^2 = (\cos\theta_T - 3\cos\theta_D \cos\theta_A)^2 = (\sin\theta_D \sin\theta_A \cos\phi - 2\cos\theta_D \cos\theta_A)^2 \tag{2.7}$$

Equation 2.5 can also be expressed as:

$$k_T(r) = \frac{1}{\tau_D}\left(\frac{R_0}{r}\right)^6 \tag{2.8}$$

Where R_0 is the distance (in A^0) between the donor and acceptor at which the transfer efficiency is 50% and given by:

$$R_0 = 0.211[\kappa^2 n^{-4} Q_D J(\lambda)]^{1/6} \tag{2.9}$$

Efficiency of energy transfer is the fraction of photons absorbed by the donor that are transfer to the acceptor non-radiatively and can be expressed as:

$$E = \frac{k_T(r)}{\tau_D^{-1} + k_T(r)} \tag{2.10}$$

Eq. 2.10 and 2.8 can be rearranged to yield:

$$E = \frac{R_0^6}{r^6 + R_0^6} \tag{2.11}$$

This equation clearly shows the strong dependence of the transfer efficiency on the distance between the donor and the acceptor. There are various ways to define the RET efficiency like in terms of relative fluorescence intensity of the donor in the presence and absence of the acceptor, fluorescence lifetime of the donor in the presence and absence of acceptor and also in terms of distance between donor and the acceptor.

$$E = 1 - \frac{\tau_{DA}}{\tau_D} = 1 - \frac{f_{DA}}{f_D} = \frac{R_0^6}{R^6 + R_0^6} \tag{2.12}$$

This distance dependent behavior of FRET makes it a very useful spectroscopic tool in structural biology, biochemistry and polymer science [16-22].

2.3.2.3 Fluorescence anisotropy

In a bulk solvent environment, all the fluorophores in their ground state are oriented randomly and the optical response from a large sample of molecules is isotropic or unpolarized in nature. However, upon excitation with a polarized light beam, the molecules whose transition dipole moment is aligned with the electric field vector of the excitation light, preferentially absorb the light with a maximum probability and excite while those at 90° remain in the ground state only. This process is known as photoselection. These excited molecules may rotate to other directions before returning to the ground state with the emission of light and causes the depolarization of emission. The depolarization of emission depends upon the rate and extent of the rotational diffusion during the lifetime of the excited state [9]. Two factors are believed to be affecting this rate of rotational diffusion. One is the viscosity of the solvent which surrounds the molecules and another is the size and shape of the molecule itself [23-27]. The extent to which optical response of the molecules is aligned to the polarization of the excited light is termed as anisotropy. To measure the fluorescence anisotropy, the sample is excited with both vertically and horizontally polarized light. The

intensity of the vertically and horizontally polarized components of the emission was measured through a polarizer after the sample holder cell and fluorescence anisotropy (r_0) was then calculated as [28]:

$$r_0 = \frac{I_{VV} - G\, I_{VH}}{I_{VV} + 2G\, I_{VH}} \tag{2.13}$$

where, G is the correction factor, I_{VV}, and I_{VH} and are the emission intensities of the sample recorded using the different orientation of the excitation and emission polarizers. The first subscript refers to the orientation of the excitation polarizer and the second subscript refers to the orientation of the emission polarizer. The steady state fluorescence anisotropy measurements were performed with the Fluoromax-4 spectrofluorimeter from Jobin Yvon, Horiba.

For fluorescence anisotropy measurements, DPH (1 μM) was incubated overnight with 100 μM liposome solutions and the temperature dependent fluorescence anisotropy were measured by exciting DPH at 360 ± 2 nm and monitoring the emission at 420 ± 4 nm. For the temperature variation experiments, the sample was allowed to equilibrate with the temperature for at least 30 minutes. During experiment, the temperature variation was observed to be less than 0.2 °C. The phase transition temperature of the unilamellar liposomes made from different mole-ratio of POPG and DPPG lipid are provided in Table 2.4

Table 2.4: *Phase transition temperature of POPG & DPPG liposomes made from different mole-ratio of POPG and DPPG lipid used.*

Liposome composition	T_m (°C)
DPPG	42.0 ± 0.4
DPPG:POPG(5:1)	38.7 ± 0.6
DPPG:POPG(3:1)	37.6 ± 0.8
DPPG:POPG(1:1)	30.8 ± 1.1
DPPG:POPG(1:3)	--
POPG	--

2.4 The SHG experimental setup

The schematic sketch of the experimental setup used for the monitoring the real time transport of molecules across the lipid bilayer of the liposomes is shown in figure 2.4. The excitation source for SHG is provided by the quasi-CW output of a Ti-Sapphire (Coherent Mira) laser pumped by a green (532 nm, Coherent Verdi 5W) laser. The quasi-CW output of a Ti-Sapphire provides femtosecond pulses tunable from 780 nm to 850 nm at a repetition rate of 82 MHz. The FWHM pulse width was ~150 fs at this wavelength range as certified by the supplier. Femtosecond laser pulses were used because of their high peak power, which is necessary for the nonlinear optical processes to be efficient. To get resonance enhanced SHG signals, the sample was excited with the laser output tuned in the range of 790 to 810 nm where the second harmonic is in resonance with the absorption spectrum of the SH probe to be used in this thesis. The typical average laser power used in all the experiments was ~ 500 mW. A half wave plate (HWP) was used to fix the polarization of the fundamental laser light in the vertical plane. A 10 cm focal length convex lens was used to focus the fundamental laser beam into the sample cell holder. After excitation of the sample, the light (fundamental as well as the second harmonic) was detected at right angle geometry by a cooled Hamamatsu MCP-PMT using an Edinburgh Instruments TCSPC system (Model LifeSpec Red). To reject the fundamental light, a band pass filter and a monochromator was used. The monochromator slit width was adjusted for a wavelength resolution of 2 nm. The SH signal was integrated for one second by using the single photon counting module of the instrument.

A typical time versus SH intensity trace is shown in Figure 2.5. During the entire experiment the solution is constantly stirred with a magnetic stirrer and the sample temperature is controlled (± 0.5 ^{0}C) by a circulating water bath. The experiment is started by recording the SH signal of a 2 mL buffer solution placed in a 1 cm pathlength quartz cuvette. After addition of LDS^{+} ions to the buffer solution, the SH signal increases moderately due to HRS generated

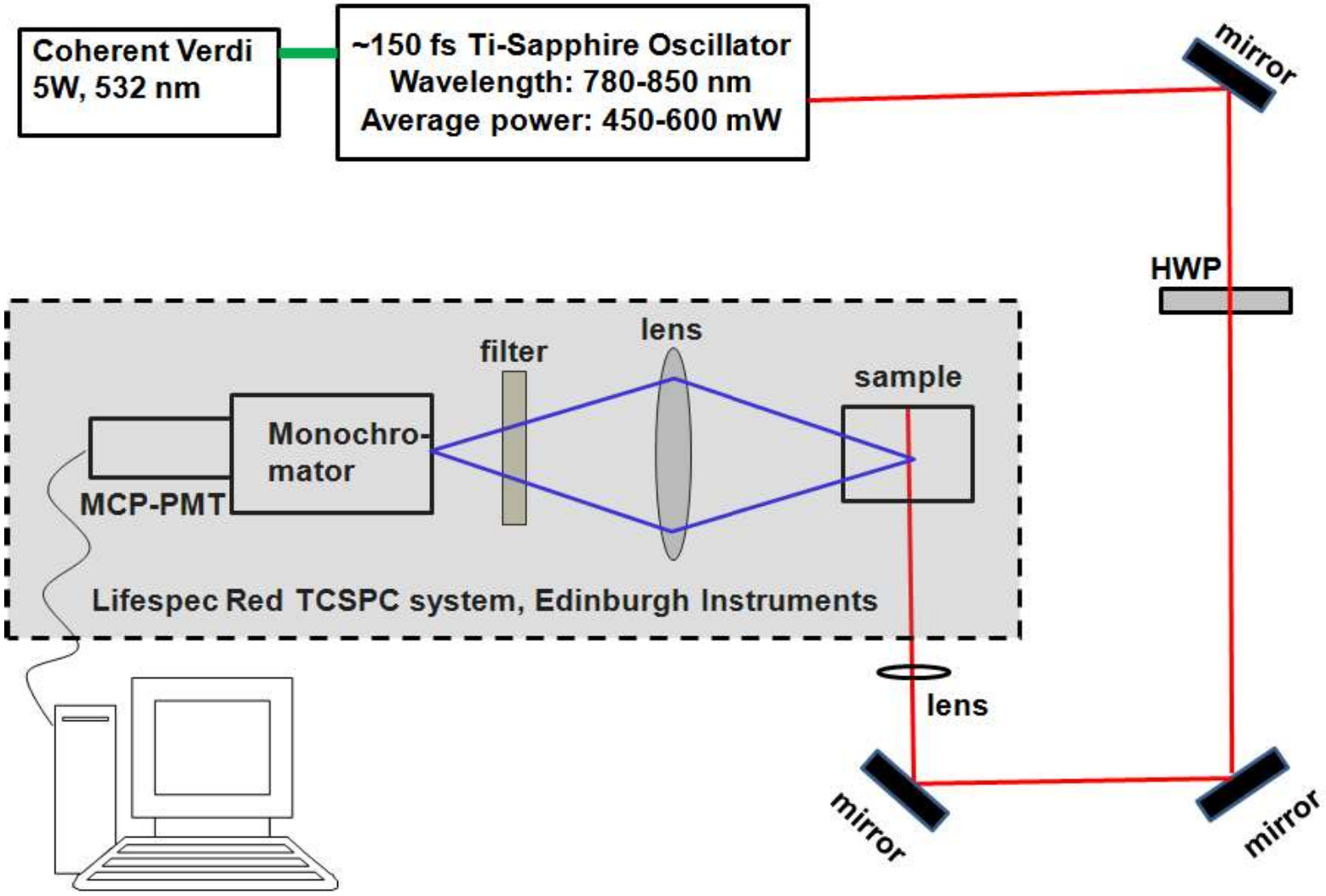

Figure2.4: *Schematic of the experimental set up used to measure HRS and SH signals.*

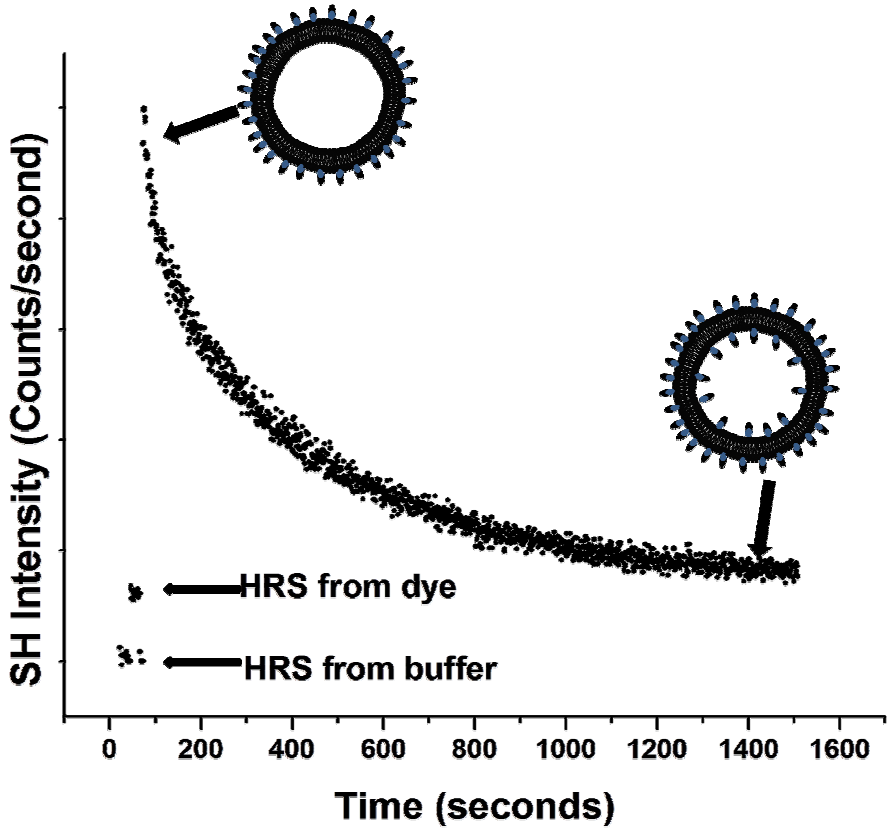

***Figure 2.5**: A typical SH decay showing how the molecular diffusion across a bilayer can be monitored in real time.*

by the LDS^+ ions. A further addition of POPG liposome into this solution results in an instantaneous (less than a second; where one second is the time resolution of this setup) increase of the SH signal due to the adsorption of the positively charged dye on the outer surface of the negatively charged liposome. With time, the SH signal decreases in an exponential fashion due to the transport of the dye from the outer to the inner bilayer. The experiment is stopped when the SH signal becomes invariant with time. The average transport time is then calculated by fitting the time dependent SH trace with exponential decay functions.

2.5 Spectroscopic characterization of the SH probe LDS^+ ion

Earlier SHG studies were done with the organic cation MG. One of the drawbacks of using MG cation is that it can be used only at acidic pH since at neutral pH, the molecule becomes neutral and loses its nonlinear characteristics. Since it is desirable to find a SH probe which can act over a wide range of pH we have searched for an alternative. It is known that hemicayanine dyes have strong hyperpolarizability values [29] and one member of this family LDS^+ ion has sufficient absorption at the SH wavelength of a Ti-Sapphire laser. This prompted us to test the suitability of LDS^+ ion as a SH probe. LDS^+ ion (perchlorate salt, from Exciton) was a gift from Prof. N. Sarkar and was used as received. The chemical structure of the LDS^+ ion is shown in Figure 2.6.

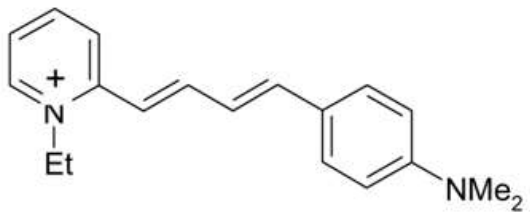

Figure 2.6: *Chemical structure of the LDS^+ ion*

The nonlinear properties (e.g. HRS) of LDS^+ ion in aqueous buffer solution at physiological pH were first investigated. The HRS characteristics of LDS^+ ion, against 840 nm laser excitation are shown in Figure 2.7. The HRS spectrum, linear relationship of the HRS intensity with LDS^+ ion concentration and the quadratic relationship of the HRS signal with the input laser power demonstrates that LDS^+ ion has reasonable nonlinear properties when excited with 840 nm femtosecond laser.

Then, we have used three different lipids and their combinations to determine which lipid or lipid mixture will bind more strongly with the dye and, consequently will give more SH signal. Figure 2.8 shows the typical time profile of the SH intensity before and after a liposome solution was injected into a LDS^+ ion solution. The initial constant signal level (after the first dotted line) is attributed to HRS originating from the dye (Figure 2.8). Immediately after the liposome solution was injected, an instantaneous increase (> 1s) in the SH signal intensity was observed. This indicates that adsorption of LDS^+ ion molecules onto the outer surface of the liposome bilayer is faster than our time resolution (1s) as well as the mixing process, which is limited by the injection time. Following the initial increase of the SHG signal, there is a decrease due to transport of the dye molecules across the liposome bilayers and adsorbing at the inner surface with an orientation opposite to that at the outer surface. The Y-axis ranges in Figure 2.8 are deliberately kept similar to show how the relative intensity of the generated SH signal depends upon the lipid composition. POPG liposomes were observed to generate the largest and POPC liposomes generate the least SH signal. Liposomes made from a 50: 50 (mol: mol) mixture of POPG/POPS and POPG/POPC were also able to generate a measurable SH signal. Our results demonstrate that the more negatively charged head group of the liposome, the larger was the extent of the adsorption giving rise to a larger SH signal.

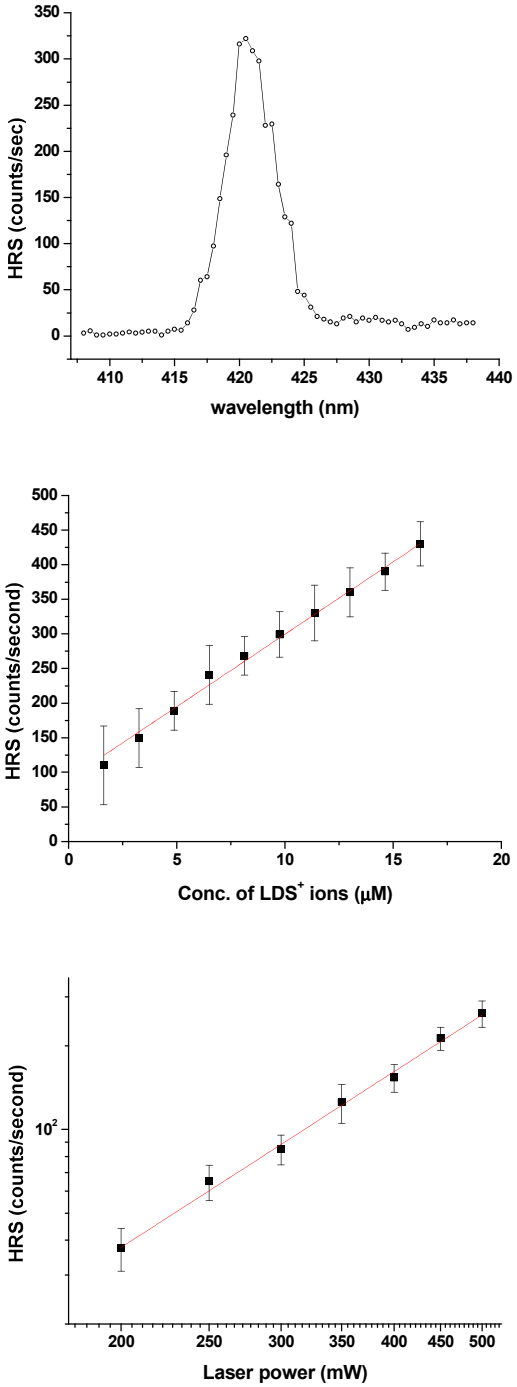

Figure 2.7: *HRS characteristics of LDS^+ ion in aqueous buffer solution at pH 7.4. Input laser power: 550 mW; wavelength: 840 nm. Top: Spectrum of the HRS signal (dye concentration 10 μM). Middle: Linear variation of HRS intensity with dye concentration. Bottom: The Quadratic variation of HRS intensity with input laser power (dye concentration 10 μM).*

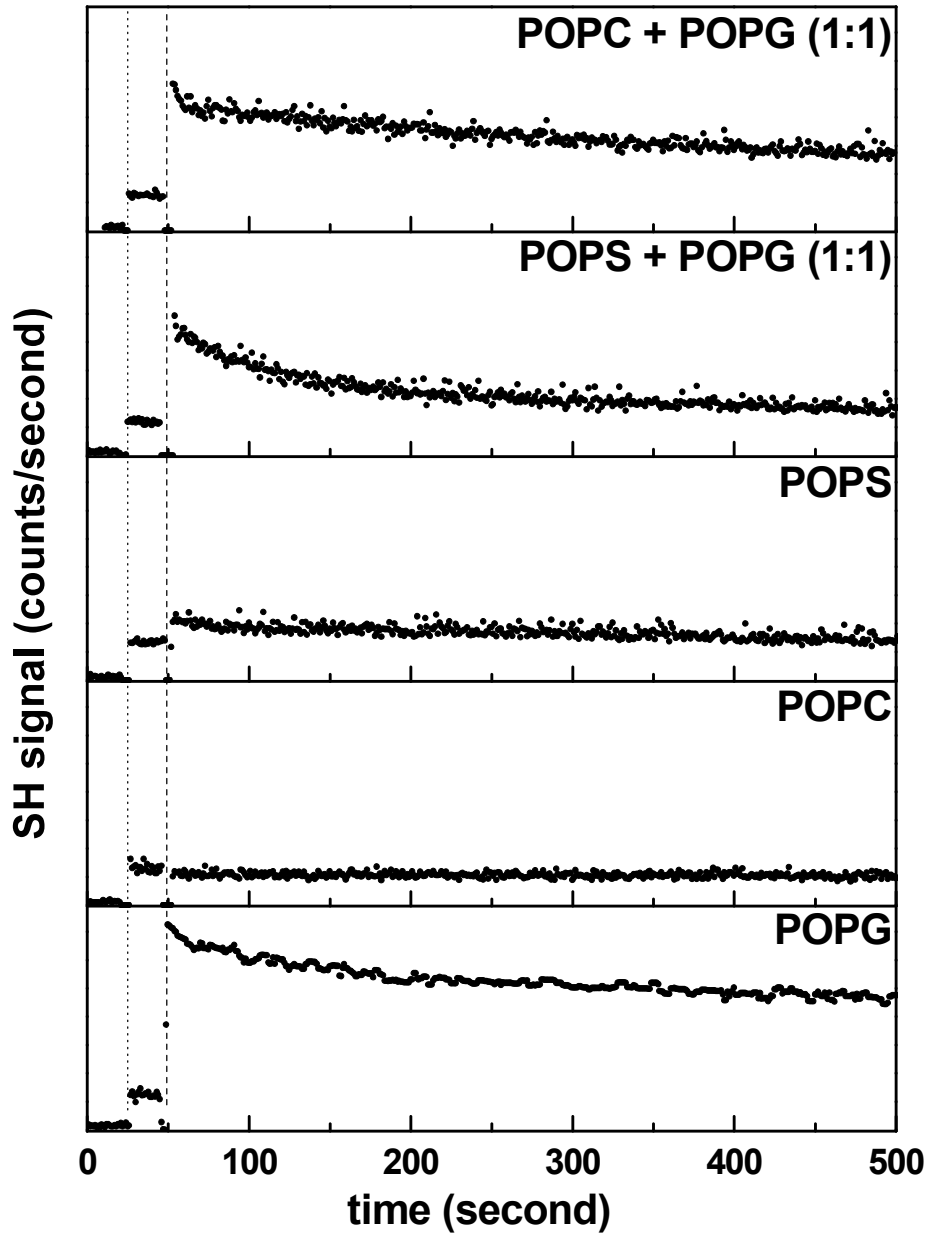

Figure 2.8: *Time dependence of SH signals observed from 6.5 μM LDS^+ ion and in presence of different types of liposomes (12.5 mM in lipid) in aqueous buffer solution at pH 7.4. The dotted line indicates addition of dye and the dashed line indicates addition of liposomes. The Y-axis in all cases spans from 10 to 1700.*

After observing that POPG liposomes gives the maximum SHG signal we have used this liposome as the model membrane system to explore the transport characteristics of the dye. The absorption and emission characteristics of the dye changes significantly in the presence of POPG liposomes (Figure 2.9) which provide further evidence that electrostatic interaction between positively charged LDS^+ ion and the anionic head group of liposomes are primarily responsible for dye adsorption onto the liposomes.

Finally, we have checked the pH range where LDS^+ ion can be used as a SH probe. The electron donor group of the LDS^+ ion, (i.e. the $–N(Me)_2$ group) is susceptible to protonation at acidic pH which would result in loss of electron delocalization thereby reducing its SH signal. Therefore an estimation of the pK_a value for this group was necessary to determine the pH range at which the dye can act as a SH probe. Figure 2.10 describes the absorption spectra of LDS^+ ion over a wide range of pH. The absorption peak of LDS^+ ion at 440 nm starts to decrease in intensity as the pH approaches 5.0 and at pH 3 a new peak appears at 360 nm. These changes in the absorption spectra are attributed to the protonation of the $–N(Me)_2$ group of the dye which results in absorption at higher energy due to loss of electron delocalization. From the plot of the absorbance ratio at 440 and 360 nm versus pH, the pK_a value of the $–N(Me)_2$ group was estimated at 4.3. Therefore, the lower limit of the pH for carrying out the transport of the dye across POPG liposomes was set at pH 4.0. We have recorded the decay characteristics of the SH electric field of LDS^+ ion after addition of POPG liposomes in the pH range of 4.0 to 8.0 which is shown in Figure 2.11. The corresponding fitted parameters; transport time constant (τ_{av}) and N_{in}/N_{out} ratio are provided in Table 2.5. Since the pK_a of the donor group of LDS^+ ion ($-NMe_2$) is at 4.3, the population of LDS^+ ion is roughly 33% and 83% at pH 4.0 and 5.0 respectively. The N_{in}/N_{out} ratio and τ_{av} values at pH 4.0 and 5.0, obtained from the observed $E_{2\omega}$ signal (which arises exclusively due to the the LDS^+ ion) reflects the effect of changing populations of the LDS^+ ion.

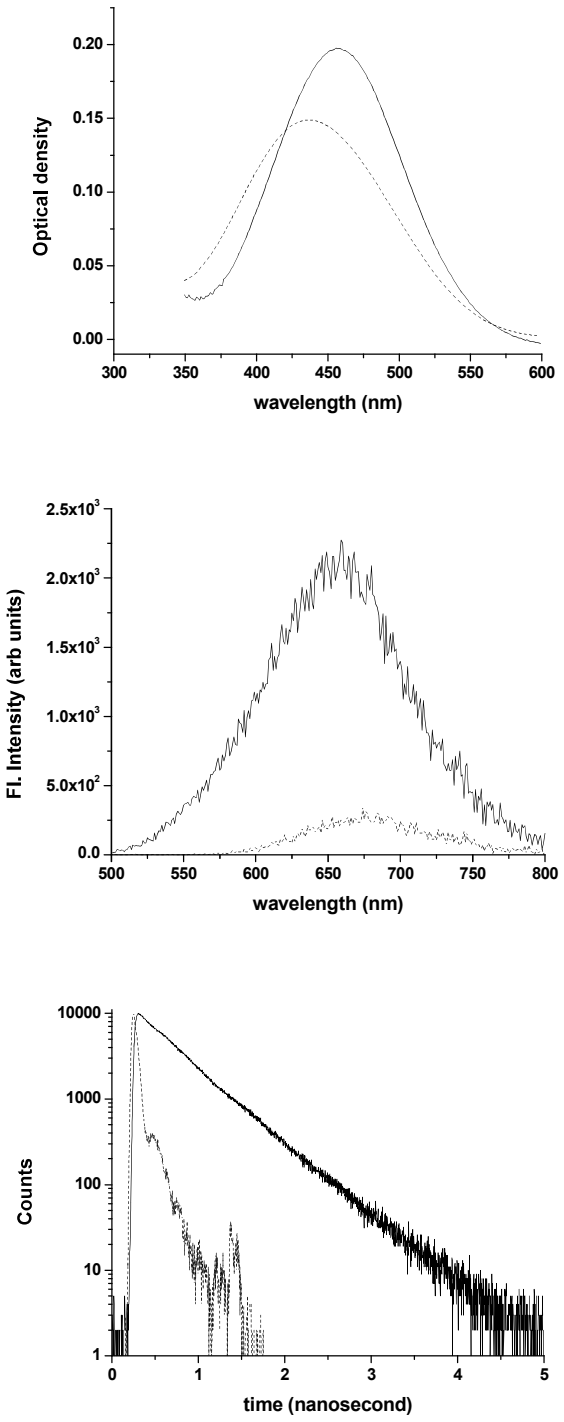

Figure 2.9: *Absorption (top), emission (middle) and fluorescence lifetime (bottom) of LDS^+ ion (2μM) in buffer (dotted) and buffer containing POPG liposomes (λ_{ex}= 420 nm) indicating interaction between dye and liposome.*

In addition, the transport of the cation was observed to be faster with increasing pH. The N_{in}/N_{out} value approaches ~0.90 as the pH of the medium is increased to 8.0. This roughly corresponds to the ratio of the area of the inner leaflet to the outer leaflet for the POPG liposomes, (size ~200 nm and bilayer thickness ~5 nm) which indicates the completion of the transport process.

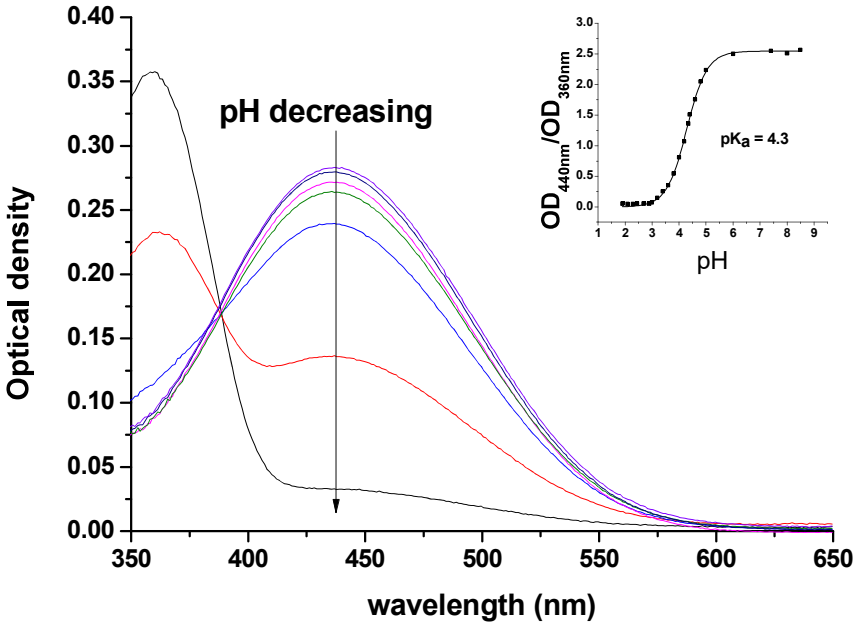

Figure 2.10: *Effect of pH on the absorption spectra of LDS^+ ion (2.5 µM). The pH values are 8.5, 8.0, 7.4, 6.0, 5.0, 4.0 and 3.0. Inset: Plot of the ratio of absorbance values of the dye at 440 and 360 nm at different pH. The inflection point obtained from the sigmoidal fit gave a pK_a of 4.3 for the $–N(Me)_2$ group.*

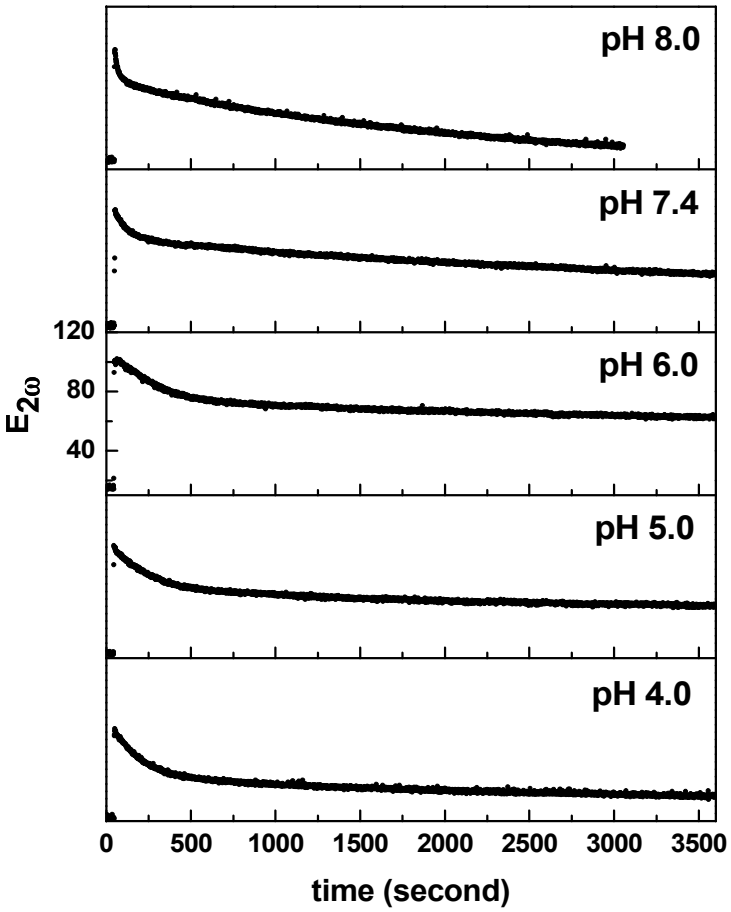

Figure 2.11: *Effect of pH on the SH electric field ($E_{2\omega}$) of 5 μM LDS^+ ion before and after addition of 50 μM POPG liposomes at 25 °C. The Y axes are similar and hence shown only for one panel.*

Table 2.5: *Fitted parameters obtained after exponential fitting of the SH electric field of LDS^+ ion after addition of POPG liposomes in the pH range of 4.0 to 8.0*

pH	a_0	a_1	τ_1	a_2	τ_2	τ_{av}	N_{in}/N_{out}
4.0	0.32	0.42	170	0.26	2600	750	0.68
5.0	0.45	0.37	199	0.18	2220	464	0.55
6.0	0.42	0.34	242	0.24	6752	1713	0.58
7.4	0.34	0.30	79	0.36	3470	1280	0.66
8.0	0.14	0.22	54	0.64	2120	1379	0.86

References

1. Peret-Almeida, L.; Cherubino, A. P. F.; Alves, R. J.; Dufosse, L.; Gloria, M. B. A. *Food Res. Int*. **2005**, *38*, 1039−1044
2. Adhikary, R.; Mukherjee, P.; Kee, T. W.; Petrich, J. W. J. *Phys. Chem. B* **2009**, *113*, 5255−5261; Adhikary, R.; Carlson, P. J.; Kee, T. W.; Petrich, J. W. *J. Phys. Chem. B* **2010**, *114*, 2997−3004
3. Moscho, A.; Orwar, O.; Chiu, D. T.; Modi, B. P.; Zare, R. N. *Proc Natl Acad sci USA* **1996,** 93, 11443−11447.
4. Tardi, P. G.; Boman, N. L.; Cullis, P. R. *J. of Drug Targeting* **1996,** *4*, 129−140.
5. Haskell, R. J. *J. Pharm. Sci.* **1998**, *87*, 125−129.
6. Hunter, R. J. *Zeta potential in Colloids Science: Principles and Applications*, Academic Press, UK, 1**988**.
7. Shaw, D. J. *Introduction to Colloidal and Surface Chemistry*, Butterworth Heinemann, UK, **1992**.
8. Rohatgi-Mukherjee, K. K. *Fundamentals of Photochemistry*; Wiley Eastern Ltd: India, **1986**.
9. Lackowicz, J. R. *Principles of fluorescence spectroscopy*, 3rd ed.; Springer; New York, **2006**.
10. Birks, J. B. *Photo Physics of Aromatic Molecules*; Wiley-Interscience: New York, **1970**.
11. Gilbert, A; Baggott, J.; Wagner, P. J. *Essential of Molecular Photochemistry*; Blackwell Science Inc.: Cambridge, USA, **1991**.
12. Sauer, M.; Hofkens, J.; Enderlein, J. *Handbook of Fluorescence Spectroscopy and Imaging*, WILEY-VCH Verlag GmbH & Co. KGaA, Weinheim, **2011**.
13. O'Connor, D. V.; Phillips, D. *Time-Correlated Single-Photon Counting*; Academic Press: London, **1984**.

14. Förster, T. *Ann. Phys.* **1948**, *2*, 55-75.

15. Stryer, L.; Haugland, P. R. *Proc. Natl. Acad. Sci.* **1967**, *58*, 719−726.

16. Matyus, L. J. *Photochem. Photobiol. B* **1992**, 12, 323−337.

17. Bottiroli, G.; Croce, A. C.; Ramponi, R. *J. Photochem. Photobiol. B* **1992**, *12,* 413−416.

18. Stryer, L.; Thomas, D. D.; Meares, C. F. *Annu. Rev. Biophys. Bioeng.* **1982**, *11*, 203−222.

19. Heman, B. *Methods Cell Biol.* **1989**, *30*, 219−243.

20. Jovin, T. M.; Arndt-Jovin, D. J. *Annu. Rev. Biophys. Biophys. Chem.* **1889**, *18*, 271−308.

21. Matayoshi, E. D.; Wang, G. T.; Krafft, G. A.; Ericson, J. *J. Science* **1990**, *247,* 954−958.

22. Taylor, D. L.; Reidler, J.; Spudich, J. A.; Stryer, L. *J. Cell Biol.* **1981**, *89*, 362−367.

23. Ito, N.; Arzhantesv, S.; Heitz, M.; Maroncelli, M. J. *J. Phys. Chem. B.* **2004**, *108*, 5771−5777.

24. Mukherjee, P.; Crank, J. A.; Sharma, P. S.; Wijeratne, A. B.; Adhikary, R.; Bose, S.; Armstrong, .; D. W.; Petrich, J. W. *J. Phys. Chem. B* **2008**, *112*, 3390−3396.

25. Ingram, J. A.; Moog, R. S.; Ito, N.; Diswas, R.; Marcincelli, M. J. *J. Phys. Chem. B* **2003**, *107*, 5926−5932.

26. Ito, N.; Arzhanstev, S.; Maroncelli, M. *Chem. Phys. Lett.* **2004**, *396,* 83−91.

27. Adhikary, R.; Bose, S.; Mukherjee, P.; Thite, A.; Kraus, G. A.; Wijeratne, A. B.; Sharma, P.; Armstrong, D. W.; Petrich, J. W. *J. Phys. Chem. B.* **2008**, *112*, 7555−7559.

28. Jablonski, A. *Bull. I'Acad. Pol. Sci. Ser. A.* **1960**, *8*, 259.

29. Duan, X. M.; Konami, H.; Okada, S.; Oikawa, H.; Matsuda, H.; Nakanishi, H. *J. Phys. Chem*. **1996**, *100*, 17780−17785. Ashwell, G. J.; Jackson, P. D.; Crossland, W. A. *Nature*, **1994**, *368*, 438−440. Kim, O. K.; Choi, L. S.; Zhang, H. Y.; He, X. H.; Shih, Y. H. *J. Am. Chem. Soc*. **1996**, *118*, 12220−12221. Xu, J.; Lu, X.; Zhou, G.; Zhang, Z. *Thin Solid Films* **1998**, *312*, 295−299.

Chapter 3

Effect of curcumin on the transport kinetics of a Hemicyanine dye, LDS^+ ions across a lipid bilayer probed by second harmonic spectroscopy

3.1. Introduction

The medicinal pigment curcumin shows a wide variety of biological effects which includes antioxidant, antiangiogenic, anticancerigenic, and wound-healing capacities [1]. Curcumin has a great affinity for biological membranes and has been shown to alter their properties [2-7]. It might thus be tempting to speculate that many of its biological activity may arise from its effect on the membrane structure. Second harmonic generation (SHG) spectroscopy has been demonstrated to probe various surfaces and interfaces at length scales of few nanometer [8]. In addition, the SHG technique has been used to monitor the transport kinetics of certain molecules across a model membrane in real time [9]. The capability of this technique has first been demonstrated using an organic cation Malachite Green [9-14] (MG) and later an organic anion chlorin-p_6 [15].

The transport kinetics of a molecule across a lipid bilayer can be monitored by the SHG technique provided it possesses a reasonable hyperpolarizability value at the excitation wavelength. In chapter 2 we have demonstrated that LDS^+ ions can be used successfully as a SH probe over a wide pH range. In this study we have used LDS^+ ions as a SH probe to investigate the effect of curcumin on the permeability of a bilayer constituted from POPG lipids.

3.2. Results

Hyper-Rayleigh Scattering (HRS) and SH measurements were performed as described in Chapter 2. SHG experiments were done as follows: First the signal from 2 mL of buffer was recorded followed by addition of micro-liter aliquots from a concentrated LDS^+ ions stock solution and finally 100 μL of liposome solution was added. The final concentration of LDS^+ ion and lipid was 6.5 and 13.6 μM respectively. For experiments involving curcumin, micro-liter aliquots from a concentrated stock solution of curcumin (1 mM) was added to the liposome solution and incubated for few minutes. The liposomal curcumin solution (100 μL) was then added to 2 mL buffer solution containing LDS^+ ions.

The time dependent decay of the second harmonic field $E_{2\omega}$ after addition of POPG liposomes to a solution of LDS^+ ions at pH 7.4 over a period of one hour is shown in Figure 3.1. Single and double exponential fits of the data are also shown from which it is evident that double exponential fit is better. Two significantly different decay times were obtained; the short (50s) time constant was similar to that observed earlier for MG cation and a long (1550s) time constant which was also observed for higher MG concentrations [11]. The decay was consistently observed to be bi-exponential over a wide range (1-10 μM) of dye concentration (data not shown). As observed in earlier studies [9-14], a notable feature of the decay kinetics is the observation that the SHG signal levels off at a value that is significantly greater than zero (corresponding to the term A_0 in the exponential fitting equation). This has been attributed to the finite population difference in the dye molecules adsorbed on the outer and inner surface of the liposome. The ratio of this population difference (in terms of N_i/N_o i.e. No. of dye molecules at the inner surface/No. of dye molecules at the outer surface) is equal to $1-A_0$ (when sum of all the pre-exponential factors are equal to unity). It is to be noted that the maximum value of N_i/N_o is ~0.9 for liposomes of diameter ~100 nm [10-14] and the

minimum value is zero which points to the case when there is no transport to the inner surface of the bilayer.

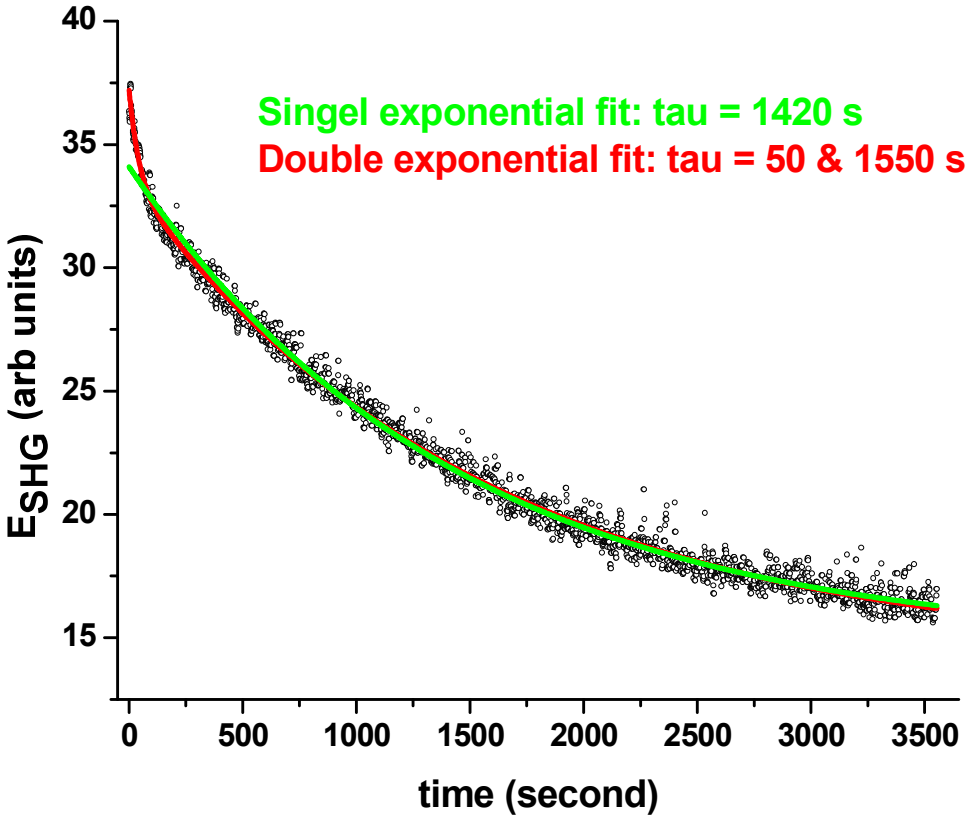

Figure 3.1: *Single and double exponential fitting of SH electric field observed from 6.5 µM* LDS^+ ions *after addition of POPG liposomes in aqueous buffer solution at pH 7.4.*

The effect of increasing the bilayer rigidity on the transport kinetics and the N_i/N_o ratio of the dye in POPG liposomes was also investigated (Figure 3.2 and 3.3). For this purpose bilayer rigidity is changed by incorporating Cholesterol (50 mol %) and changing the temperature. The decays of $E_{2\omega}$ at different temperatures with and without Cholesterol are shown in Figure 3.2. It can be seen from Figure 3.2 and 3.3 that cholesterol and temperature significantly affect the transport kinetics and the N_i/N_o ratio.

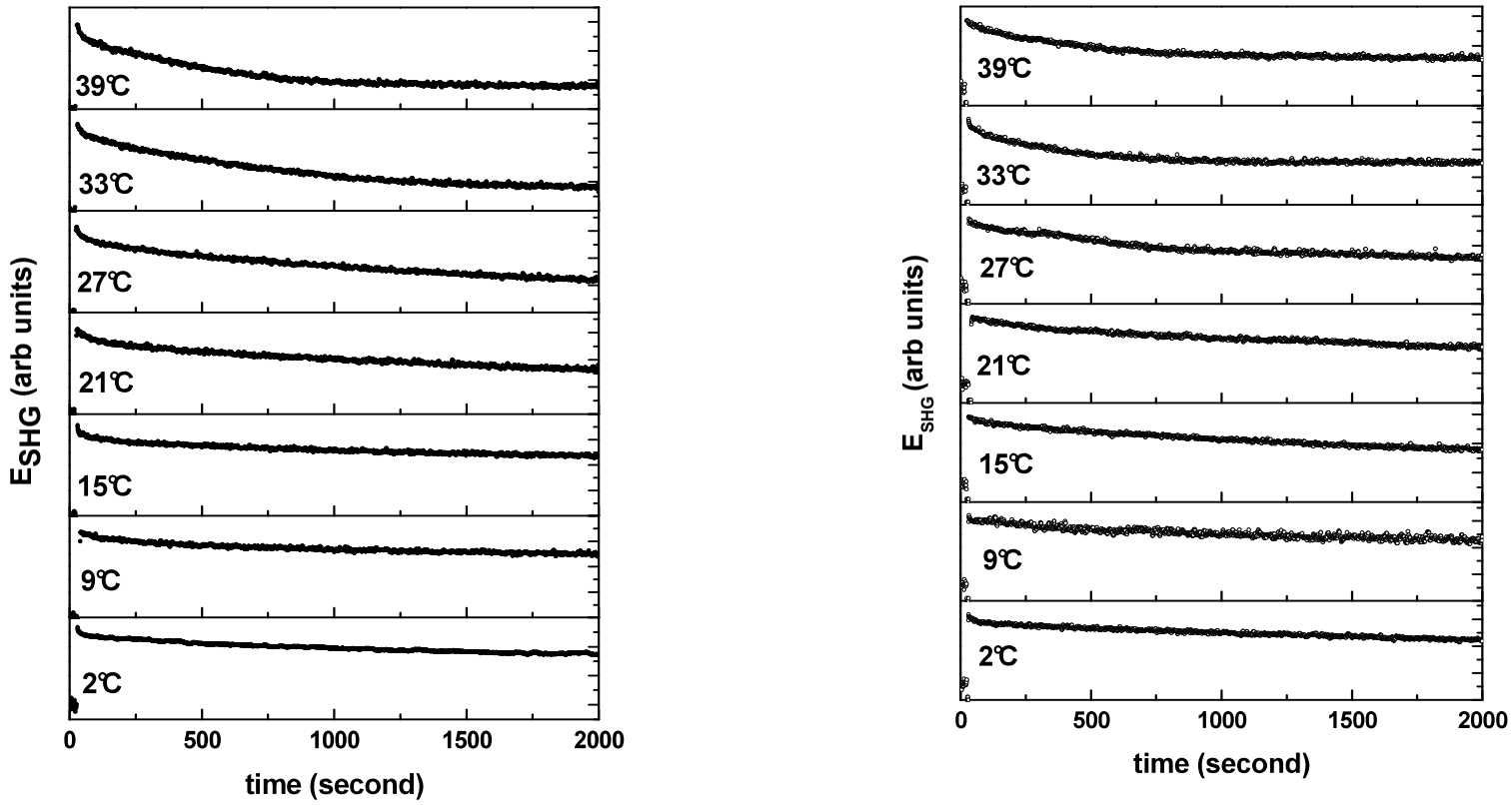

Figure 3.2: *Decays of SH electric field observed from 6.5 μM LDS^+ ions after addition of POPG liposomes (13.6 μM in lipid, left) & POPG liposomes (containing 50 mol % Cholesterol; 13.6 μM in lipid, right) at different temperatures.*

Although all the decays are recorded in a 2000s time window it is evident from Figure 3.2 that this time window is still not sufficient enough to capture the entire kinetics and hence the fitted time constants have little significance. Nevertheless the N_i/N_o ratio will give a qualitative idea about the transport of the dye in this time scale. A plot of the N_i/N_o ratio is shown in Figure 3.3. The N_i/N_o ratio starts to differ after 15 °C and at 40 °C it can be concluded that ~70% LDS^+ ions have diffused across the barrier compared to ~50% in the presence of 50 mol % Cholesterol.

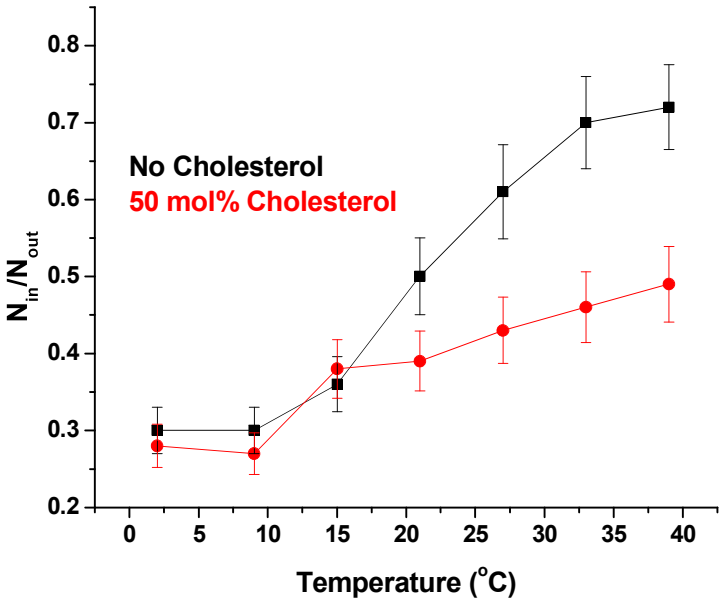

Figure 3.3: *The corresponding N_i/N_o ratio calculated from the data shown in Figure 3.2*

The effect of liposomal curcumin on the transport kinetics of the dye in POPG liposomes are shown in Figure 3.4. There is a drastic change in the decay of the SH field, it being much faster in the presence of 1.33 µM curcumin (which corresponds to ~ 0.1 molecule of curcumin per lipid; pure POPG or 50:50 POPG:Cholesterol) at all conditions room temperature or low temperature, POPG lipids with or without cholesterol.

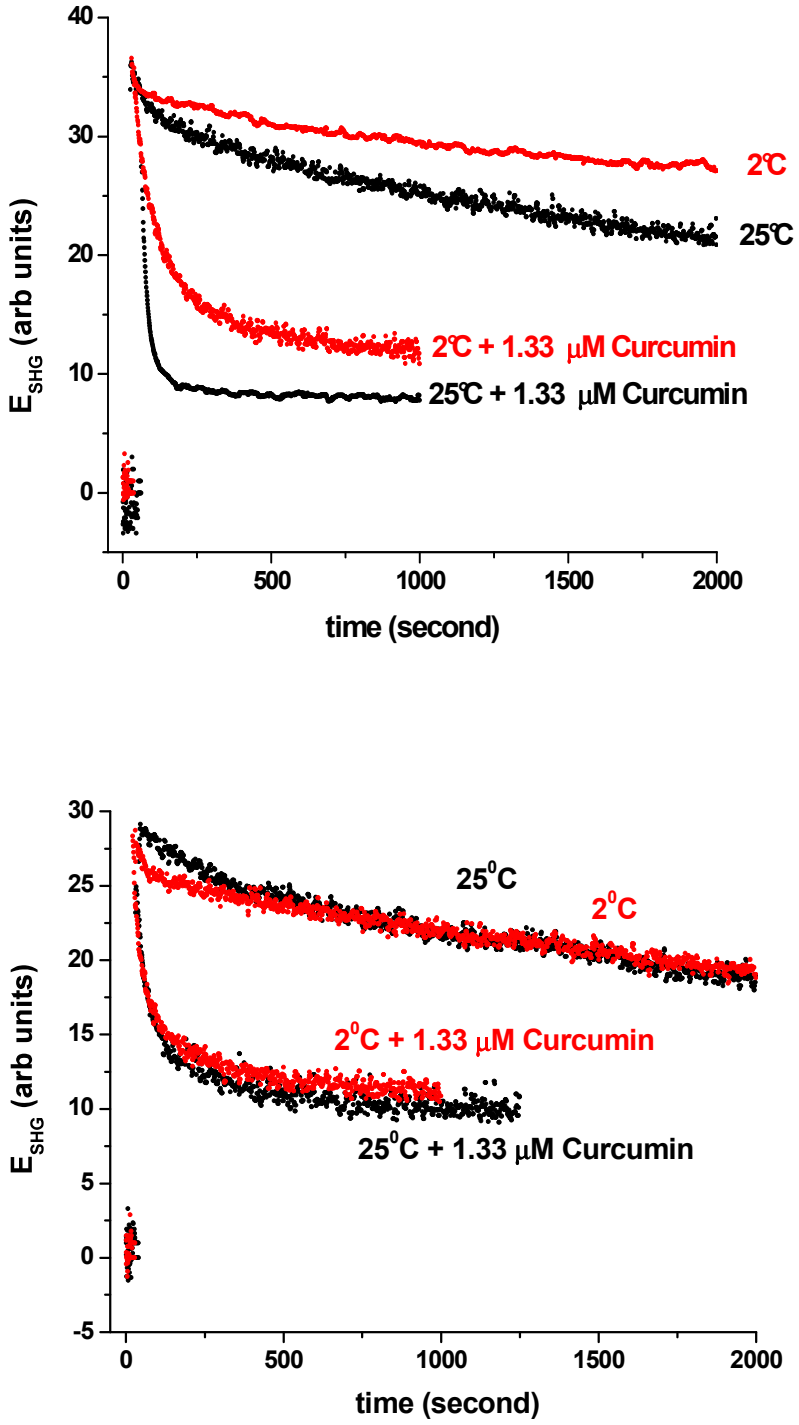

Figure 3.4: *Effect of curcumin: Decays of SH electric field observed from 6.5 μM LDS^+ ions after addition of POPG liposomes (top) and Cholesterol-POPG liposomes (bottom) containing 1.33 μM curcumin in aqueous buffer solution at pH 7.4 at low (2 °C, red curve) and room temperature (25 °C, black curve).*

The changes in the transport time constants and the N_i/N_o ratio for different curcumin content are shown in Figure 3.5 and summarized in Table 3.1. At room temperature, the average transport time of LDS^+ ions changes from 780s to 29s in POPG liposomes containing 1.33 μM curcumin, a ~27 times decrease with increase in the N_i/N_o ratio from 0.60 to 0.71.

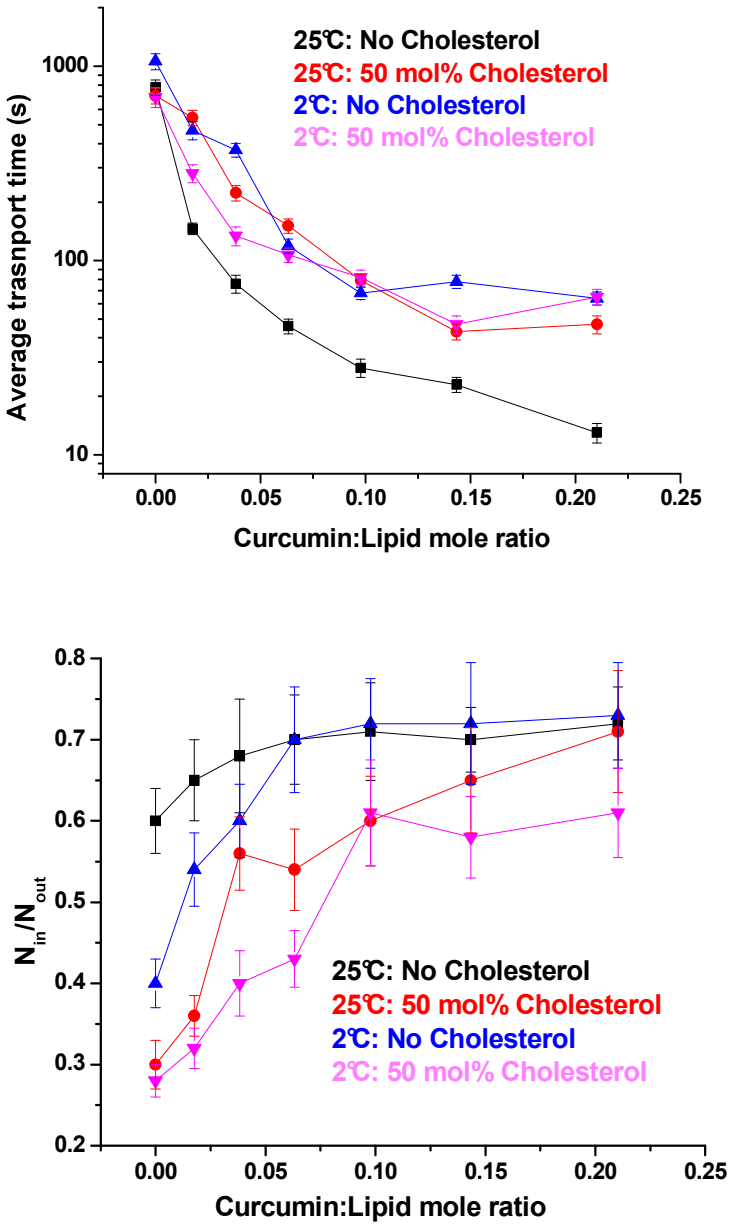

Figure 3.5: *Transport time constants of LDS^+ ions in various conditions with varying amount of curcumin (upper figure) and corresponding N_i/N_o ratio (lower figure).*

Table 3.1: *Transport time constants of LDS^+ ions (6.5 μM) in presence of curcumin obtained from the decay of SH electric field*[a]

Curcumin:Lipid[b]	$\tau_1(a_1)$	$\tau_2(a_2)$	A_0	τ_{av}	N_{in}/N_{out}
POPG liposome: Temperature 25 °C					
0.0 (0)	50(10%)	1550(50%)	40%	780	0.60
0.02 (0.24)	35 (19%)	270 (46%)	35%	131	0.65
0.04 (0.52)	30 (25%)	160 (43%)	32%	76	0.68
0.06 (0.86)	30 (62%)	230 (12%)	30%	46	0.70
0.10 (1.33)	20 (65%)	160 (10%)	29%	29	0.71
0.14 (1.95)	17 (63%)	170 (7%)	30%	23	0.70
0.21 (2.86)	10 (65%)	100 (7%)	28%	14	0.72
POPG liposome: Temperature 2 °C					
0.0 (0)	65(8%)	3180(22%)	70%	705	0.30
0.02 (0.24)	20(11%)	1260(43%)	46%	544	0.54
0.04 (0.52)	50(14%)	470(46%)	40%	223	0.60
0.06 (0.86)	40(26%)	320(44%)	30%	151	0.70
0.10 (1.33)	40(44%)	220(28%)	28%	79	0.72
0.14 (1.95)	35(58%)	160(14%)	28%	43	0.72
0.21 (2.86)	35(63%)	250(10%)	27%	47	0.73
50:50 (mol%) Cholesterol-POPG liposome: Temperature 25 °C					
0.0 (0)	--	1060(30%)	70%	1060	0.30
0.02 (0.24)	40(9%)	1360(27%)	64%	371	0.36
0.04 (0.52)	160(26%)	1420(30%)	44%	468	0.56
0.06 (0.86)	70(36%)	470(20%)	46%	119	0.54
0.10 (1.33)	30(40%)	280(20%)	40%	68	0.60
0.14 (1.95)	20(52%)	520(13%)	35%	78	0.65
0.21 (2.86)	10(50%)	280(21%)	29%	64	0.71
50:50 (mol%) Cholesterol-POPG liposome: Temperature 2 °C					
0.0 (0)	60(8%)	3200(21%)	71%	695	0.29
0.02 (0.24)	80(14%)	1500(18%)	68%	281	0.32
0.04 (0.52)	90(12%)	440(28%)	60%	134	0.40
0.06 (0.86)	95(17%)	350(26%)	57%	107	0.43
0.10 (1.33)	25(39%)	220(33%)	39%	82	0.61
0.14 (1.95)	20(42%)	240(16%)	42%	47	0.58
0.21 (2.86)	20(45%)	350(16%)	39%	65	0.61

[a]*The observed time constants (τ_i) are in seconds and the values in parentheses (a_i) represents corresponding pre-exponential factors. The errors in τ_i, a_i and N_{in}/N_{out} ratio are estimated to be about 10% based on experiments performed on three different liposome samples.*

[b]*The numbers represents the mole:mole ratio and the values in parentheses correspond to molar concentrations of curcumin.*

At the highest curcumin concentration used in this study, 2.86 µM, (corresponding to ~ 0.2 molecules of curcumin per lipid) the transport time of LDS-698 decreases by a factor of ~56 times. For other cases (POPG liposomes at 2 °C or POPG liposomes containing Cholesterol at 25 °C and 2 °C) the amount of decrease cannot be compared quantitatively as estimation of the transport time without curcumin is not accurate with a time window of 2000s.

Finally, it would be interesting to know the effect of other lipophilic molecules present in the bilayer on the transport kinetics of LDS^+ ions. For this purpose we choose two well known lipophilic molecules DPH and Nile Red. Figure 3.6 compares the effect of DPH, Nile Red and curcumin incorporated in the bilayer of POPG liposomes on the transport kinetics of LDS^+ ions.

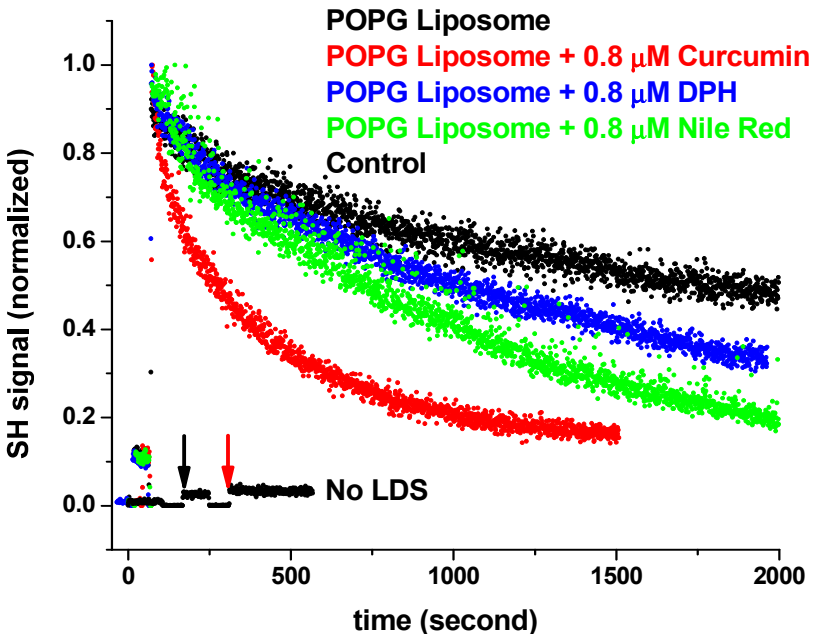

Figure 3.6: *Control experiments: Normalized decays of SH signal of 6.5 µM* LDS^+ ions *after addition of POPG liposomes (black) and POPG liposomes containing ~0.8 µM curcumin (red); ~0.8 µM DPH (blue) and ~0.8 µM Nile Red (green). Also shown is the signal from only liposomes (added at the black arrow) and liposomes containing 3.0 µM curcumin (added at the red arrow).*

The decays of the SH signal of LDS^+ ions becomes faster when DPH and Nile Red (0.8 μM each) are present in the bilayer, but when compared to similar concentrations of liposomal curcumin, their effect is, clearly, less pronounced. In addition we also show that SH signal from only POPG liposomes and POPG liposomes containing 3 μM curcumin (or, 3 μM DPH or NR, data not shown) is insignificant thus ruling out any contribution in the SH signal from these lipophilic molecules.

3.3. Discussions

It has been proposed that lipophilic drugs may alter the physical properties of the membrane. An indirect proof of this hypothesis comes from the fact that alterations of membrane protein's activity have been detected in presence of several lipophilic drugs [16-20]. Studies on curcumin have shown that it affects a large number of unrelated membrane proteins [2]. To explain this it has been proposed that curcumin can regulate the action of membrane proteins indirectly by changing the physical properties of the membrane rather than direct binding to the protein [21]. Subsequently it has been demonstrated that curcumin is capable of altering the properties of model and cell membranes [2-7]. For example, it has been observed to disrupt biological membranes [3-4] (at high concentration), modulate bilayer material properties [2], has a thinning effect on membranes [5], and it exerts a strong effect on model membrane structure [6-7]. It is therefore expected that liposomal curcumin should also affect the transport of molecules across a model membrane.

To study the kinetics of transport in real time we have used the SHG method [9-15]. The SHG method is surface specific; SH signals arise only from the surface of the liposomes, signals from bulk are very weak and thus do not interfere. The hemicyanine dye (LDS^+ ions) is positively charged and hence it is expected that it will bind to negatively charged liposomes. The observed SH signal of the dye in presence of various liposomes having

different head groups (for details see Chapter 2, Figure 2.8) confirms that binding is indeed electrostatic. This is consistent with the results of a previous report where the effect of bilayer surface charge density on molecular adsorption and transport has been studied using a positively charged dye Malachite Green (MG) [11]. However, compared to Malachite Green [9-14] (transport time constant ~100s), the transport of LDS^+ ions across a PG bilayer is significantly slower (average transport time 780s, Table 3.1). Transport of a molecule across a lipid bilayer should depend upon its interaction with the polar and nonpolar part of the bilayer. Since the chemical structures of MG and LDS^+ ions are quiet different their interaction with the polar and nonpolar regions of the bilayer is expected to be different and consequently their observed transport times should also expected to be different. At this point it may be noted that very few studies have been reported on the transport characteristics of *different* dyes across a lipid barrier using the SHG technique and thus lacks sufficient data for a general interpretation of the observed transport times. Since the SH signals arise only from the dye molecules bound to the surface of the liposomes, it is necessary to have an estimate about the absolute surface coverage i.e. number of LDS^+ ions bound to one liposome. The absolute surface coverage can be estimated by measuring the electric field of the SH signal at long times (i.e. at equilibrium) at different dye concentrations [11]. Using malachite green as the SH probe and POPG liposomes, the absolute surface coverage were estimated to be $\sim 10^4$ dye molecules per liposome [11]. Although this experiment has not been done, it may be assumed that absolute surface coverage is similar here since the concentration ranges of the dye and liposomes used in this study were similar to that used earlier (except the fact that the dyes being positively charged, are different). Increasing the bilayer rigidity (by incorporation of Cholesterol or by changing temperature) slows down the transport: this has been observed earlier [11,15] and in this study also (Figure 3.2). At 2 °C, with or without Cholesterol, the SH decay is almost flat indicating that LDS^+ ions is adsorbed on the outer bilayer but unable

to diffuse to the inner bilayer in the 2000s time window. The temperature dependent variation in the N_{in}/N_{out} ratio observed in Cholesterol and non-Cholesterol containing POPG liposomes (Figure 3.3) shows that up to 15 °C the transport is similar in nature and then it starts to differ significantly owing to the extra rigidity of the bilayer provided by Cholesterol.

The transport times of the dye was observed to be markedly dependent on the amount of curcumin whose lipophilic nature has been established in a previous study [6]. In the presence of 2.86 μM curcumin (~0.2 molecule of curcumin per lipid molecule) the decrease in the transport time observed in PG liposomes at 25 °C is ~56 times. For similar amount of curcumin, the average transport time for LDS^+ ions increases from 14 to 65s (a ~5 times increase) when POPG liposomes at 25 °C are replaced by POPG liposomes containing Cholesterol at 2 °C. Thus, it shows that liposomal curcumin facilitates faster transport even when the bilayer rigidity has been enhanced by a combined effect of Cholesterol and low temperature. This is also reflected by the N_{in}/N_{out} ratio (Figure 3.5, lower figure) especially when the rigidity of the bilayer is increased. It is pertinent to note that earlier studies have shown that presence of Cholesterol prevents peptide-induced membrane disruption by increasing the cohesion and stiffness of the lipid bilayer membrane [22]. The transport kinetics of MG across a membrane in presence of an ionophore gramicidin A (gA) were studied earlier. The kinetics observed were significantly faster in presence of gA which has been attributed to the gA assisted transport of the other cations (Na^+, H_3O^+) present in the system. As a result the N_{in}/N_{out} ratio of MG almost doubled (0.4 to 0.8) in the presence of gA. However in this study, the N_{in}/N_{out} ratio changes from 0.6 to 0.7 in presence of curcumin indicating that it does not act as an ionophore. As stated earlier, lipophilic drugs are expected to alter the membrane properties. Experiments performed on DPH and Nile Red containing liposomes show that membrane altering properties of curcumin are far superior compared to these well known lipophilic molecules. In two recent studies the effect of curcumin on

membrane organization has been studied by a variety of techniques [6-7]. It has been concluded that curcumin is oriented in the bilayer with its main axis parallel to the acyl chains and interacting with the polar head groups of the lipid. The length of the curcumin molecule has been estimated to be about 16 A^0, which is comparable to the typical length of a lipid molecule [6, 23]. At higher concentrations (the one used in this study) it has been suggested that curcumin forms higher order oligomeric structures in the membrane that span the bilayer [6]. Thus the bilayer environment encountered by LDS^+ ions in the presence of curcumin is altered and is likely to be more polar than the one constituted by nonpolar methyelene ($-CH_2-$) units. This altered polarity is expected to make the transport process faster for the positively charged dye. However, it might be noted that same argument should also apply when DPH and Nile Red are present in the bilayer and consequently the transport of LDS^+ ions should be similar. It appears therefore that an important factor in this regard is how the modification of the bilayer environment depends upon the interaction between the lipophilic drug and the polar head group of the lipid. Compared to DPH, both Nile Red and curcumin has polar functional groups like keto and hydroxyl groups which might interact (say, hydrogen bonding) with the polar head group region of the lipid and consequently change the bilayer properties. Thus different lipophilic drugs might affect the bilayer differently and as a consequence, transport of molecules (cationic, in this case) may get affected remarkably which is clearly shown in this study. Finally, it would be interesting to use the SHG technique to study how membrane transport are affected in the presence of membrane active molecules like antimicrobial or amyloid pedtides, since NMR studies have shown that they siginificantly alter the membrane properties [24].

3.4. Conclusion

In conclusion, we have studied the kinetics of transport of the hemicyanine dye LDS^+ ions across POPG model membrane bilayers by the surface selective SHG technique. The transport is initiated by electrostatic adsorption of the dye to the outer surface of the liposomes and its time constant is affected by the rigidity of the bilayer. In presence of the liphophilic drug curcumin, the transport of LDS^+ ions is enhanced remarkably and gets only slightly affected by bilayer rigidity. Control experiments with other lipophilic molecules like DPH and Nile Red showed that this enhancement may depend upon the interaction of the lipophilic molecule with the polar head group region of the lipid which, consequently is expected to depend on the chemical structure of the lipophilic molecule.

References

1. Aggarwal, B. B.; Sundaram, C.; Malini, N.; Ichikawa, H. *In Molecular Targets and Therapeutic Uses of curcumin in Health and Disease*; Aggarwal, B. B., Surth, Y. J., Eds.; Springer: New York, 2007. Ruby, A. J.; Kuttan, G.; Babu, K. D.; Rajasekharan, K. N.; Kuttan, R.; *Cancer Lett*. **1995**, *94*, 79−83. Lantz, R. C.; Chen, G. J.; Solyom, A. M.; Jolad, S. D.; Timmermann, B. N.; *Phytomedicine* **2005**, *12*, 445−452. Goel, A.; Kannumakkara, A. B.; Aggarwal, B. B.; *Biochem. Pharamacol*. **2008**, *75*, 787−809. Shi, M.; Cai, Q.; Yao, L.; Mao, Y.; Ming, Y.; Ouyang, G.; *Cell Biol. Int***. 2006**, *30*, 221−226. Surh, Y.-J.; *Food Chem. Toxicol*. **2002**, *40*, 1091−1097. Joe, B.; Vijaykumar, M.; Lokesh, B. R.; *Crit. Rev. Food. Sci. Nutr*. **2004**, *44*, 97−111. Maheshwari, R. K.; Singh, A. K.; Gaddipati, J.; Srimal, R. C.; *Life Sci*. **2006**, *78*, 2081−2087. Anand, P.; Thomas, S. G.; Kunnumakkara, A. B.; Sundaram, C.; Harikumar, K. B.; Sung, B.; Tharakan, S. T.; Misra, K.; Priyadarsini, I. K.; Rajasekharan, K. N.; Aggarwal, B. B.; *Biochem. Pharmacol*. **2008**, *76*, 1590−1611.
2. Ingolfsson, H. I.; Koeppe, R. E.; Andersen, O. S. *Biochemistry* **2007**, *46*, 10384–10391.
3. Jaruga, E.; Salvioli, S.; Dobrucki, J.; Chrul, S.; Bandorowicz-Pikuła, J.; Sikora, E.; Franceschi, C.; Cossarizza, A.; Bartosz, G. *FEBS Lett*. **1998**, *433*, 287−293.
4. Jaruga, E.; Sokala, A.; Chrulb, S.; Bartosza, G. *Exp. Cell Res*. **1998**, *245*, 303.
5. Hung, W. C.; Chen, F. Y.; Lee, C. C.; Sun, Y.; Lee, M. T.; Huang, H. W. *Biophys. J.* **2008**, *94*, 4331−4338.
6. Barry, J.; Fritz, M.; Brender, J. R.; Smith, P. E.; Lee, D. K.; Ramamoorthy, A. *J. Am. Chem. Soc*. **2009**, *131*, 4490−4498.
7. Perez-Lara, A.; Ausili, A.; Aranda, F. J.; Godos, A.; Torrecillas, A.; Corbalan-Garcia, S.; Gomez-Fernandez, J. C. *J. Phys. Chem*. *B* **2010**, *114*, 9778–9786.
8. Eisenthal, K. B. *Chem. Rev*. **2006**, *106*, 1462−1477.
9. Srivastava, A.; Eisenthal, K. B. *Chem. Phys. Lett*. **1998**, *292*, 345−351.

10. Yan, E. C. Y.; Eisenthal, K. B. *Biophys. J*. **2000**, *79*, 898−903.

11. Liu, Y.; Yan, E. C. Y.; Eisenthal, K. B. *Biophys. J*. **2001**, *80*, 1004−1012.

12. Shang, X. M.; Liu, Y.; Yan, E.; Eisenthal, K. B. *J. Phys. Chem. B* **2001**, *105*, 12816−12822.

13. Liu, J.; Shang, X. M.; Pompano, R.; Eisenthal, K. B. *Faraday Discuss*. **2005**, *129*, 291−299.

14. Liu, J.; Subir, M.; Nguyen, K.; Eisenthal, K. B. *J. Phys. Chem. B* **2008**, *112*, 15263−15266.

15. Saini, R. K.; Gupta, P. K.; Das, K. *J. Phys. Chem B* **2012**, *116*, 4199−4205.

16. Oezdirekcan, S.; Nyholm, T. K. M.; Raja, M.; Rijkers, D. T. S.; Liskamp, R. M. J.; Killian, J. A. *Biophys. J*. **2008**, *94*, 1315–1325.

17. Adachi, S.; Nagao, T.; Ingolfsson, H. I.; Maxfield, F. R.; Andersen, O. S.; Kopelovich, L.; Weinstein, I. B. *Cancer Res*. **2007**, *67*, 6493−6501.

18. Lundbaek, J. A.; Birn, P.; Tape, S. E.; Toombes, G. E. S.; Sogaard, R.; Koeppe, R. E.; Gruner, S. M.; Hansen, A. J.; Andersen, O. S. *Mol. Pharmacol*. **2005**, *68*, 680–689.

19. Hwang, T. C.; Koeppe, R. E.; Andersen, O. S. *Biochemistry* **2003**, *42*, 13646–13658.

20. Lundbaek, J. A. *J. Gen. Physiol*. **2008**, *131*, 421–429.

21. Bilmen, J. G.; Khan, S. Z.; Javed, M. U. H.; Michelangeli, F. *Eur. J. Biochem*. **2001**, *268*, 6318–6327.

22. Ramamoorthy, A.; Lee, D-K.; Narasimhaswamy, T.; Nanga, R. P. R. *Biochim. et Biophys. Acta Biomembranes*. **2010**, *1798*, 223–227.; Brender, J. R.; McHenry, A. J.; Ramamoorthy, A. *Front. Immunol.* **2012**, *3*, 1-3. McHenry, A. J.; Sciacca, M. F. M.; Brender, J. R.; Ramamoorthy, A. *Biochim. et Biophys. Acta Biomembranes.* **2012**, *1818*, 3019–3024.

23. Parimita, S. P.; Ramshankar, Y. V.; Suresh, S.; Row, T. N. G. *Acta Crystallogr. Sect. E* **2007**, *63*, o860–o862.

24. Henzler Wildman, K. A.; Lee, D.-K.; Ramamoorthy, A. *Biochemistry* **2003**, *42*, 6545−6558. Ramamoorthy, A.; Thennarasu, S.; Lee, D-K.; Tan, A.; Maloyy, L. *Biophys. J.* **2006**, *91*, 206–216. Brender, J. R.; Lee, E. L.; Cavitt, M. A.; Gafni, A.; Steel, D. G.; Ramamoorthy, G. *J. Am. Chem. Soc.* **2008**, *130*, 6424–6429. Brender, J. R.; Hartman, K.; Gottler, L. M.; Cavitt, M. E.; Youngstrom, D. W.; Ramamoorthy, A. *Biophys. J.* **2009**, *97*, 2474–2483.

Chapter 4

A comparative study on the effect of curcumin and chlorin-p_6 on the transport of the LDS cation across a negatively charged POPG bilayer: Effect of pH

4.1 Introduction

The interaction between a drug and a lipid bilayer can alter several important biophysical properties of membranes such as the membrane potential, fluidity and permeability [1-15]. In the previous chapter we have observed that the transport (and hence membrane permeability) of LDS^+ ions across a POPG bilayer becomes significantly faster when curcumin is present in the bilayer by using the interface selective second harmonic spectroscopic technique [16]. Drug induced alteration in lipid membrane permeability are expected to depend on the chemical structure of the drug, and if the drug contains ionizable functional groups, the pH of the medium. In this work we have therefore attempted to compare the membrane permeability effect of curcumin and chlorin-p_6 (Cp_6: a porphyrin based photosensitizer) on POPG liposomes using LDS^+ ion as a probe over a pH range of 4.0 to 8.0 using the SH spectroscopic technique. Further, using fluorescently labeled POPG liposomes, steady state fluorescence resonance energy transfer (FRET) studies were conducted to find out the pH dependent bilayer localization of both the drugs. The results of SHG and FRET studies were used to get an idea about how the membrane permeability depends upon the position of the drug in the POPG bilayers. The chemical structures of chlorin-p_6 and DPH-PC used in this study are shown in Figure 4.1.

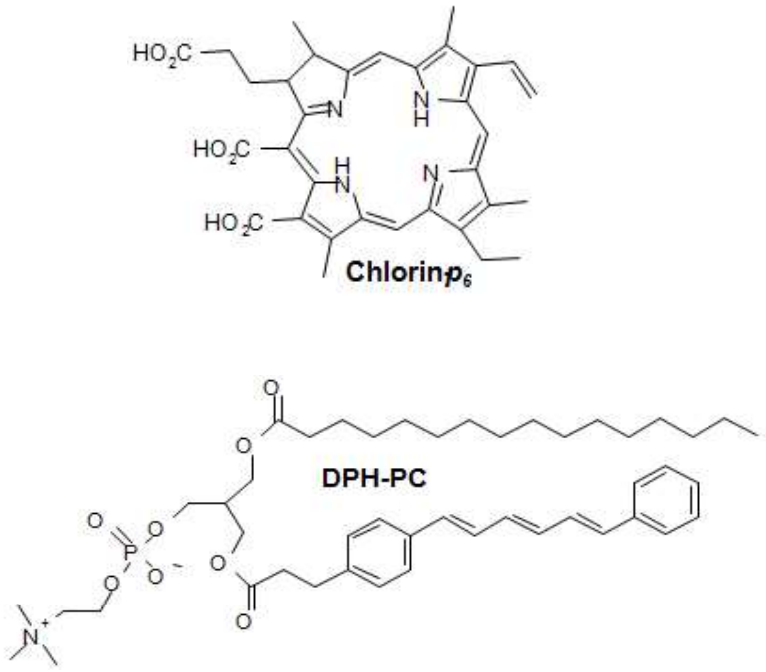

Figure 4.1: *Chemical structures of chlorin-p_6 (Cp_6), DPH-PC lipid.*

4.2 Results

The average laser power used in the SHG experiments was 600 mW. Micro-liter aliquot from a concentrated stock solution of curcumin was added to the liposome solution and incubated for few minutes for attaining equilibrium between the drug and the liposome. For Cp_6, following our previous study [17], the incubation time was kept at 30 minutes to ensure full equilibrium between the drug and the liposome. SH experiments were done as follows: First the signal from 2 mL of buffer containing 5 μM LDS^+ ions was recorded followed by addition of 50 μL of liposome (with/without drug) solution at 50 second time point. The time corresponding to liposome addition were denoted as t = 0 in all the figures. The concentration of lipid was kept at 50 μM and the concentration of both curcumin and Cp_6 were kept at 3 μM.

The lower limit of the pH for carrying out the transport of LDS^+ ions across POPG liposomes was set at pH 4.0 as discussed in chapter 2. Additionally, the upper limit of pH was fixed at 8.0 since several studies have showed that curcumin degrades near physiological pH [18-20]. Figure 4.2 describes the changes in SH electric field ($E_{2\omega}$) of LDS^+ ions (5 μM) before and after addition of POPG (50 μM) liposomes at different pH. Before the addition of liposomes the observed $E_{2\omega}$ is due to hyper-rayleigh scattering from the dye. Addition of liposomes produces an instantaneous increase of $E_{2\omega}$ due to adsorption of the cationic dye to the outer surface of the anionic headgroups of POPG lipids. Subsequently $E_{2\omega}$ decreases with time as LDS^+ ions transports from the outer to inner bilayer. The normalized $E_{2\omega}$ values ($E_{2\omega}$ values are normalized w.r.t. their maxima, i.e. immediately following liposome addition) are plotted for a reason that will be discussed later and also due to the fact that normalization provides a better clarity on the effect of pH as well as the drugs on the $E_{2\omega}$ characteristics of LDS^+ ions. The decays of $E_{2\omega}$ are fitted to exponential decay functions of the following form:

$$E_{2\omega}(t) = A_0 + \sum a_i \exp(-t/\tau_i) \qquad (4.1)$$

The observed decays of $E_{2\omega}$ were consistently observed to be bi-exponential and the fitting parameters are provided in Table 4.1.

The driving force for the transport of the LDS^+ ions from the outer to the inner bilayer of the POPG liposomes originates from the potential difference created between the outer and inner bilayer due to electrostatic adsorption of the LDS^+ ions on the outer bilayer surface [21-25]. The observed bi-exponential decays of $E_{2\omega}$ could arise due to initial rapid transport of the cation from the outer bilayer to the inner bilayer (~100 seconds, Table 4.1) and as the inner bilayer gets populated with the LDS^+ ions the potential difference decreases causing the transport rate of the LDS^+ ions to be slower (~1000 seconds, Table 4.1).

As observed earlier [22-25] a notable feature of the decay characteristics of $E_{2\omega}$ is the observation that it levels off at a value that is significantly greater than zero (corresponding to

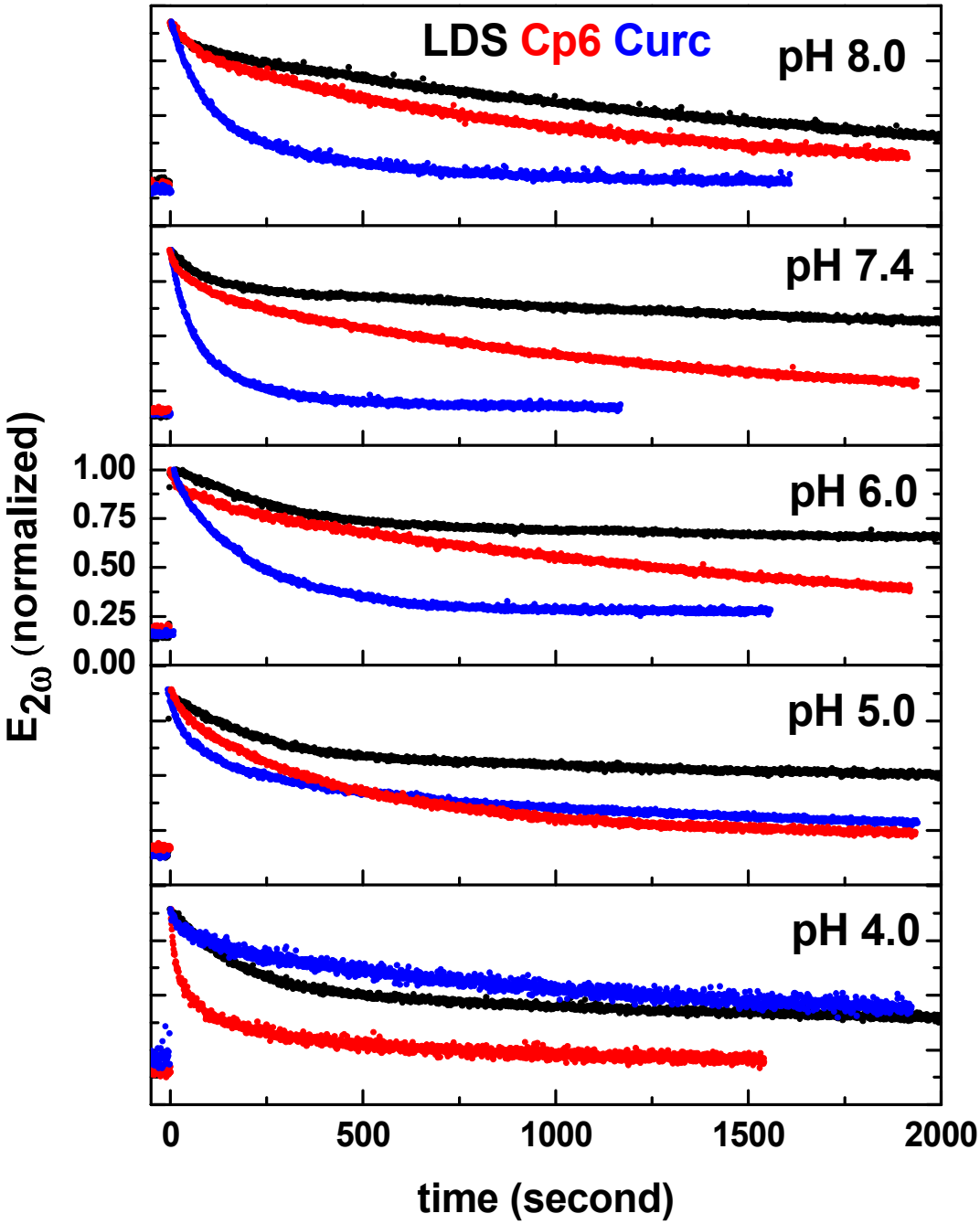

Figure 4.2: *Effect of pH on the SH electric field of 5 μM LDS^+ ions before and after addition of 50 μM POPG liposomes at 25 °C. Liposomes are added at t = 0 time point. The black curves denote only liposomes; red and blue curves denote liposomes containing 3 μM of Cp_6 and curcumin respectively. All the curves are normalized with respect to the maximum $E_{2\omega}$ value.*

the term A_0 in eqn. 4.1). This has been attributed to the finite population difference in the dye molecules adsorbed on the outer (N_{out}) and inner (N_{in}) surface of the liposome and the term 1-A_0 represents the N_{in}/N_{out} ratio. The transport kinetics of LDS^+ ions after addition of POPG liposomes containing either curcumin or C*p*$_6$ (3 μM each) changes significantly. In presence of the drugs, the decays of $E_{2\omega}$ (from LDS^+ ions) depend both on the pH of the medium and the drug (curcumin/C*p*$_6$) present in the bilayer. It is clear from Figure 4.2 that at acidic pH (4.0) bilayer permeability is significantly increased by C*p*$_6$ whereas near physiological pH bilayer permeability is markedly enhanced by curcumin.

To get an idea about how the bilayer transport of LDS^+ ions is affected by the drugs over the pH range used in this study we have compared the relative changes of two transport parameters: average transport time constant (τ_{av}; where, $\tau_{av} = a_1\tau_1 + a_2\tau_2$) and the relative changes of the N_{in} and N_{out} values. The N_{in}/N_{out} ratios under different experimental conditions are listed in Table 4.1. However it is pertinent to note that the transport kinetics of LDS^+ ions across the bilayer reached equilibrium at ~500 second in the presence of 3 μM C*p*$_6$ at pH 4.0 (or 3 μM curcumin at pH 7.4) whereas in the absence of the drugs at least an one hour is needed to attain equilibrium. Therefore, the N_{in}/N_{out} ratio of LDS^+ ions at equilibrium obtained by exponential fitting actually represents the N_{in}/N_{out} values at *widely different time points*. On the other hand, following the addition of liposomes at t = 0, $E_{2\omega}(t)$ will be proportional to $[N_{out}(t) - N_{in}(t)]E_\omega E_\omega$ at any time t. Therefore, if the $E_{2\omega}$ values are normalized to unity at t = 0, then under similar experimental conditions the drug induced relative changes of the quantity: $[N_{out}(t) - N_{in}(t)]$ or $\Delta N(t)$ can be compared by simply taking the ratio of $E_{2\omega}$ values at that particular time t. It is important to note that by comparing the different $E_{2\omega}(t)$ i.e. $\Delta N(t)$ values a fair idea about the transport process can be gained at any time without the need to fit the experimental data. The smaller the value of ΔN (t) will correspond to a faster rate of transport across the bilayers

Table 4.1: *Fitted parameters for the decay of SH electric field of LDS^+ ions after addition of different POPG liposomes at different pH*[a]

pH[b]	a_0	a_1	τ_1	a_2	τ_2	τ_{av}	N_{in}/N_{out}
4.0	0.32	0.42	170	0.26	2600	750	0.68
+ 3μM Cp6 $Cp_6^{-1} : Cp_6^{-2} \approx 6.3$	0.08	0.81	29	0.11	390	65	0.92
+ 3μM Curc	0.40	0.19	90	0.41	1143	486	0.60
5.0	0.45	0.37	199	0.18	2220	464	0.55
+ 3μM Cp6 $Cp_6^{-1} : Cp_6^{-2} \approx 0.6$	0.19	0.31	44	0.50	494	262	0.81
+ 3μM Curc	0.23	0.47	69	0.296	790	266	0.77
6.0	0.42	0.34	242	0.24	6752	1713	0.58
+ 3μM Cp6 $Cp_6^{-3} : Cp_6^{-2} \approx 0.1$	0.12	0.19	84	0.69	1947	1351	0.88
+ 3μM Curc	0.22	0.18	79	0.6	235	155	0.78
7.4	0.34	0.30	79	0.36	3470	1280	0.66
+ 3μM Cp6 $Cp_6^{-3} : Cp_6^{-2} \approx 2.5$	0.18	0.30	57	0.52	1166	629	0.82
+ 3μM Curc $Curc^0 : Curc^{-1} \approx 4.0$	0.10	0.67	47	0.23	184	74	0.90
8.0	0.14	0.22	54	0.64	2120	1379	0.86
+ 3μM Cp6 $Cp_6^{-3}:Cp_6^{-2} \approx 10$	0.21	0.26	57	0.53	1016	557	0.79
+ 3μM Curc $Curc^0 : Curc^{-1} \approx 2.5$	0.14	0.63	81	0.23	418	147	0.86

[a]*The fitted values represent the decays of the SH electric field of LDS^+ ions under various conditions where the experimental time windows vary considerably. For example, in the presence of only POPG liposomes decays of $E_{2\omega}$ were recorded on a much longer time scale (see chapter 2) to get an accurate estimation of the time constants. All the time constants are in second*

[b]*The ratio of the abundant ionic species of the drugs at different pH (obtained from their corresponding pK_a values) are provided in grey background.*

Figure 4.3 shows the relative changes in the τ_{av} and ΔN_{1000s} (at t = 1000s) values at different pH. Both the drugs used in this study have functional groups that can be ionized depending upon the pH of the medium. This ionization is expected to affect the hydrophobic/hydrophilic balance of the drug thereby affecting its bilayer localization. It is evident from Figures 4.2 and 4.3 that pH plays an important role in the drug induced membrane permeability of LDS^+ ions. Therefore, to get an idea about how membrane permeability depends upon the bilayer localization of the drug, FRET studies were carried out using POPG liposomes containing DPH labeled PC phospholipid. Since the fluorescence spectra of DPH overlaps nicely with the absorption spectra of both the drugs (Figure 4.4) in the presence of POPG liposomes it is expected that FRET will occur between DPH and the drugs.

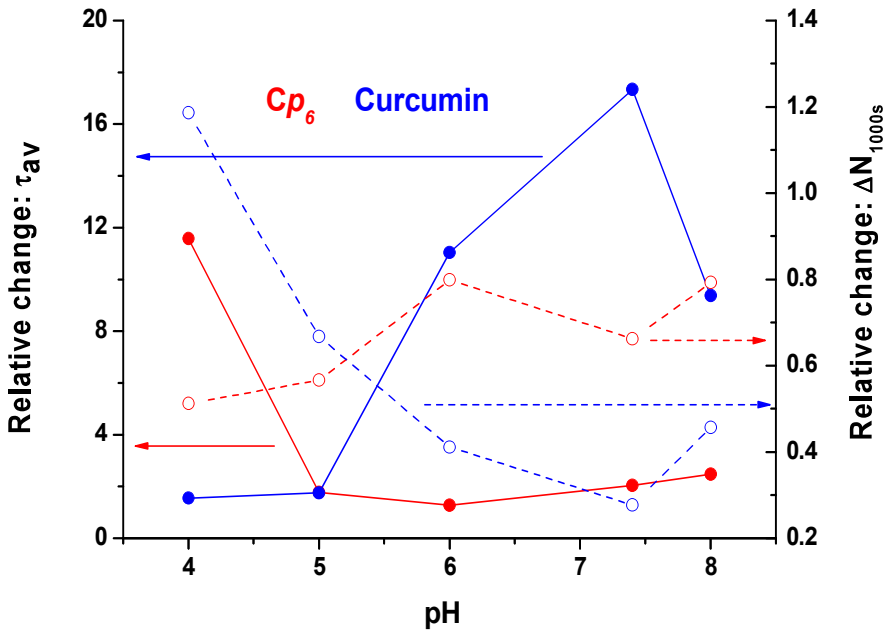

Figure 4.3: *Relative changes in: i) average transport time constant τ_{av} (solid data points connected by solid lines) and ii) $\Delta N_{1000\,s}$ (hollow data points connected by dashed lines) of* LDS^+ *ions. Relative changes are calculated by normalizing with the corresponding value in the absence of the drugs.*

The R_0 values for the FRET pairs DPH- Cp_6 and DPH-Curcumin were estimated to be 34.9 ± 0.8 and 42.5 ± 1.0 A^0 respectively (Table 4.2).

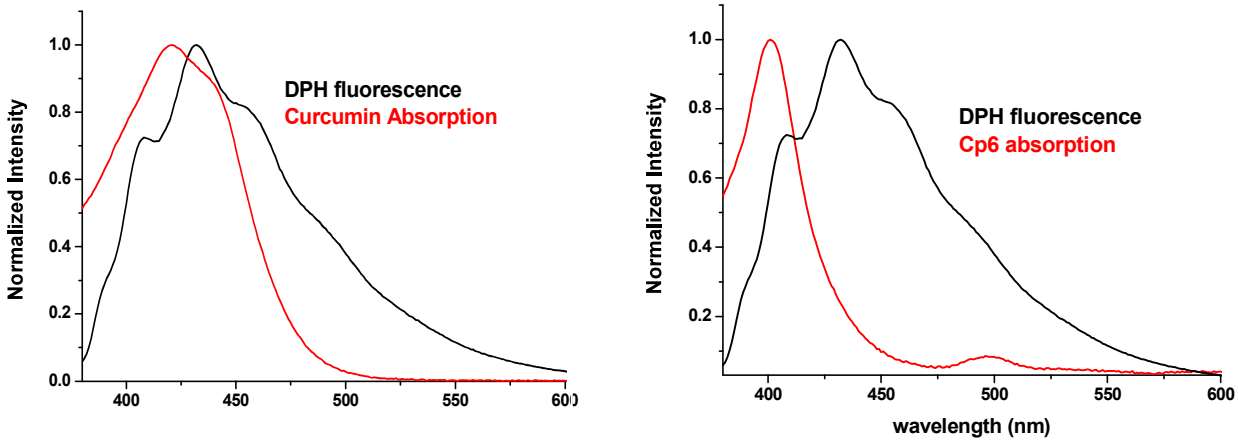

Figure 4.4: *Overlap between the emission of DPH-PC and curcumin (left) and DPH-PC and Cp6 (right) in POPG liposomes at pH 5.0. DPH-PC: 1 µM; curcumin & Cp6: 3 µM*

Table 4.2: *FRET parameters used to calculate the average center-to-center distance (d_x) between DPH and the drugs.*

RET pair	**J(λ) (x 10^{14} $M^{-1}cm^{-1}nm^4$)**	**R_0 (A^0)**	**d_x (A^0)[a] (Av. center-to-center distance)**
DPH-Curcumin	8.45 ± 0.95	42.5 ± 1.0	33.9 ± 0.4 at pH 4.0 35.0 ± 0.4 at pH 5.0 36.4 ± 0.5 at pH 6.0
DPH-Cp_6	2.59 ± 0.50	34.9 ± 0.8	34.6 ± 0.5 at pH 4.0 37.4 ± 0.4 at pH 5.0 41.6 ± 0.6 at pH 6.0 42.1 ± 0.3 at pH 4.0 43.6 ± 0.5 at pH 8.0

[a]*The d_x values are calculated at a drug concentration of 3 µM. The errors represent the standard deviation obtained from three different experiments using three freshly made DPH labeled POPG liposomes*

Figure 4.5 shows the FRET efficiency between DPH-Cp_6 and DPH-Curcumin with increasing concentrations of the drugs at various pH calculated from the steady state fluorescence intensity of the donor DPH. The FRET efficiency curves increases with increasing concentration of the drugs and then tends to saturate. While the FRET efficiency between DPH and Cp_6 were observed to significantly decrease with increase in the pH of the medium, the FRET efficiency between DPH and curcumin at acidic pH range (4.0 to 6.0) were observed to marginally decrease with increase in the pH of the medium.

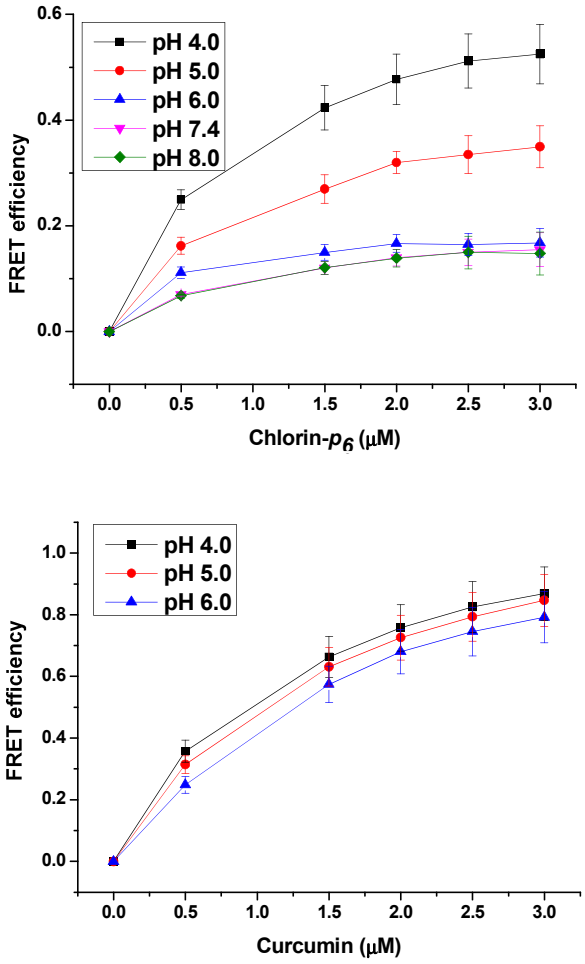

Figure 4.5: *pH dependent FRET efficiency (λ_{ex} = 360 nm) between DPH-PC and Cp_6 (upper figure) and between DPH-PC and curcumin (lower figure). FRET efficiency (defined as: 1-F_{DA}/F_D; where F_{DA} and F_D is the fluorescence intensity of DPH in the presence and absence of curcumin or Cp_6, respectively) was obtained by monitoring the fluorescence maxima of DPH-PC at 432 nm. In these experiments the lipid concentration was kept at 150 μM (DPH-PC: POPG = 1:150*

4.3 Discussion

The main objective of this work was to study the pH dependence of curcumin and Cp_6 induced changes in the transport of the LDS^+ ions across a POPG bilayer. The pH dependence of drug induced bilayer permeability was assessed by monitoring the relative changes in the two calculated parameters: average transport time constant (τ_{av}) and ΔN_{1000s} values. The observed trends in the relative τ_{av} and ΔN_{1000s} values show that the permeability of the POPG bilayer containing curcumin (drug:lipid = 0.06) against the LDS^+ ions increases remarkably as the pH is increased, it peaks at 7.4 (~17x decrease in τ_{av} with corresponding $\Delta N_{1000s} \approx 0.3$; Figure 4.3) and then decreases significantly at pH 8.0. The decrease in curcumin induced bilayer permeability at pH 8.0 could be explained by the fact that at this pH the amount of neutral curcumin population (which is expected to be in the bilayer) decreases by 29% (Table 4.1). Interestingly an opposite trend is observed when relative τ_{av} and ΔN_{1000s} values are compared for POPG liposomes in presence of similar amount of Cp_6 (drug:lipid = 0.06). Cp_6 induced bilayer permeability was observed to be maximum at pH 4.0 (~10x decrease in τ_{av} with corresponding $\Delta N_{1000s} \approx 0.5$; Figure 4.3), a further increase in the pH of the medium decreased the drug induced membrane permeability and any further increase in pH did not affect the bilayer permeability significantly.

Curcumin and Cp_6 are amphiphilic in nature due to the presence of ionizable functional groups (-COOH groups in Cp_6 and –OH groups in curcumin). The pK_a values of some of these functional groups are either within the pH range used in this study or closer to it. Therefore depending upon the pH of the medium these drugs can be charged or neutral which is expected to affect their lipophilicity. Cp_6 can exist as Cp_6^{-1}, Cp_6^{-2} and Cp_6^{-3} depending upon the pH of the medium. The first and second pK_a of the –COOH groups of Cp_6 are at 7.0 and 4.8 [26-27]. The ratios of the various forms of Cp_6 present at different pH are shown in Table 4.1. So, at pH 4.0 where Cp_6^{-1} species (more hydrophobic) is the majority, the bilayer

permeability gets significantly enhanced whereas at pH 8.0 where Cp_6^{-3} species (more hydrophilic) is abundant the change in the bilayer permeability is modest.

The average center-to-center distance (d_x) between DPH and the drugs were estimated from the FRET efficiency and corresponding R_0 values (Table 4.2). The d_x values of DPH and Cp_6 in the POPG bilayer increases from 34.6 ± 0.5 to 43.6 ± 0.8 A^0 as the solution pH increases from 4.0 to 8.0. The d_x values of DPH and curcumin in the POPG bilayer increases from 33.9 ± 0.4 to 36.4 ± 0.5 A^0 as the solution pH increases from 4.0 to 6.0. It can be seen from Table 4.2 and Figure 4.3 that the increase in the d_x values has a marked effect on the transport characteristics of the LDS^+ ions. For example an increase in the d_x value of Cp_6 from 34.6 ± 0.5 at pH 4.0 to 41.6 ± 0.6 at pH 6.0 results in a 9 fold decrease while an increase in the d_x value of curcumin from 33.9 ± 0.4 at pH 4.0 to 36.4 ± 0.5 at pH 6.0 results in a 7 fold increase in the relative transport time constant of the cation. It therefore appears that with increasing pH, the outward movement of curcumin and Cp_6 (with respect to the bilayer center) *affects the membrane permeability in an opposite way*.

In order to search for an explanation for this opposite effect, we note that: i) the length (long axis) of both the drugs are comparable to the length of a POPG molecule and, ii) it is reasonable to assume that in the bilayer the ionizable group/groups of the drugs should be closer to the liposome-water interface. Earlier reports have indicated that interaction of the functional groups of curcumin (phenolic –OH and enolic –OH) with the polar head groups of the choline moiety of the phosphatidyl choline lipids (DMPC and DPPC) plays a major role in modulating the bilayer organization [14-15]. Based on FRET results, the proximity between the enolic –OH group of the drug and the polar head groups of POPG is likely to get enhanced with increasing pH, which might cause the significant enhancement the bilayer permeability by curcumin. One way to test this hypothesis would be to investigate with curcumin derivatives where the enolic –OH group of the molecule is replaced by some inert

group say, -OMe. Cp_6, on the other hand, have the three –COOH groups at one end of the molecule. With an increase in solution pH the outward movement of the drug is likely to reduce the proximity between the –COOH group of the drug and the polar head groups of POPG as suggested by the FRET study. Therefore Cp_6 induced bilayer permeability gets significantly reduced with increase in solution pH.

4.4 Conclusion

In conclusion, we have studied the transport kinetics of the LDS^+ ions across POPG liposomes in the pH range of 4.0 to 8.0 in the presence and absence of two amphiphilic drugs, curcumin and Cp_6. Our results show that transport (and consequently bilayer permeability) of LDS^+ ions across the bilayer is governed by the nature of the drug and pH of the medium. While Cp_6 significantly enhanced the transport of LDS^+ ions at pH 4.0, curcumin gradually enhanced the transport of the cation as the pH is increased which become maximum near physiological pH (7.4) and decreased a bit at pH 8.0. FRET studies confirmed that the bilayer localization of Cp_6 is pH dependent, due to the presence of the carboxyl groups. Combining the results of FRET studies and the relative population of the various ionic/nonionic species of Cp_6 at different pH leads to the suggestion that the reduced distance between the carboxyl group of Cp_6 and polar head groups of the lipid might be responsible for the observed enhanced permeability of LDS^+ ions at acidic pH. Understanding how pH plays a role in curcumin induced bilayer permeability is more complex as the drug itself gets degraded near physiological pH. However the results obtained from the SHG and FRET studies suggest the possibility that interaction between anionic species of the drug ($Curc^{-1}$) and the polar head groups of the lipids might result in significant modulation of the bilayer organization.

References

1. Peetla, C.; Stine, A.; Labhasetwar, V. *Molecular Pharmaceutics* **2009**, *6*, 1264–1276.
2. Grancelli, A.; Morros, A.; Cabanas, M. E.; Domenech, O.; Merino, S.; Vazquez, J. L.; Montero, M. T.; Vinas, M.; Hernandez-Borrell, J. *Langmuir* **2002**, *18*, 9177–9182.
3. Berquand, A.; Fa, N.; Dufrene, Y. F.; Mingeot-Leclercq, M. P. *Pharm. Res*. **2005**, *22*, 465–475.
4. Barcelo, F.; Prades, J.; Funari, S. S.; Frau, J.; Alemany, R.; Escriba, P. V. *Mol. Membr. Biol*. **2004**, *21*, 261–268.
5. Cheng, H. Y.; Randall, C. S.; Holl, W. W.; Constantinides, P. P.; Yue, T. L.; Feuerstein, G. Z. *Biochim. Biophys. Acta, Biomembr*. **1996**, *1284*, 20–28.
6. Corvis, Y.; Barzyk, W.; Brezesinski, G.; Mrabet, N.; Badis, M.; Hecht, S.; Rogalska, E. *Langmuir* **2006**, *22*, 7701–7711.
7. Agasosler, A. V.; Tungodden, L. M.; Cejka, D.; Bakstad, E.; Sydnes, L. K.; Holmsen, H. *Biochem. Pharmacol*. **2001**, *61*, 817–825.
8. Hidalgo, A. A.; Caetano, W.; Tabak, M.; Oliveira, O. N. *Biophys. Chem*. **2004**, *109*, 85–104.
9. Feng, S. S.; Gong, K.; Chew, J. *Langmuir* **2002**, *18*, 4061–4070.
10. Preetha, A.; Huilgol, N.; Banerjee, R. *Colloids Surf. B* **2006**, *53*, 179–186.
11. Preetha, A.; Huilgol, N.; Banerjee, R. *J. Membr. Biol*. **2007**, *219*, 83–91.
12. Hung, W. C.; Chen, F. Y.; Lee, C. C.; Sun, Y.; Lee, M. T.; Huang, H. W. *Biophys. J.* **2008**, *94*, 4331-4338.
13. Sun, Y.; Lee, C-C.; Hung, W-C.; Chen, F-Y.; Lee, M-T.; Huang, H. W. *Biophys. J.* **2008**, *95*, 2318–2324.
14. Barry, J.; Fritz, M.; Brender, J. R.; Smith, P. E.; Lee, D. K.; Ramamoorthy, A. *J. Am. Chem. Soc*. **2009**, *131*, 4490-4498.

15. Perez-Lara, A.; Ausili, A.; Aranda, F. J.; Godos, A.; Torrecillas, A.; Corbalan-Garcia, S.; Gomez-Fernandez, J. C. *J. Phys. Chem. B* **2010**, *114*, 9778–9786.

16. Varshney, G. K.; Saini, R. K.; Gupta, P. K.; Das, K. *Langmuir* **2013**, *29*, 2912−2918.

17. Saini, R. K.; Varshney, G. K.; Dube, A.; Gupta, P. K.; Das, K. *J. Mol. Struc*. **2014**, *1074*, 22−26.

18. Bernabe-Pineda, M.; Ramirez-Silva, M. T.; Romero-Romob, M.; Gonzalez-Vergara, E.; Rojas-Hernandez, A. *Spectrochim. Acta Part A* **2004**, 60, 1091–1097.

19. Leung, M. H. M.; Colangelo, H.; Kee, T. W. *Langmuir* **2008**, *24*, 5672−5675.

20. Wang, Z.; Leung, M. H. M.; Kee, T. W.; English, D. S. *Langmuir* **2010**, *26*, 5520–5526.

21. Srivastava, A.; Eisenthal, K. B. *Chem. Phys. Lett*. **1998**, *292*, 345−351.

22. Yan, E. C. Y.; Eisenthal, K. B. *Biophys. J*. **2000**, *79*, 898−903.

23. Liu, Y.; Yan, E. C. Y.; Eisenthal, K. B. *Biophys. J*. **2001**, *80*, 1004−1012.

24. Liu, J.; Shang, X. M.; Pompano, R.; Eisenthal, K. B. *Faraday Discuss*. **2005**, *129*, 291−299.

25. Liu, J.; Subir, M.; Nguyen, K.; Eisenthal, K. B. *J. Phys. Chem. B* **2008**, *112*, 15263−15266.

26. Datta, A.; Dube, A.; Jain, B.; Tiwari, A.; Gupta, P. K. *Photochem. Photobiol*. **2002**, *75*, 488.

27. Saini, R. K.; Gupta, P. K.; Das, K. *J. Phys. Chem. B* **2012**, *116*, 4199−4205.

Chapter 5

Effect of bilayer partitioning of curcumin on the adsorption and transport of a cationic dye across POPG liposomes probed by second harmonic spectroscopy

5.1 Introduction

The lipid bilayer of cell membranes is a natural binding site for several types of amphipathic molecules, like proteins, drugs, detergents etc. It is important to study the binding of a drug to a membrane because drug-membrane binding can cause changes in the bilayer properties and thus affect the functions of embedded proteins [1-2]. Amphipathic drugs can bind to the membrane-water interface or intercalate into the nonpolar chain region of the membrane. One such example of an amphipathic drug is curcumin (Figure 5.1) which shows a wide spectrum of pharmacological effects [3-6]. The results of recent studies suggest that curcumin can regulate various structurally-unrelated membrane proteins by changing the properties of the surrounding lipid bilayer rather than directly binding to proteins [7-8]. Consequently several studies have been performed in model membrane systems to understand how curcumin affects the bilayer properties by different bio-physical techniques [9-14]. However majority of these studies [9, 11-13] were carried out under an equilibrium condition, i.e. after curcumin was bound to the membrane. A few studies [10, 14] where direct observation of membrane properties were carried out while curcumin is added revealed some interesting aspects of the membrane binding properties of this amphipathic drug.

It has been observed that surface area of individual giant unilamellar vesicles (GUVs) of DOPG lipid increases upon binding of curcumin from solution by the micropipette aspiration

technique [10]. The rate of increase is faster up to a curcumin: lipid molar ratio (C/L) of 0.02 and becomes slower thereafter. Combining this with results obtained from earlier studies on X-ray lamellar diffraction measurements of the thickness of DOPG bilayers as a function of curcumin content [9] a two-state model was proposed for curcumin binding to DOPG bilayer. Curcumin initially binds to the aqueous bilayer interface and then at higher concentrations gradually partition to a state where it is inserted into the hydrocarbon region of the bilayers [10]. In another study using total internal reflection fluorescence microscopic technique, it was observed that curcumin induces fusion of lipid raft domains at low concentrations by changing the boundary between the ordered and disordered phases [14].

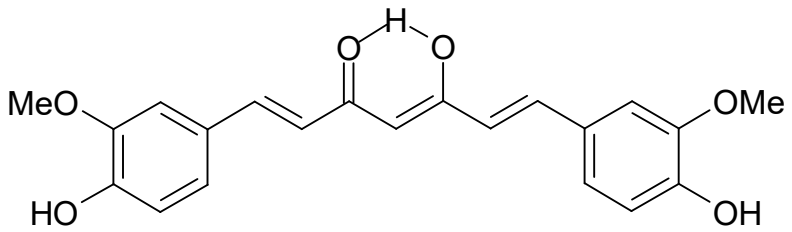

Figure 5.1: *Chemical structure of curcumin*.

Second Harominc (SH) spectroscopic technique has the ability to probe the interfacial region exclusively due to symmetry considerations [15]. Generation of SH light requires that the medium must lack a center of symmetry which is applicable at the lipid bilayer interface. Interfacial adsorption of a molecule/ion and its transport across a bilayer can therefore be monitored by the SH technique provided it possesses a reasonable hyperpolarizability value at the excitation wavelength [13, 16-19]. We have earlier monitored the transport of a cationic hemicyanine dye, LDS^+ ion, across a negatively charged POPG bilayer by the SH spectroscopic technique and observed that when POPG liposomes were incubated with

curcumin the transport of LDS^+ ions across the bilayer was significantly faster [13]. Since it has been observed that partitioning of curcumin from solution to a bilayer is accompanied by membrane area expansion and membrane thinning [9-11, 14] it would be interesting to see whether this will affect the *interfacial binding* of small organic molecules with lipid bilayer. In this work we report how the adsorption and transport of LDS^+ ions across a POPG bilayer changes when curcumin is added to the solution and compare our results with previous studies [9-10].

5.2 Results

The average laser power used in the SHG experiments was 600 mW. The SH experiments were conducted as follows: The SH intensity of LDS^+ ions (5 μM) in buffer solution was monitored with time. At t = 50 second, 50 micro-liter concentrated POPG solution was added to make the final concentration of POPG as 50 μM. Unless otherwise stated micro-liter aliquots from a concentrated stock solution of curcumin were added to the liposome solution at t = 100 second to get the desired curcumin:lipid (C/L) ratio. Figure 5.2 describes the changes in the SH field ($E_{2\omega}$) of LDS^+ ions after addition of POPG liposomes (at 50 second) for three different conditions:

a) Without curcumin.

b) POPG liposomes which were earlier incubated with curcumin (C/L = 0.1) for few minutes.

c) Curcumin (C/L = 0.1) was added *50 second after the addition of POPG liposomes*.

The instantaneous increase (< 1 second) in the $E_{2\omega}$ signal of LDS^+ ions after addition of POPG liposomes at 50 second time point for all the three curves in Figure 5.2 is due to the rapid electrostatic absorption of the positively charged dye on the negative charged outer bilayer surface as has been demonstrated in numerous studies earlier [13, 16-19].

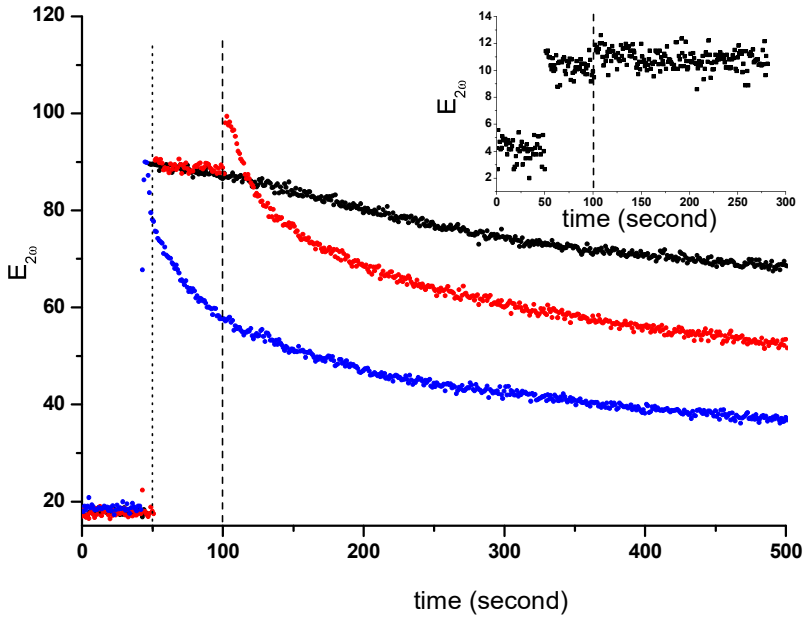

Figure 5.2: *SH electric field ($E_{2\omega}$) of LDS^+ ions (5 μM) under different conditions at pH 5.0 and room temperature.* ***Black:*** *In presence of POPG liposomes (50 μM) which were added at 50 second time point;* ***Blue:*** *In presence of POPG liposomes (50 μM) incubated with curcumin (C/L = 0.10), which were added at 50 second time point;* ***Red:*** *In presence of POPG liposomes (50 μM) added at 50 second time point and curcumin (C/L = 0.10) added at 100 second time point.* ***Inset:*** *SH electric field ($E_{2\omega}$) arising from pH 5.0 buffer to which POPG liposomes (50 μM) was added at 50 second time point and curcumin (C/L = 0.50) was added at 100 second time point.*

After addition of POPG liposomes $E_{2\omega}$ of LDS^+ ions decreases gradually due to transport of the LDS^+ ions from the outer to inner lipid bilayer (case a). Consistent with our earlier studies the rate of decrease of the $E_{2\omega}$ of LDS^+ ions gets significantly faster when POPG liposomes contain curcumin (case b). However when curcumin is added to the solution containing LDS^+ ions and POPG liposomes, it generates an *additional instantaneous increase* in the $E_{2\omega}$ signal of LDS^+ ions (case c). This phenomenon is observed whenever curcumin is added as shown in Figure 5.3. In order to see whether this is due to $E_{2\omega}$ generated by the curcumin molecules itself, we have monitored the $E_{2\omega}$ signal of POPG liposomes in presence of only curcumin

which is shown as an inset in Figure 5.2. The time course of $E_{2\omega}$ signal coming from a pH 5.0 buffer solution increases marginally after addition of POPG liposomes (added at 50 second) but remains more or less unchanged even after addition of curcumin (added at 100 second) whose concentration is five times higher than that used in Figure 5.2 b and 5.2 c. Therefore, the instantaneous increase in the $E_{2\omega}$ signal of LDS^+ ions following addition of curcumin does not arise due to $E_{2\omega}$ of curcumin. In the presence of POPG liposomes the $E_{2\omega}$ signal of LDS^+ ions at any time is directly proportional to the population difference between the LDS^+ ions molecules residing at the outer and inner lipid bilayer. The *additional instantaneous increase* in the $E_{2\omega}$ signal of LDS^+ ions (case c) indicates that addition of curcumin affects this population difference. Therefore the instantaneous increase of the $E_{2\omega}$ signal of LDS^+ ions (red curve, Figure 5.2), immediately after addition of curcumin, can be attributed to an instantaneous increase of the number of LDS^+ ions molecules adsorbed on the outer bilayers.

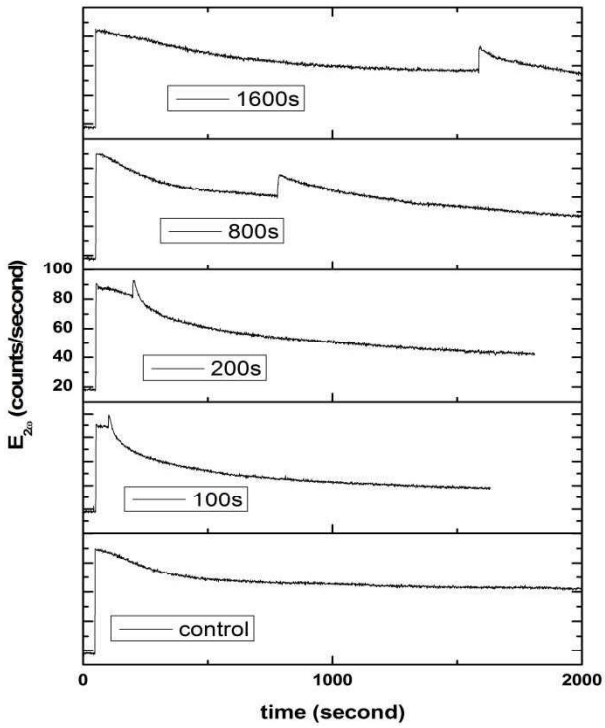

Figure 5.3: *Effect of addition of curcumin (C/L = 0.02) to a solution containing LDS^+ ions and POPG liposomes (corresponding to case c of Figure 5.2). The instantaneous increase in the $E_{2\omega}$ signal of LDS^+ ions happens whenever curcumin is added.*

It would be interesting to see whether this phenomenon is a particular one (for LDS^+ ion only) or a general one (for any organic cations). Therefore, we have repeated the same experiment corresponding to curve c of Figure 5.2, but replaced the LDS^+ ion by either Malachite Green or Auramine-O cation both of which have appreciable SH signals at 800 nm excitation [15]. Although no instantaneous increase in the $E_{2\omega}$ signal of these two cations were observed after addition of curcumin at room temperature (data not shown), lowering the temperature of the solution (3 °C) indeed resulted in an instantaneous increase in the $E_{2\omega}$ signal of these two cations which is shown in Figure 5.4, along with LDS^+ ions. These results therefore suggest that addition of curcumin changes the outer bilayer of the POPG liposomes in such a way so as to induce an increase in the number of cationic molecules adsorbed on the negatively charged outer bilayer.

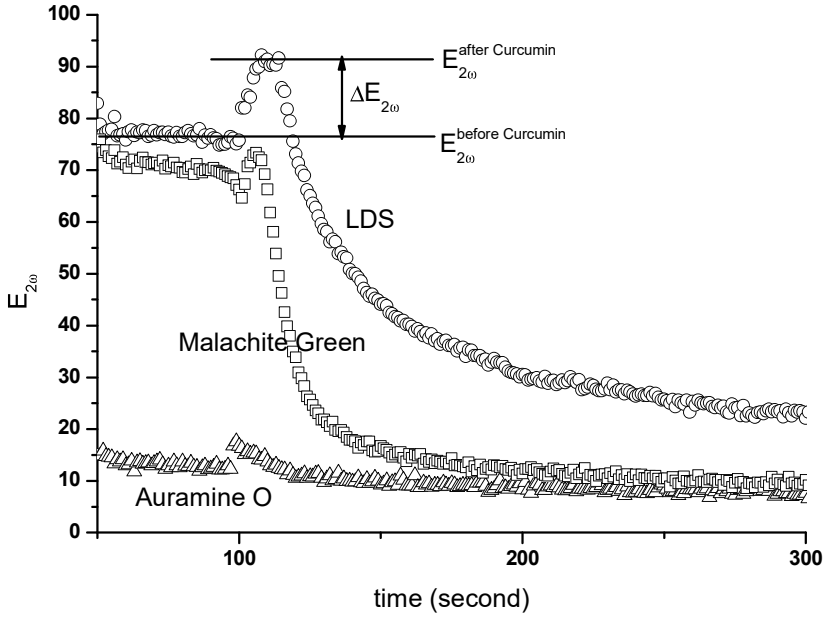

Figure 5.4: *Changes in $E_{2\omega}$ of LDS^+ (circles), Malachite Green (squares) and Auramine-O (triangles) in the presence of POPG liposomes (50 μM) before and after addition of curcumin (C/L = 0.1; added at 100 second time point) in pH 5.0 buffer at 3 °C. Estimation of curcumin associated fractional changes in the $E_{2\omega}$ of LDS^+ ions is also shown.*

In order to quantify the observed changes in the $E_{2\omega}$ signal due to curcumin, we have chosen LDS^+ ions as the probe molecule and kept the temperature at 3 °C because as evident from Figure 5.4, changes in the $E_{2\omega}$ signal after addition of curcumin of LDS^+ ions is largest among the three cations. Curcumin induced fractional changes in the $E_{2\omega}$ signal of LDS^+ ions can now be quantified as:

$$E^f_{2\omega} = \Delta E_{2\omega} / E^0_{2\omega} \qquad (5.1)$$

where $\Delta E_{2\omega}$ is the *maximum observed difference* of the SH electric field of LDS^+ ions before and after addition of curcumin (Figure 5.4). Since the $E_{2\omega}$ signal of LDS^+ ions after addition of POPG liposomes remains unchanged (it remains constant for several hundred seconds which is consistent with our earlier report [13]) before addition of curcumin it is reasonable to assume (as per Eqn. 1) that the $E_{2\omega}$ signal of LDS^+ ions (in presence of POPG liposomes at 3 °C) will be directly proportional to the number of LDS^+ ions adsorbed on the outer bilayer of the liposomes for the initial few hundreds of seconds. Therefore, curcumin induced fractional increase in the $E_{2\omega}$ signal of LDS^+ ions can be directly correlated to the fractional increase in the number of LDS^+ ions molecules adsorbed on the outer lipid bilayer. In the following sections we have attempted to investigate curcumin induced fractional changes of SH electric field ($E^f_{2\omega}$) of LDS^+ ions under various environmental conditions.

Curcumin is an amphiphilic molecule having three acidic hydroxyl groups among which the enolic hydroxyl group is the most reactive having a pK_a of ≈ 8.4 [20,11]. In order to investigate whether the ionization of the enolic hydroxyl group should affect the $E^f_{2\omega}$ of LDS^+ ions we did a pH variation study. Figure 5.5 shows the changes in $E^f_{2\omega}$ of LDS^+ ions with changes in the pH of the medium. As shown in the inset of Figure 5.5, a change in the pH of the medium (from 5.0 to 8.5) causes $E^f_{2\omega}$ of LDS^+ ions to change significantly. The fractional increase in the SH electric field of LDS^+ ions at pH 5.0 was observed to be twice (~17%) as much as that observed for pH 8.5 (~8%). Since with increase in pH, the formation of enolic

anion of curcumin is favored it indicates that neutral species of curcumin is more effective in increasing the $E^f_{2\omega}$ of LDS^+ ions. Therefore in the subsequent studies we have kept the medium pH at 5.0

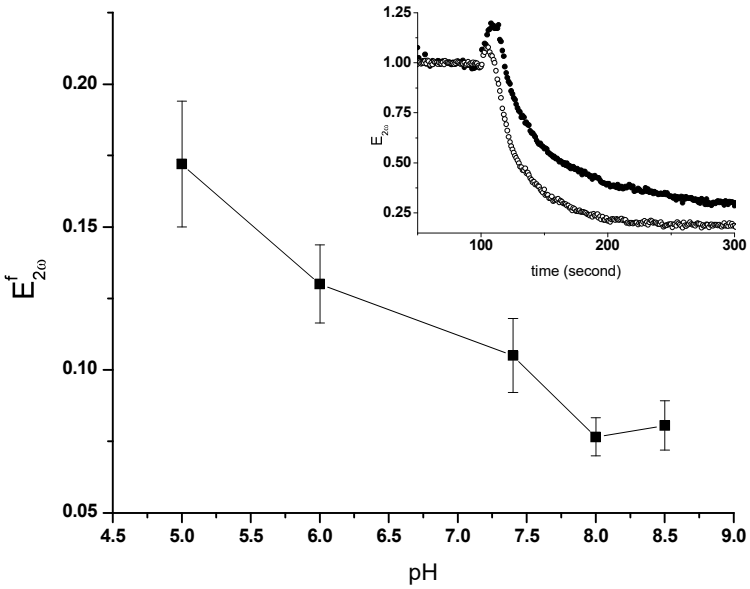

Figure 5.5: *The variation in the $E^f_{2\omega}$ of LDS^+ ions in presence of POPG liposomes (C/L = 0.1) with pH of the medium at 3 °C. Inset: Time dependent changes of the $E_{2\omega}$ signal of LDS^+ ions in presence of POPG liposomes before and after addition of curcumin at pH 5.0 (black circles) and at pH 8.5 (hollow circles). The $E_{2\omega}$ signals of LDS^+ ions were normalized before addition of curcumin to unity for clarity.*

.

The changes in the $E_{2\omega}$ signal of LDS^+ ions with changing curcumin:lipid (C/L) mole ratio are provided in Figure 5.6. It is evident from Figure 5.6 that the transport of the cation remains more or less similar up to a C/L value of 0.02 and starts to become significantly faster thereafter. Transport rate constants of LDS^+ ions under different C/L mole ratio were obtained by fitting with an exponential decay function as mentioned in our early work [13]. To extract the decay time constants of the individual curves they were fitted after the curcumin induced jump in the $E_{2\omega}$ signal of LDS^+ ions is completed.

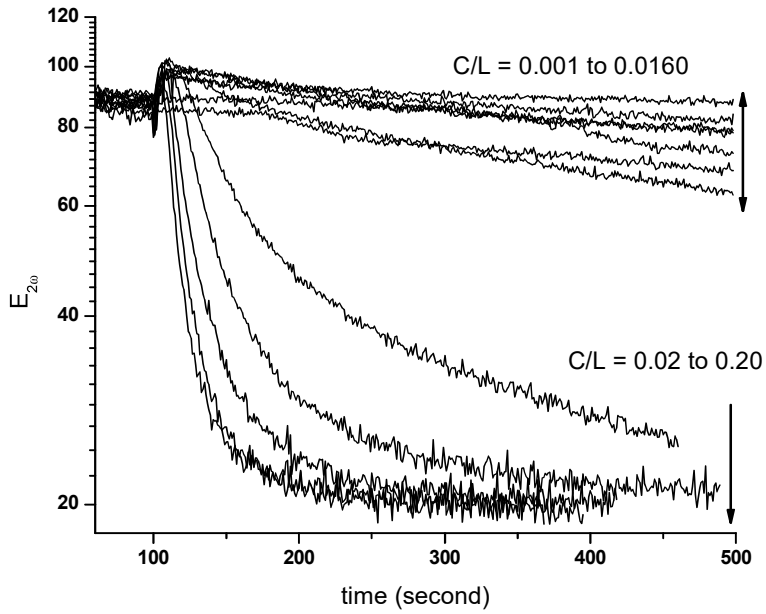

Figure 5.6: *Changes in the $E_{2\omega}$ signal of LDS^+* ions *due to addition of curcumin (C/L varied from $1x10^{-3}$ to 0.2) to a solution containing LDS^+ ions and POPG liposomes. Curcumin was added at t = 100 second time point.*

Figure 5.7 shows the changes in $E^f_{2\omega}$ and transport rated constant (k_T) values of LDS^+ ions with changing curcumin:lipid (C/L) mole ratio. Representative time dependent $E_{2\omega}$ signal of LDS^+ ions at two different C/L ratio ($4.0x10^{-3}$ to $4.0x10^{-2}$) are shown in the inset for a qualitative assessment on the effect of increasing curcumin concentration. It is interesting to note that with increasing C/L ratio the observed trends of $E^f_{2\omega}$ and k_T values of LDS^+ ions, are not similar at lower C/L ratio. While the increase in the $E^f_{2\omega}$ of LDS^+ ion is initially rapid the transport rate of the cation remains quite similar up to a C/L ratio of ≤ 0.02. For C/L ratio being ≥ 0.02, while the $E^f_{2\omega}$ values remains more or less constant there is a significant (~40 times) followed by a modest increase in the k_T values of LDS^+ ions. It is pertinent to note that the observed trend in the variation of $E^f_{2\omega}$ with C/L ratio is quite similar to earlier studies where it was observed that bilayer thinning and surface area expansion of a DOPC bilayer increases rapidly up to a C/L ratio of 0.02 and saturates thereafter [9-10].

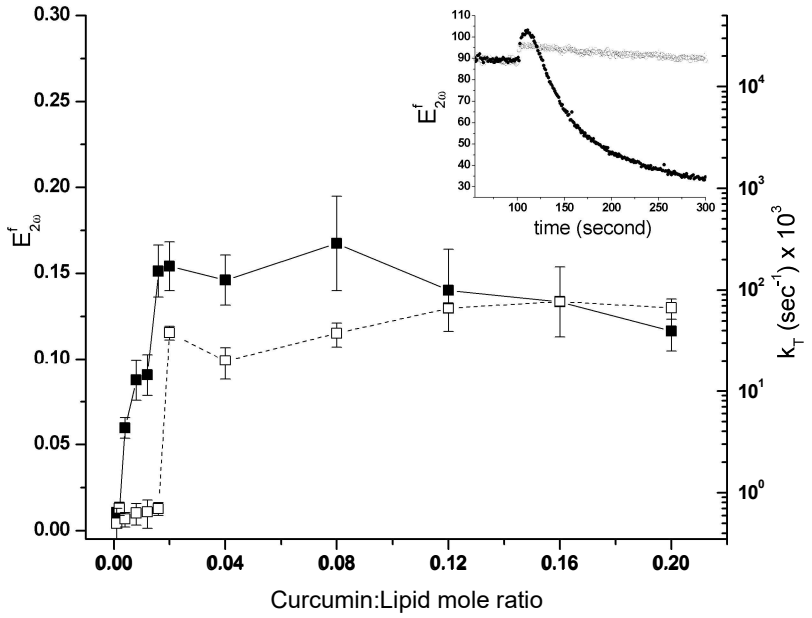

Figure 5.7: *Changes in the $E^f_{2\omega}$ (filled, solid lines) and transport rate constant (k_T) values (hollow, dashed lines) of LDS^+ ions in presence of POPG liposomes at pH 5.0 with variation in the C/L mole ratio at 3 °C. Inset: Representative time dependent $E_{2\omega}$ signal of LDS^+ ions for C/L mole ratio of $4.0x10^{-2}$ (solid circles) and $4.0x10^{-3}$ (hollow transparent circles).*

Figure 5.5 to 5.7 describes the effect of curcumin with respect to its concentration and ionic species without the presence of any electrolytes. Since biological membranes are always suspended in presence of different electrolytes such as NaCl, KCl etc. it would be prudent to investigate the effect of curcumin in presence of these ions. Therefore we have studied the effect of NaCl keeping the curcumin:Lipid molar ratio at 0.10. Figure 5.8 shows the effect of increasing NaCl concentration on the curcumin induced changes in the $E^f_{2\omega}$ values of LDS^+ ions. With increasing NaCl concentration $E^f_{2\omega}$ of LDS^+ ions increases and at the highest NaCl concentration (20 mM) used in this study the magnitude of increase was nearly two fold compared to the situation when no electrolyte (i.e. NaCl) is present

.

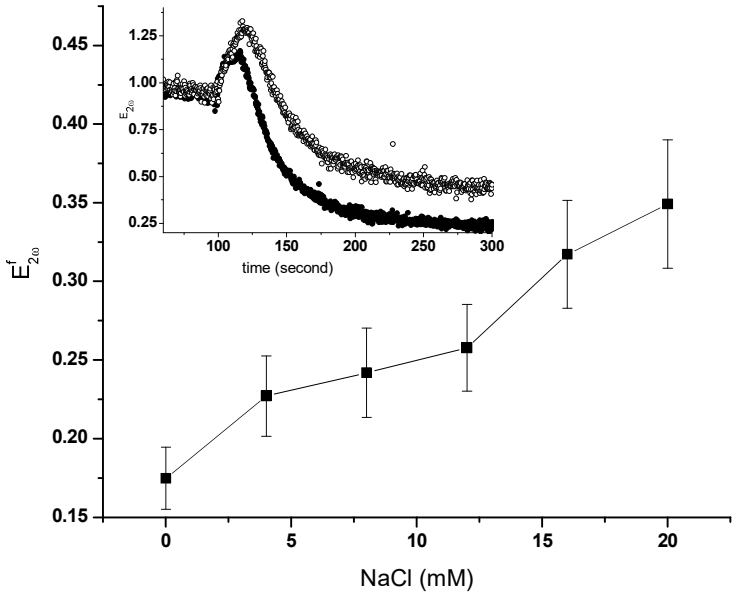

Figure 5.8: *Changes in the $E^f_{2\omega}$ of LDS^+ ions in presence of POPG liposomes and curcumin (C/L = 0.1) with increasing amounts of an electrolyte, NaCl at pH 5.0 and 3 °C. Inset: Representative time dependent changes of the $E_{2\omega}$ signal of LDS^+ ions in presence of POPG liposomes before and after addition of curcumin at pH 5.0 and 3 °C. Solid and hollow circles represent NaCl concentrations of 0 and 20 mM respectively. The $E_{2\omega}$ signals were normalized before addition of curcumin to unity for clarity.*

5.3 Discussions

In this work we have investigated the adsorption and transport process of the LDS^+ ions across a negatively charged POPG bilayer *while curcumin is added to the bilayer* by the interface selective Second-Harmonic spectroscopic technique. Results presented in Figures 5.2 and 5.4 suggest that the observed increase in the $E_{2\omega}$ signal of LDS^+ ions upon curcumin addition is due to creation of additional binding sites for the LDS^+ ions on the outer bilayer of POPG liposomes by curcumin.

Curcumin (Figure 5.1) has three acidic protons out of which the enolic proton is most acidic (pK_a ~ 8.4) [20-21]. Results of several photophysical studies carried out on curcumin suggests that inter-molecular hydrogen bonding between the enolic proton of curcumin and a

hydrogen-bond-acceptor group in polar protic solvents is possible [22-29]. Since the molecule also has a strong affinity for membranes [8-12] it is quite likely that there will be hydrogen bonding interactions between the drug and the polar head groups of the lipid when the drug is bound to the membrane. Results obtained from the pH experiment (Figure 5.5) shows that the observed 50% decrease in the $E^{f}_{2\omega}$ of LDS^{+} ions when the pH is increased from 5.0 to 8.5 correlates with the ≈ 50% decrease in the concentration of the neutral form of the drug at pH 8.5. Therefore our results indicate that hydrogen bonding between the enolic proton of curcumin and the polar headgroup of the POPG liposomes is crucial for the creation of additional binding sites for LDS^{+} ions.

The observed changes in the $E^{f}_{2\omega}$ and k_T values of LDS^{+} ions (Figure 5.7) with changes in C/L ratio indicate the presence of two distinct regimes:

1) C/L ratio ≤ 0.02: At this regime addition of curcumin generates more binding sites for LDS^{+} ions without affecting its transport rate across the bilayer.
2) C/L ratio ≥ 0.02: In this regime addition of curcumin does not generates any more binding sites for LDS^{+} ions but causes the transport of the cation to become significantly faster across the bilayer.

If the proposed two-state binding model of the drug with bilayer (DOPG or POPG) as suggested earlier is correct then results presented in Figure 5.7 suggests that surface associated state of the drug is responsible for creation of extra binding sites for the LDS^{+} ions whereas the bilayer intercalated state of the drug is responsible for the enhanced transport of LDS^{+} ions. It is reasonable to expect that when the drug is intercalated in the bilayer the energy barrier (associated within the hydrophobic domain of the bilayer) for the LDS^{+} ions to cross the bilayer will be lowered as curcumin is a polar molecule having a dipole moment of ~10 Debye [30].

However in order to understand why it should lead to an increment in cation binding sites we need to consider the effect of other ions (i.e. electrolytes) present in the solution. Several Molecular Dynamics (MD) simulation studies have found that strong ion–lipid interactions in POPG lipids stabilize the bilayer by reducing lipid-lipid repulsion arising due to similar charge of the lipid head groups [31-34]. These interactions occur with positively charged counter ions (e.g. Na^+) and carbonyl oxygens present in the POPG head groups via formation of ion-lipid and lipid-ion-lipid complexes. Results obtained from atomistic [31] and coarse-grained [33] MD simulations show that interactions with anti microbial peptides (AMP) with POPG membranes are associated with the release of these counter ions from the membrane interface. The entropy increase due to the counter ion release from the electric double layer surrounding the membrane is attributed as one of the origins of the attraction between the strongly charged POPG membrane and AMP. In a particular case the mechanism for degradation of a POPG membrane upon binding to a cationic AMP was ascribed to the counter ion release by the AMP thereby destroying the cationic bridges between charged lipid head groups and de-stabilizing the bilayers [34].

The adsorption and subsequently the transport of LDS^+ ion is initiated by electrostatic force of attraction between the dye and the negatively charged bilayer. For reasons discussed above, the negative charge of the bilayer will be somewhat screened due to the presence of Na^+–lipid interactions as the liposomes are suspended in sodium phosphate buffer solution. Therefore any factor that affects this interaction is expected to alter the bilayer surface charge density which in turn will affect the electrostatic adsorption of LDS^+ ions with the bilayer. Since it has been reported that curcumin forms hydrogen bond with the carbonyl oxygens in a DPPC bilayers [11-12] we propose that addition of curcumin to a POPG liposome solution suspended in sodium phosphate buffer medium disturbs the Na^+–lipid interactions by formation of intermolecular hydrogen bond between the enolic hydrogen of curcumin and

carbonyl oxygen of the DOPG lipid. This hypothesis is consistent with our experimental observations (Figure 5.5) that the enolate anion of curcumin is less conducive for increasing the $E^{f}_{2\omega}$ of LDS^{+} ions. Replacement of the Na^{+} ions with electrically neutral curcumin molecules is expected to enhance the electrostatic force of attraction between LDS^{+} ions and the negatively charged POPG bilayer by increasing the bilayer surface charge density which would explain our experimental observations. It is interesting to note that although the bilayer surface charge screening increases with increasing Na^{+} ion concentration (by adding NaCl to the solution), curcumin is still able to disturb the Na^{+}–lipid interaction (Figure 5.8) which demonstrates the lipophilic character of the molecule. It is pertinent to note that this alteration of bilayer surface charge density by curcumin should depend upon relative orientation of the molecule with the bilayer. The chemical structure of curcumin (Figure 5.1) indicates that interaction between the enolic hydrogen of curcumin and the carbonyl oxygens of the POPG bilayer is likely to be maximum when the drug will reside at the surface of the bilayer rather than intercalate within hydrocarbon region of the bilayer. It is pertinent to note here that water near the bilayer also plays a crucial role for several biochemical processes such as adsorption, ionic transport and membrane protein orientation. Several recent studies using the heterodyne detected electronic sum frequency generation technique have shed light upon how lipid head groups affect the interfacial pH and orientation of interfacial water molecules [35-37]. In addition MD studies also showed that formation of the Na^{+}-lipid complexes becomes energetically more stable when a water molecule is shared between them [32-35]. Finally, the results obtained by us are summarized in a cartoon (Figure 5.9) which tries to explain the experimental observations. Addition of LDS^{+} ions to a POPG liposome solution results in electrostatic adsorption of the dye to the negatively charged bilayer surface. The amount of adsorption of the cation depends upon the surface charge density of the bilayer governed by the Na^{+}–lipid interactions. Addition of curcumin (C/L ratio ≤ 0.02) results in replacement of

Na^+–lipid complexes by formation of curcumin-lipid complexes which helps further adsorption of the LDS^+ ions at the outer bilayer due to an increase in the negative charge density of the bilayer surface. Further addition of curcumin results in partitioning of the drug inside the bilayer where the long axis of the molecule is oriented perpendicular to aqueous-bilayer interfacial plane. In this geometry the polar curcumin molecule reduces the hydrophobic character of the hydrophobic domain of the bilayer and as a result the transport of the LDS^+ ions across the bilayer gets faster.

5.4 Summary and conclusions

The function of membrane bound proteins is sensitive to their hydrophobic as well as hydrophilic interactions with the bilayers [35]. The hydrophobic interaction happens inside the bilayer, with the hydrophobic part of the bilayer whereas the hydrophilic interaction occurs at the aqueous-bilayer interface with the polar head groups of the lipids and the surrounding ions. A disturbance in these interactions is expected to affect their functionality and for curcumin our results combined with previous results [9-10] are expected to provide further insights about the ability of this drug to regulate various structurally-unrelated membrane proteins by changing the properties of the lipid bilayer. Finally, we note that a closer inspection of Figures 5.2 and the inset of Figure 5.7 reveal that the increase in the $E_{2\omega}$ signal of LDS^+ ions, immediately following addition of curcumin, is not instantaneous at low temperature. This indicates that disruption of Na^+–lipid interactions and formation of curcumin-lipid hydrogen bonding is a kinetically controlled process. Attempts will be made to investigate this aspect in the next study.

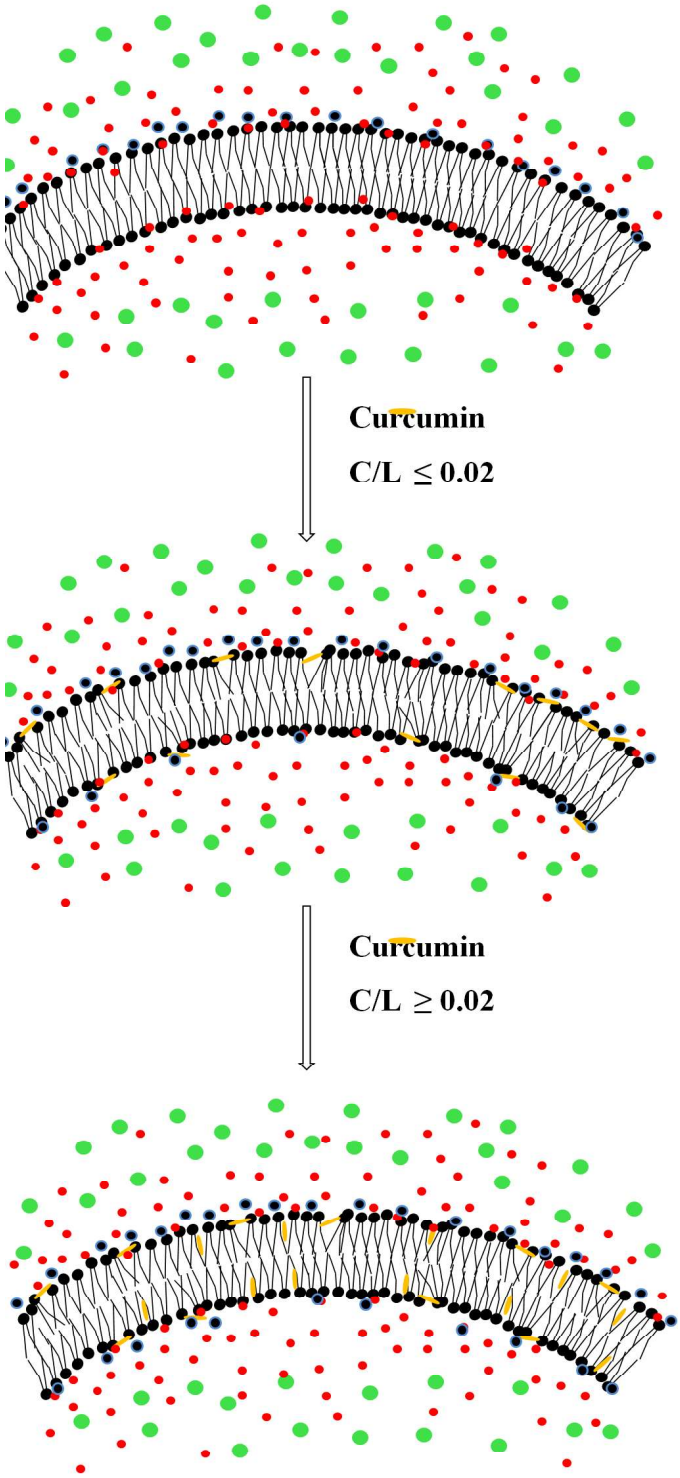

Figure 5.9: *Cartoon showing how curcumin binds and disturbs the POPG bilayer and affects the adsorption and transport of the LDS^+ ions. The LDS^+ ions adsorb initially on the outer bilayer (top) of the POPG liposomes and then transports to the inner bilayer (bottom).*

References

1. Schreier, S.; Malheiros, S. V. P.; de Paula, E. *Biochimica et Biophysica Acta* **2000,** *1508*, 210−234.
2. Peetla, C.; Stine, A.; Labhasetwar, V. *Molecular Pharmaceutics* **2009**, *6*, 1264−1276.
3. Gupta, S. C.; Patchva, S.; Aggarwal, B. B. *The AAPS Journal* **2013**, *15*, 195−218.
4. Ravindran, J.; Prasad, S.; Aggarwal, B. B. *The AAPS Journal* **2009**, *11*, 495-510.
5. Hatcher, H.; Planalp, R.; Cho, J.; Torti, F. M.; Torti, S. V. *Cellular and Molecular Life Sciences* **2008**, *65*, 1631−1652.
6. Maheshwari, R. K.; Singh, A. K.; Gaddipati, J.; Srimal, R. C. *Life Sciences* **2006**, *78*, 2081−2087.
7. Bilmen, J. G.; Khan, S. Z.; Javed, M. U. H.; Michelangeli, F.*Eur. J. Biochem* **2001**, *268*, 6318−6327.
8. Ingolfsson, H. I.; Koeppe, R. E.; Andersen, O. S. *Biochemistry* **2007,** *46,* 10384−10391.
9. Hung, W. C.; Chen, F. Y.; Lee, C. C.; Sun, Y.; Lee, M. T.; Huang, H. W.*Biophys. J.* **2008**, *94*, 4331−4338.
10. Sun, Y.; Lee, C-C.; Hung, W-C.; Chen, F-Y.; Lee, M-T.; Huang, H. W. *Biophys. J.* **2008**, *95*, 2318−2324.
11. Barry, J.; Fritz, M.; Brender, J. R.; Smith, P. E.; Lee, D. K.; Ramamoorthy,A. *J. Am. Chem. Soc*. **2009**, *131*, 4490−4498.
12. Perez-Lara, A.; Ausili, A.; Aranda, F. J.; Godos, A.; Torrecillas, A.; Corbalan-Garcia, S.; Gomez-Fernandez, J. C. *J. Phys. Chem. B* **2010**, *114*, 9778−9786.
13. Varshney, G. K.; Saini, R. K.; Gupta, P. K.; Das, K. *Langmuir* **2013**, *29*, 2912−2918.
14. Tsukamotoa, M.; Kuroda, K.; Ramamoorthy, A.; Yasuhara, K.*Chem. Comm*. **2014**, *50*, 3427−3430.
15. Eisenthal, K. B.*Chem. Rev*. **2006**, *106*, 1462−1477.

16. Srivastava, A.; Eisenthal, K. B.*Chem. Phys. Lett*. **1998**, *292*, 345−351.

17. Liu, Y.; Yan, E. C. Y.; Eisenthal, K. B. *Biophys. J*. **2001**, *80*, 1004−1012.

18. Liu, J.; Subir, M.; Nguyen, K. *J. Phys. Chem. B* **2008**, *112*, 15263−15266.

19. Saini, R. K.; Dube, A.; Gupta, P. K.; Das, K. *J. Phys. Chem. B* **2012**, *116*, 4199−4205.

20. Bernabe-Pineda, M.; Ramirez-Silva, M. T.; Romero-Romob, M.; Gonzalez-Vergara, E.; Rojas-Hernandez, A. *Spectrochim. Acta Part A* **2004**, *60*, 1091−1097.

21. Wang, Z.; Leung, M. H. M.; Kee, T. W.; English, D. S. *Langmuir* **2010**, *26*, 5520−5526.

22. Adhikary, R.; Mukherjee, P.; Kee, T. W.; Petrich, J. W. *J. Phys. Chem. B* **2009,** *113*, 5255−5261.

23. Adhikary, R.; Carlson, P. J.; Kee, T. W.; Petrich, J. W. *J. Phys. Chem. B* **2010,** *114*, 2997−3004.

24. Ghosh, R.; Mondal, J. A.; Palit, D. K. *J. Phys. Chem. B* **2010**, *114*, 12129−12143.

25. Ke, D.; Wang, X.; Yang, Q.; Niu, Y.; Chai, S.; Chen, Z.; An, X.; Shen, W. *Langmuir* **2011**, *27*, 14112−14117.

26. Erez, Y.; Presiado, I.; Gepshtein, R.; Huppert, D. *J. Phys. Chem. A* **2011**, *115*, 10962−10971.

27. Erez, Y.; Presiado, I.; Gepshtein, R.; Huppert, D. *J. Phys. Chem. A* **2012**, *116*, 2039−2048.

28. Saini, R. K.; Das, K. *J. Phys. Chem. B* **2012**, *116*, 10357−10363.

29. Saini, R. K.; Das, K. *J. Lumin.* **2014**, *145*, 832-837.

30. Shen, L.; Ji, H. F. *Spectrochim. Acta Part A* **2007**, *67*, 619-623.

31. Zhao, W.; Rog, T.; Gurtovenko, A. A.; Vattulainen, I.; Karttunen, M. *Biophys. J*. **2007**, *92*, 1114−1124.

32. Zhao, W.; Rog, T.; Gurtovenko, A. A.; Vattulainen, I.; Karttunen, M. *Biochimie* **2008**, *90*, 930−938.

33. Tolokh, I. S.; Vivcharuk, V.; Tomberli, B.; Gray, C. G. *Phys. Rev. E* **2009**, *80*, 031911.

34. Von Deuster, C. I.; Knecht, V. *Biochim. Biophys. Acta Biomembr*. **2011**, *1808*, 2867−2876.

35. Mondal, J. A.; Nihonyanagi, S.; Yamaguchi, S.; Tahara, T. *J. Am. Chem. Soc*. **2010**, *132*, 10656−10657.

36. Mondal, J. A.; Nihonyanagi, S.; Yamaguchi, S.; Tahara, T. *J. Am. Chem. Soc*. **2012**, *134*, 7842−7850.

37. Kundu, A.; Yamaguchi, S.; Tahara, T. *J. Phys. Chem. Lett*. **2014**, *5*, 762−766.

38. Sachs, J. N.; Engelman, D. M. *Ann. Rev. Biochem*. **2006**, *75*, 707−12.

Chapter 6

Effect of curcumin addition on the adsorption and transport of a cationic dye across DPPG-POPG liposomes probed by second harmonic spectroscopy

6.1 Introduction

A lot of biological phenomena are triggered due to some events taking place at a biological interface. One of the most ubiquitous biological interface is the aqueous-membrane interface where events like adsorption and transport can lead to significant changes in cellular functioning. A powerful approach to study interfacial phenomena is based on the spectroscopic methods of second harmonic and sum-frequency generation (SHG & SFG respectively) [1-5]. The reason behind the selectivity of these spectroscopic techniques to exclusively probe the interfacial region lies on the fact that that these second-order processes are electric dipole forbidden in centrosymmetric media but allowed in non-centrosymmetric media such as an interface. Several types of interfacial phenomena has been probed by SHG and SFG spectroscopy [1-5]. Among them, the adsorption and transport kinetics of several organic ions across a lipid bilayer has been monitored by the SHG technique [6-17]. The principle behind this has been already discussed in Chapter 1.

Although the adsorption and bilayer transport of an ion is primarily driven by the electrostatic force of attraction between the oppositely charged ion and the bilayer head group, it can change drastically during the partitioning of a lipophilic molecule from aqueous to bilayer phase [8,10,13-18]. For example, utilizing the SHG spectroscopic technique we have shown that, curcumin, a well known drug, increases the adsorption and transport of a cationic

hemicyanine dye, LDS^+, across a negatively charged POPG (1-palmitoyl-2-oleoyl-sn-glycero-3-phospho-(1'-rac-glycerol) bilayer while partitioning from the aqueous to the bilayer phase (Chapter 5). Interestingly, the increase in the adsorption of LDS^+ ions was attributed to curcumin induced release of Na^+ counter-ions from the bilayer head group region.

There have been numerous reports of strong counter-ion lipid head-group interactions in liposomes having either charged or zwitterionic head groups (e.g. phosphatidylcholine: PC; phosphatidylserine: PS; phosphatidylglycerol: PG) [19-27]. In particular this interaction is quite relevant for liposomes where the head groups are charged (e.g. PG) and the formation of counter ion-lipid complexes are necessary to balance the repulsive force arising due to similar charge of the lipid head groups and preserve the integrity of the bilayers [19-20,26-27]. Anything which disrupts the counter ion-lipid complexes are therefore expected to de-stabilize the bilayer by increasing the electrostatic repulsion between the like charged head groups of the lipid. In fact it has been shown that de-stabilization of POPG bilayer by some cationic polymers [28-29] as well as cationic anti-microbial peptides [30-31] is associated with the counter-ion release from the head group region due to the electrostatic binding between the macromolecule and the PG head group.

Since it is well known that a lipid bilayer consisting of saturated acyl chains (e.g. 1,2-dipalmitoyl-sn-glycero-3-phospho-(1'-rac-glycerol): DPPG) will be more rigid compared to that consisting of unsaturated acyl chains (e.g. POPG) it would be interesting to get at least a qualitative idea about the relative strength of the counter-ion–DPPG and counter-ion–POPG head-group interactions. Therefore, by monitoring the curcumin induced changes in the adsorption properties of the LDS^+ ions using the interface selective SHG spectroscopic technique we have attempted to compare the strength of these counter-ion PG head-group interactions. Results obtained showed a remarkable dependence of the adsorption properties of the LDS^+ ion with respect to bilayer acyl chain saturation/un-saturation (S/U) ratio which

we have tried to explain on the basis of different types of Na^+–lipid interactions present in liposomes constituted from a mixture of DPPG and POPG lipids.

6.2 Results

The average laser power used in the SHG experiments was 500 mW. The SH experiments were conducted as follows: The SH intensity of 50 μM liposome in buffer was monitored with time. At t = 0 second, a concentrated stock solution of LDS^+ ions was added to make the final concentration of LDS^+ ions 5 μM. Micro-liter aliquots from a concentrated stock solution of curcumin were added at t = 400 second to get the desired curcumin:lipid (C/L) ratio. We have prepared six different liposomes by varying the POPG:DPPG mole ratio from 1:0 to 0:1. These are characterized with respect to their size and zeta potential at 25 °C and listed in Table 6.1. The temperature dependent changes in the fluorescence anisotropy values of the membrane probe DPH for these liposomes is shown in Figure 6.1. It is well known that fluorescence anisotropy of DPH depends upon the bilayer rigidity [31]. It can be seen from Figure 6.1 that for some liposomes (POPG:DPPG mole ratio of 0:1, 1:5, 1:3 and 1:1) the temperature dependent trends of the fluorescence anisotropy values of DPH are "S" shaped indicating a phase transition (gel to liquid crystalline state) of the bilayer within the temperature range studied. These are fitted with a sigmoidal function to extract the phase transition temperature (T_m; provided in Table 2.4) from the inflection point. For pure DPPG liposomes the T_m was located at ~42.0 °C which is close to the reported value of 41 °C [38]. As the acyl chain un-saturation percentage increases the temperature dependent changes in the DPH anisotropy values becomes more diffuse signifying the increased disorder in the acyl chains. Accordingly the T_m values decreases and for liposomes having a higher mole-fraction of the un-saturated lipid POPG (POPG:DPPG mole ratio of 3:1 and 1:0), the temperature

dependent changes in the DPH anisotropy values follows a linear pattern indicating that at this temperature range there is no phase transition of the bilayer.

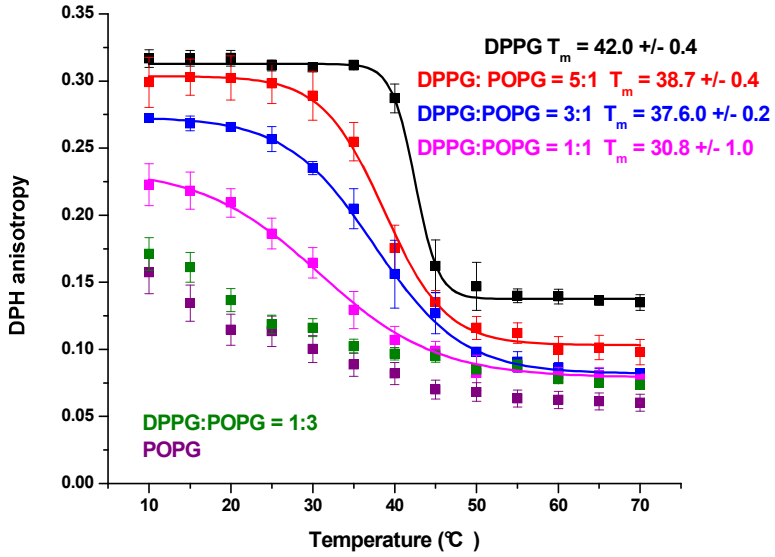

Figure 6.1: *Temperature dependent changes in the fluorescence anisotropy of the membrane probe DPH in presence of the six liposomes prepared from a mixture of POPG and DPPG lipids. The observed trends in the DPH fluorescence anisotropy suggests that out of the six liposomes, only four show a gel-liquid crystalline phase transition in the experimental temperature range. The solid lines are sigmoidal fits of the individual data point for these four sets of liposomes. The melting transition temperatures (T_m) obtained from the inflection point of the sigmoidal curve is also shown.*

We have recorded the time dependent changes of the SH intensity signal (at different temperatures) generated from a solution of these different DPPG-POPG liposomes to which 5 μM LDS^+ ions were added at t = 0 second and subsequently 5 μM curcumin (curcumin:lipid ratio: C/L = 0.10) was added at t = 400 second. After converting the SH intensity signal to SH electric field ($E_{2\omega}$), the temperature dependent $E_{2\omega}$ traces for each liposome are provided in Figure 6.2.

Figure 6.2

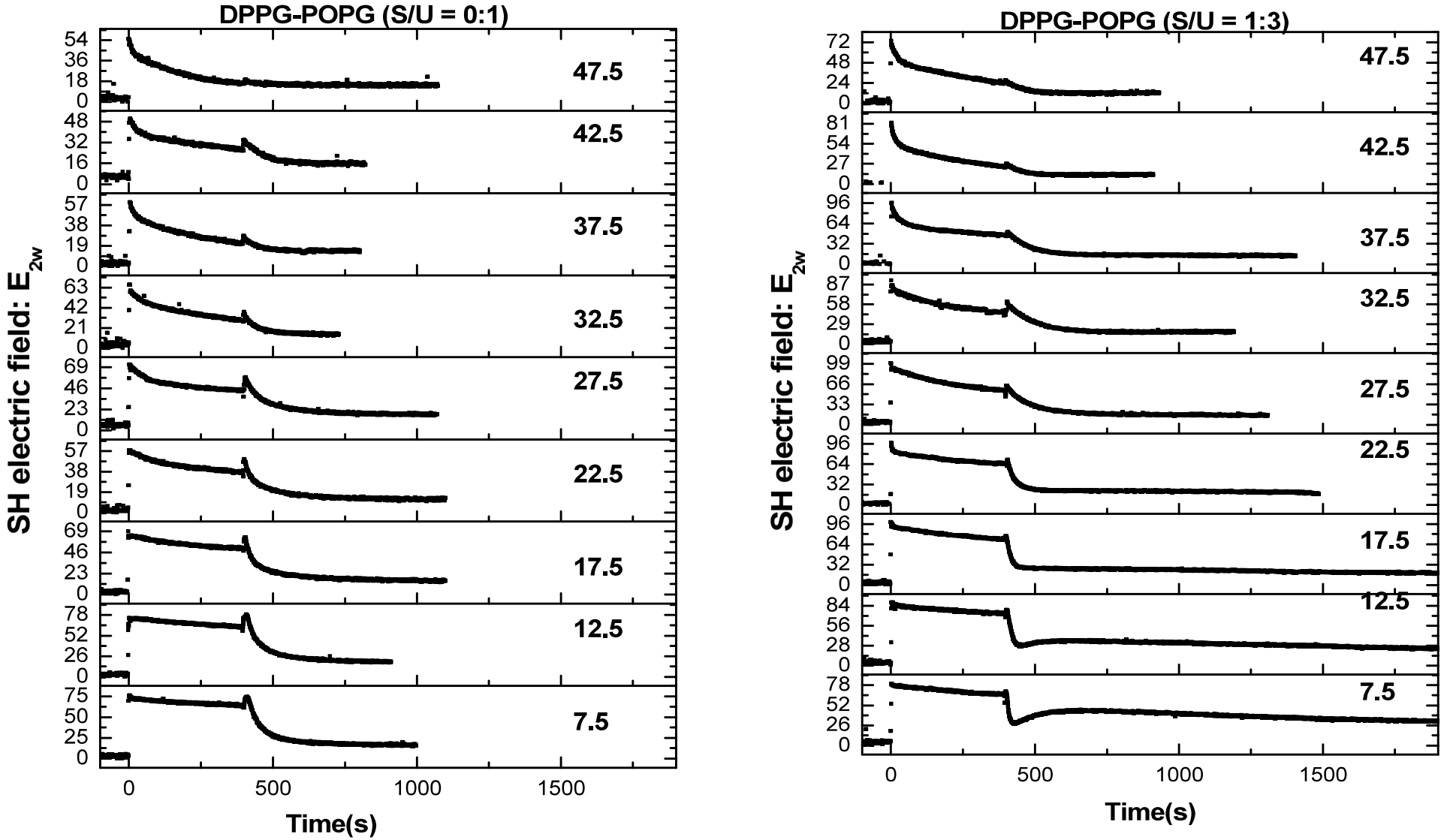
DPPG-POPG (S/U = 0:1)
DPPG-POPG (S/U = 1:3)
SH electric field: E_{2w}
47.5
42.5
37.5
32.5
27.5
22.5
17.5
12.5
7.5
Time(s)
0
500
1000
1500

Figure 6.2 (continued)

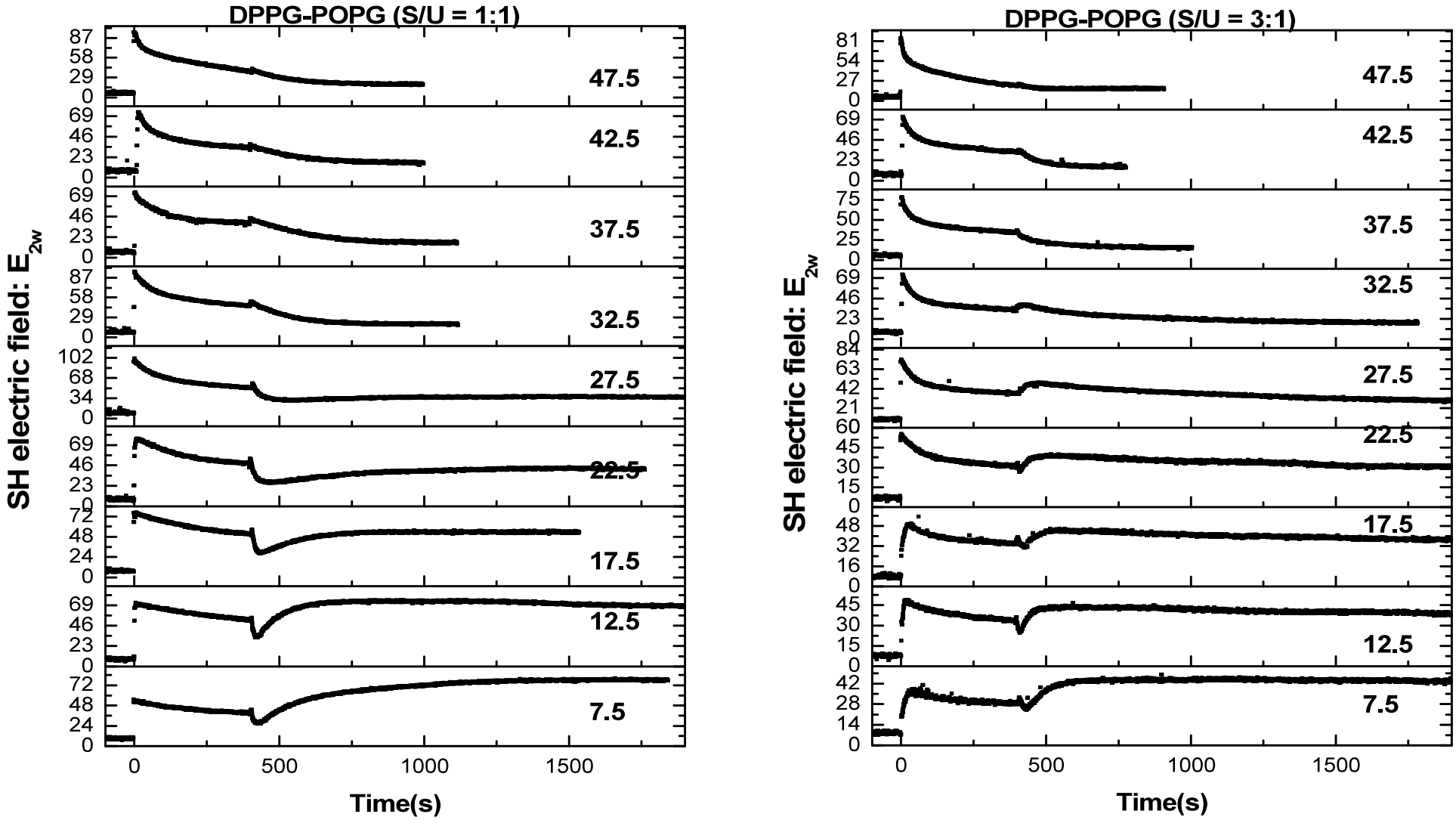

Figure 6.2 (continued)

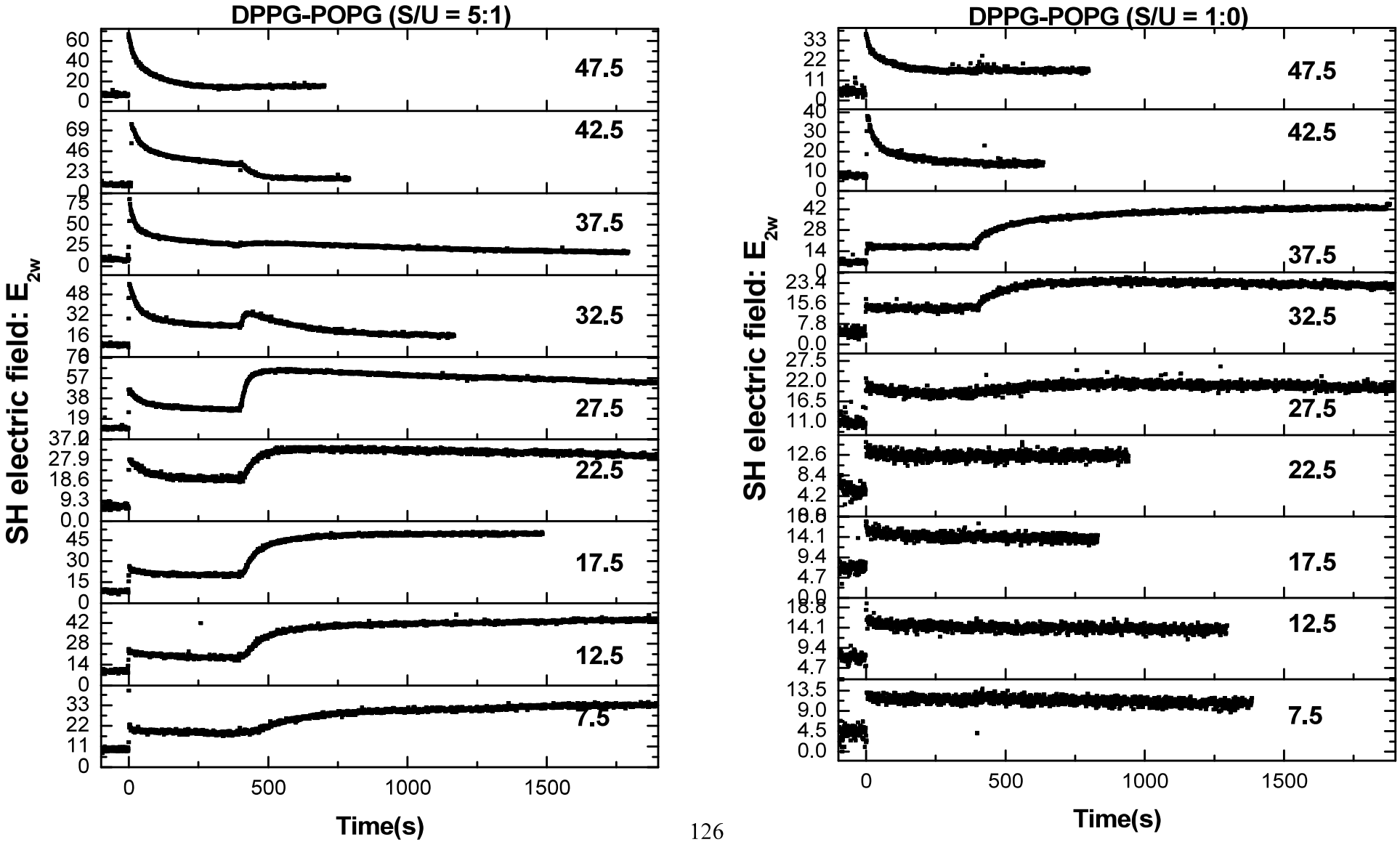

Figure 6.2: *Time dependent changes in the SH electric field ($E_{2\omega}$) generated from a mixture consisting of 50 μM liposome, 5 μM LDS^+ ions (added at t = 0s) and 5 μM curcumin (added at t = 400s) at three different temperatures. Changes the $E_{2\omega}$ signal of the LDS^+ ions upon addition of curcumin is seen to depend on the S/U ratio.*

Before addition of LDS^+ ions the observed $E_{2\omega}$ signal arises due to Hyper-Rayleigh scattering from the liposomes [17]. For all the cases, the instantaneous (< 1 second) increase in the $E_{2\omega}$ ($\Delta E_{2\omega}^{t0}$) as soon as LDS^+ ions were added is due to the rapid electrostatic adsorption of the LDS^+ ions on the negative charged outer bilayer surface as has been demonstrated in numerous studies earlier [6-18]. Therefore, the SH electric field, after addition of LDS^+ ions, is dominated by the $E_{2\omega}$ signal of LDS^+ ions ($E_{2\omega}(LDS^+)$) which then decreases gradually due to transport of the LDS^+ ions from the outer to inner lipid bilayers [16]. Although all the liposomes showed similar zeta potential values, it was observed that bilayer rigidity plays a crucial role in the adsorption of the LDS^+ ions ($\Delta E_{2\omega}^{t0}$) on the outer surface of the bilayer. At 7.5 °C, as the lipid acyl chain S/U ratio is increased the magnitude of the $\Delta E_{2\omega}^{t0}$ was observed to decrease; this was especially significant for DPPG:POPG liposomes having S/U ratio of 5:1 and 1:0, indicating that the gel-state of the bilayer is perhaps, not conducive enough for adsorption and subsequently the transport of the LDS^+ ions across the negatively charged bilayer. The instantaneous increase in measured SH signal following addition of LDS^+ ions ($\Delta E_{2\omega}^{t0}$) could be due to a combination of the HRS signal coming from the LDS^+ ions free in solution and LDS^+ ions adsorbed on the outer surface of the DPPG liposomes. One way of checking this is to compare the HRS signal generated from LDS^+ ions in absence of any liposomes with the $\Delta E_{2\omega}^{t0}$ signal. The measured SH electric signal of LDS^+ ions is 13 ± 2 counts per second under similar experimental conditions. Comparing this with the $\Delta E_{2\omega}^{t0}$ signal for the DPPG liposomes (Figure 6.2) indicates that there is insignificant adsorption of the LDS^+ ions on the outer surface of the DPPG liposomes till 37.5 °C. Above this temperature, the adsorption and subsequently the transport of the LDS^+ ions across the DPPG

bilayer can be observed. As the bilayer changes its state from the gel to liquid-crystalline phase, a significant increase in the $\Delta E_{2\omega}^{t0}$ values of the LDS^+ ions were observed indicating that the disordered state of the bilayer is now conducive enough for adsorption on the outer surface of the bilayer (Figure 6.2).

When curcumin (C/L = 0.10) is added at t = 400 second time point the $E_{2\omega}$ (LDS^+) signal was observed to change remarkably depending on the POPG:DPPG mole ratio (Figure 6.2). The instantaneous increase in the $E_{2\omega}$ (LDS^+) signal does not arises due to curcumin as demonstrated earlier in our previous study [17]. Over the entire temperature range of 7.5-47.5 °C, as soon as curcumin is added to a mixture of POPG liposomes and LDS^+ ions, the $E_{2\omega}$ (LDS^+) signal was observed to increase instantaneously (<1 second) followed by a decrease of the signal. Curcumin induced increase of the $E_{2\omega}$ (LDS^+) signal were observed to be temperature dependent: first they increases; reaches saturation (22.5 to 37.5 °C); and then starts to decrease. While this characteristic changes in the $E_{2\omega}$ (LDS^+) signal following curcumin addition is consistent with our previous study [17], when similar experiment is repeated using liposomes made from DPPG lipids, the increase in the $E_{2\omega}$ (LDS^+) signal could only be observed inside a narrow temperature window (27.5 to 37.5 °C) and contrary to POPG liposomes, the rate of increase in the $E_{2\omega}$ (LDS^+ ions) signal were not instantaneous but were observed to increase slowly over the entire experimental time window (Figure 6.2). When liposomes having different mole percentage of POPG and DPPG lipids were used, it was observed that depending upon the temperature, the curcumin induced characteristic changes in the $E_{2\omega}$ (LDS^+ ions) signal are either similar to that observed for only POPG or DPPG liposomes or a combination of both. Finally, at higher temperatures, the effect of curcumin on the $E_{2\omega}$ (LDS^+ ions) signal starts to level off. Overall the curcumin induced changes in the $E_{2\omega}$ (LDS^+ ions) signal observed in POPG-DPPG liposomes can be broadly classified into:

1) A fast kinetics (K_{POPG}) represented by an instantaneous (<1 second) rise followed by a fast decay of the $E_{2\omega}$ (LDS^+ ions) signal observed in the case of POPG liposomes.
2) A slow kinetics (K_{DPPG}) represented by a slow rise of the $E_{2\omega}$ (LDS^+ ions) signal (which remains constant thereafter within the experimental time window) observed in the case of DPPG liposomes.
3) A combination of K_{POPG} and K_{DPPG} kinetics observed in the $E_{2\omega}$ (LDS^+ ions) signal for liposomes made from POPG and DPPG lipids.
4) At higher temperatures, the K_{POPG} and K_{DPPG} kinetics merge together to form a single kinetics: K_{mix}; whose characteristics is similar to that of K_{POPG}.

Figure 6.3 shows a time expanded trace of a particular $E_{2\omega}$ (LDS^+ ions) signal (taken from Figure 6.2) where, following curcumin addition, the presence of both K_{POPG} and K_{DPPG} kinetics are clearly observed. The parameters related to the K_{POPG} and K_{DPPG} kinetics are: i) fractional increase in the $E_{2\omega}$ (LDS^+ ions) signal and ii) time constant of the decay of the $E_{2\omega}$ (LDS^+ ions) signal following the increase. Following our earlier work, we define curcumin induced fractional increase in the $E_{2\omega}$ (LDS^+ ions) signal as [17]:

$$\Delta E_{2\omega}^{fi} = \Delta E_{2\omega} / E_{2\omega}^{ti} \qquad (6.2)$$

where $\Delta E_{2\omega}$ is the *maximum observed difference* of the SH electric field as defined in Figure 6.3 and the index "i" refers to the individual kinetics. The following parameters corresponding to K_{POPG}, K_{DPPG} and K_{mix} kinetics are then calculated for each trace:

$\Delta E^{f1}{}_{2\omega}$ = fractional increase of the instantaneous signal of $E_{2\omega}$ (LDS^+ ions) signal occurring in the K_{POPG} regime.

$\Delta E^{f2}{}_{2\omega}$ = fractional increase of the instantaneous signal of $E_{2\omega}$ (LDS^+ ions) signal occurring in the K_{DPPG} regime associated with a time constant termed as tau^{f2}.

$\Delta E^{f12}{}_{2\omega}$ = fractional increase of the instantaneous signal of $E_{2\omega}$ (LDS^+ ions) signal at high temperatures for the POPG-DPPG liposomes.

For each trace, values corresponding to the parameters $\Delta E^{f1}{}_{2\omega}$, $\Delta E^{f2}{}_{2\omega}$, tau^{f2}, $\Delta E^{f12}{}_{2\omega}$ and the associated decays of the $E_{2\omega}$ (LDS^+ ions) signal were estimated and presented in Table 6.1. The time constants corresponding to the decay and rise time of the $E_{2\omega}$ (LDS^+ ions) signal (where both K_{POPG} and K_{DPPG} regimes are present) were obtained by part-by-part exponential fitting of the traces.

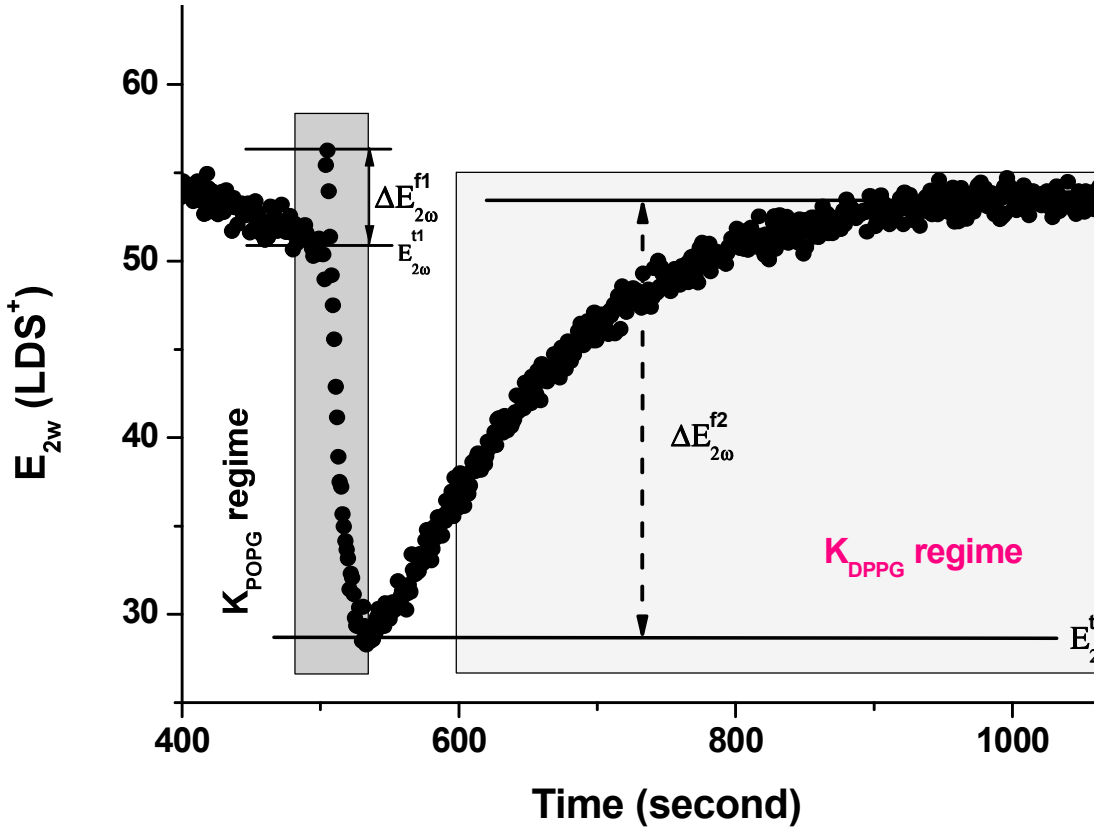

Figure 6.3: *A time-expanded trace of the $E_{2\omega}$ signal of the LDS^+ ions is shown to highlight the curcumin induced changes. The trace represents the changes in the $E_{2\omega}$ signal of the LDS^+ ions in presence of liposomes made from a POPG:DPPG S/U ratio of 1:1 at 17.5 °C, where curcumin (curcumin:lipid mole ratio = 0.10) is added at t = 400 second. The curcumin induced changes consists of an: 1) instantaneous (<1 second) increase; 2) a sharp decrease; followed by a 3) slow rise of the $E_{2\omega}$ signal of the LDS^+ ions. The method of estimation of the parameters, $\Delta E^{f1}{}_{2\omega}$ and $\Delta E^{f2}{}_{2\omega}$ are also shown. The time constants associated with the fast decay (K_{POPG} regime) and rise (K_{DPPG} regime) of the $E_{2\omega}$ signal of the LDS^+ ions are done by exponential fitting of the corresponding regions.*

Table 6.1: *Fitted parameters for the kinetic characteristics of the $E_{2\omega}$ (LDS^{+}) signal following curcumin addition at t = 400 second at different temperatures*

POPG						
Temp (°C)	**Ads & transport (after curcumin addition at t = 500s)**					
	K_{POPG}		**K_{DPPG}**		**K_{mix}**	
	$\Delta E^{f1}_{2\omega}$	**Decay**	**$\Delta E^{f2}_{2\omega}$ (tau^{f2})**	**Decay**	**$\Delta E^{f12}_{2\omega}$**	**Decay**
7.5	0.15±0.012	40±6				
12.5	0.22±0.02	27±5				
17.5	0.25±0.025	16±3				
22.5	0.32±0.036	15±2				
27.5	0.32±0.03	30±5				
32.5	0.33±0.04	48±7				
37.5	0.31±0.037	46±6				
42.5	0.27±0.034	65±9				
47.5	0.17±0.02	74±7				
POPG:DPPG = 3:1						
7.5	0.05±0.01	8±2	0.60±0.01 (110±20)	1000±150		
12.5	0.06±0.01	15±4	0.26±0.03 (80±14)	3000±600		
17.5					0.06±0.01	15±3
22.5					0.09±0.02	28±7
27.5					0.15±0.03	90±15
32.5					0.20±0.01	90±20
37.5					0.11±0.01	80±14
42.5					0.17±0.01	44±10
47.5					0.13±0.01	54±7
POPG:DPPG = 1:1						
7.5	0.10±0.01	5±2	1.93±0.3 (250±40)			
12.5	0.06±0.01	6±3	1.32±0.2 (150±20)			
17.5	0.11±0.01	9±2	0.93±0.1 (120±15)			
22.5	0.11±0.01	13±4	0.57±0.1 (70±7)			
27.5	0.14±0.02	23±6	0.16±0.1 (30±5)			
32.5					0.13±0.05	124±30
37.5					0.16±0.05	200±35
42.5					0.14±0.07	160±23
47.5					0.17±0.04	126±18
POPG:DPPG = 1:3						
Temp (°C)	Ads & transport (after curcumin addition at t = 500s)					
	K_{POPG}		K_{POPG}		K_{POPG}	
	$\Delta E^{f1}_{2\omega}$	Decay	$\Delta E^{f2}_{2\omega}$ ($\Delta E^{g1}_{2\omega}$)	Decay	$\Delta E^{f12}_{2\omega}$	Decay
7.5	0.12±0.02	8±2.0	0.78±0.10 (64±7)			
12.5	0.06±0.01	4±1.0	0.69±0.11 (31±5)			
17.5	0.15±0.02	5±1.5	0.42±0.09 (40±6)	1100±150		
22.5	0.08±0.01	6±2.0	0.44±0.06 (27±5)	1400±180		
27.5			0.31±0.05 (18±3)	842±100		
32.5			0.22±0.01 (5±2)	344±70		
37.5					0.10±0.02	105±15

42.5					0.08±0.01	65±10
47.5					0.03±0.01	32±5
POPG:DPPG = 1:5						
7.5			0.83±0.10 (220±30)			
12.5			1.36±0.08 (90±15)			
17.5			1.55±0.09 (82±12)			
22.5			0.70±0.07 (45±10)	1200±200		
27.5			1.33±0.10 (10±3)	3000±800		
32.5			0.39±0.10 (13±2)	200±50		
37.5			0.08±0.01 (85±2)	930±120		
42.5						
47.5						
DPPG						
7.5						
12.5						
17.5						
22.5						
27.5			0.2±0.08 (440±50)			
32.5			0.8±0.10 (110±25)			
37.5			1.6±0.20 (70±10)			
42.5						
47.5						

Error bars represent standard deviation of three experiments performed with freshly prepared liposomes.

Figure 6.4 describes how these parameters ($\Delta E^{f12}{}_{2\omega}$, $\Delta E^{f1}{}_{2\omega}$, $\Delta E^{f2}{}_{2\omega}$ and tau^{f2}) of the LDS^{+} ion depends upon lipid acyl chain S/U ratio and temperature for a fixed C/L mole ratio (0.10). Each individual graphs corresponding to a particular lipid S/U ratio are color coded into different zones to highlight the presence of different kinetic regimes (blue: K_{POPG} and K_{DPPG}; green: K_{DPPG}; grey: K_{POPG} and white: K_{mix}) associated with varying lipid acyl chain S/U ratio and temperature. In addition the temperature dependent fluorescence anisotropy values of DPH for each liposome were also superimposed on each graph to provide an idea about how the different kinetic regimes are associated with the gel, gel-LC and the LC phase state for liposomes having a particular S/U ratio.

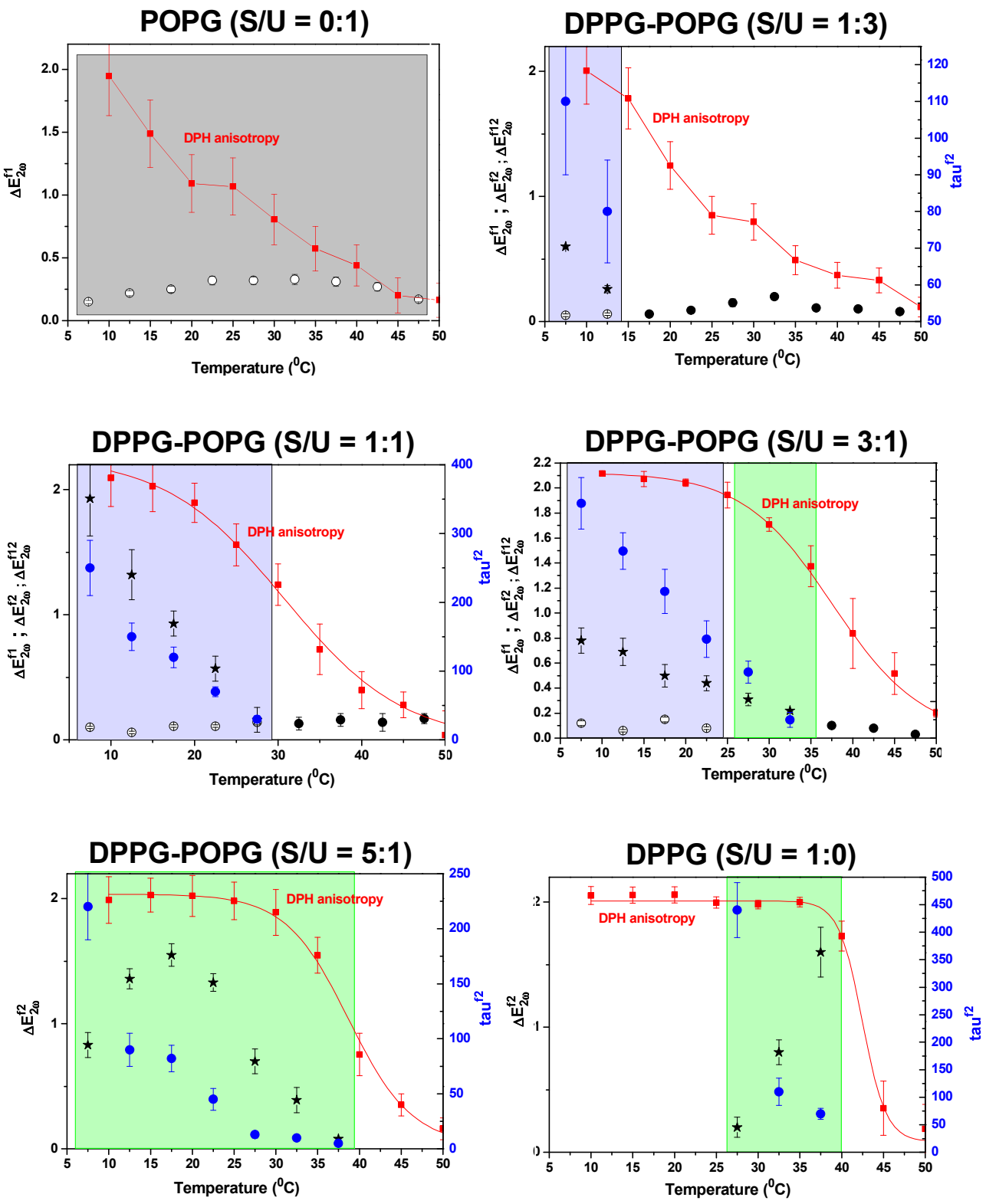

Figure 6.4: *A plot of the various parameters ($\Delta E^{f1}{}_{2\omega}$: open black circles, $\Delta E^{f2}{}_{2\omega}$: black stars, tau^{f2}: blue circles, and $\Delta E^{f12}{}_{2\omega}$: closed black circles) corresponding to the K_{POPG}, K_{DPPG} and K_{mix} regime versus temperature for each of the six set of liposomes.*

By looking at the different color zones in Figure 6.4 the following points can be summarized:

1) Both fast (K_{POPG}) and slow (K_{DPPG}) kinetics are observed at lower temperature range when the bilayer is in the gel state. This temperature range was observed to be dependent on the S/U ratio. For example, liposomes which have a 1:3 S/U ratio, signature of both K_{POPG} and K_{DPPG} in the $E_{2\omega}$ (LDS^+ ions) signal was observed till 12.5 °C, which increases to 27.5 °C and 22.5 °C for liposomes having S/U ratio of 1:1 and 3:1 respectively. In addition, for liposomes having a S/U ratio of 3:1, only the slow (K_{DPPG}) kinetics could be observed in a narrow temperature range (25-35 °C).
2) When the S/U ratio was further increased to 5:1 curcumin induced changes resulted exclusively the K_{DPPG} kinetic part, which was observed till 37.5 °C. The $E_{2\omega}$ (LDS^+ ions) signal was observed to increase slowly with time and in most cases not decay within the experimental time window.
3) In addition, while the magnitude of the fractional increase of the $E_{2\omega}$ (LDS^+ ions) signal corresponding to the K_{POPG} and K_{mix} regime ($\Delta E^{f1}{}_{2\omega}$ and $\Delta E^{f12}{}_{2\omega}$) were observed to be more or less similar over the entire temperature range, the magnitude of the same for the K_{DPPG} regime ($\Delta E^{f2}{}_{2\omega}$ and its associated rise time: tau^{f2}) were observed to decrease with increase in temperature.

Figure 6.4 suggests that the gel state of the bilayer favors the simultaneous occurrence of both fast (K_{POPG}) and slow (K_{DPPG}) kinetics provided that the lipid acyl chain S/U ratio lies in the range of 3:1 to 1:3. In an attempt to investigate how the K_{POPG} and K_{DPPG} kinetics are affected with C/L ratio we have used the liposome with S/U ratio 1:1 and monitored the changes in the $E_{2\omega}$ (LDS^+ ions) signal. Two temperatures are selected where one temperature corresponds to the gel state (10 °C) and the other corresponds to the transition from the gel to the LC state (20 °C). For each of these temperatures the C/L ratio is varied (from 0.002 to

0.200) and curcumin induced changes in the $E_{2\omega}$ (LDS^+ ions) signal were recorded (similar to experiments reported in Figure 6.2). Figure 6.5 describes the effect of changing C/L ratio on the $E_{2\omega}$ (LDS^+ ions) signal at two different temperatures for the 1:1 S/U ratio liposome. Figure 6.6 describes how the following parameters: $\Delta E^{f1}{}_{2\omega}$, $\Delta E^{f2}{}_{2\omega}$ and tau^{f2} of the LDS^+ ion depends upon the C/L mole ratio and temperature. Like Figure 6.4, here also the individual graphs are further divided into similar color zones to understand better the presence of individual kinetic regimes (blue: K_{POPG} and K_{DPPG}; and grey: K_{POPG}). It is clear from Figure 6.6 that at a lower C/L ratio the gel state of the bilayer is more conducive for the simultaneous occurrence of both K_{POPG} and K_{DPPG} kinetics.

6.3 Discussions

The objective of this study was to investigate the relative strength of the Na^+–POPG and Na^+–DPPG interactions by monitoring curcumin induced changes in the adsorption and transport properties of the LDS^+ ions across a PG bilayer containing POPG and DPPG lipids. To carry out this objective we have prepared six different liposomes made from POPG and DPPG lipids, where, by varying the acyl chain S/U ratio, the ordering in the hydrophobic chain region of the bilayer have been systematically manipulated. As expected, with increasing S/U ratio more ordering was introduced in the acyl chains and it resulted in four liposomes which showed distinct gel to LC phase transition characteristics within the temperature range used in this study (Figure 6.1).

Before we discuss the curcumin induced changes in the $E_{2\omega}$ (LDS^+ ions) signal we must note that the interaction of curcumin with lipid bilayers depends upon the bilayer rigidity and this has been shown to be higher (two times) for un-saturated PC liposomes compared to saturated PC liposomes [34]. Therefore, in our case, as the S/U ratio is increased, curcumin binding with the PG bilayer is expected to decrease, i.e. the bilayer concentration of the drug is expected to be lower.

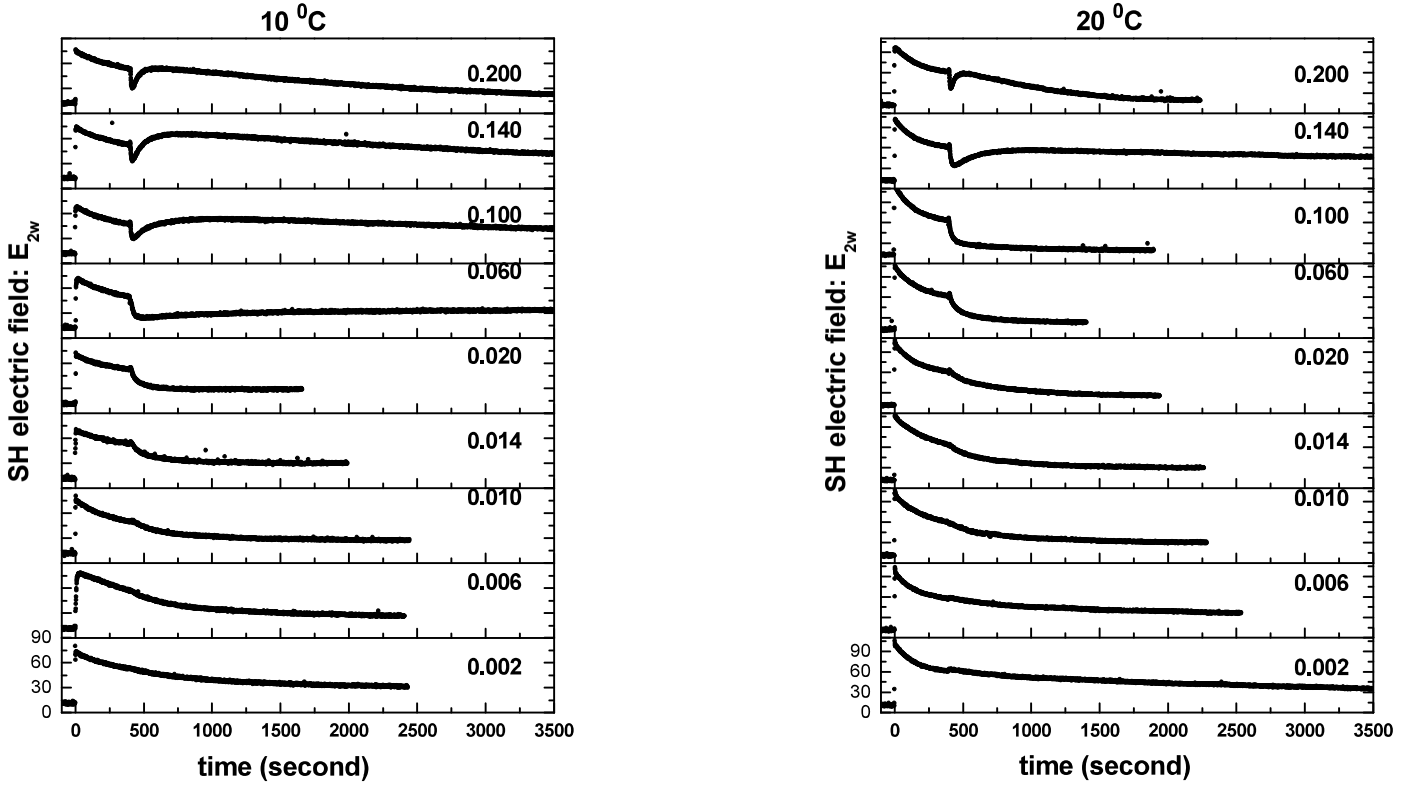

Figure 6.5: *The effect of increasing C/L ratio: Time dependent changes in the SH electric field ($E_{2\omega}$) generated from a mixture consisting of 50 μM 1:1 POPG: DPPG liposomes, 5 μM LDS^+ions (added at t = 0s) and curcumin (added at t = 400s) at 10 and 20 °C. The individual curcumin:lipid (C/L) mole ratio are indicated in each panel. The Y-axis for each panel corresponding to a particular temperature was kept same for clarity*

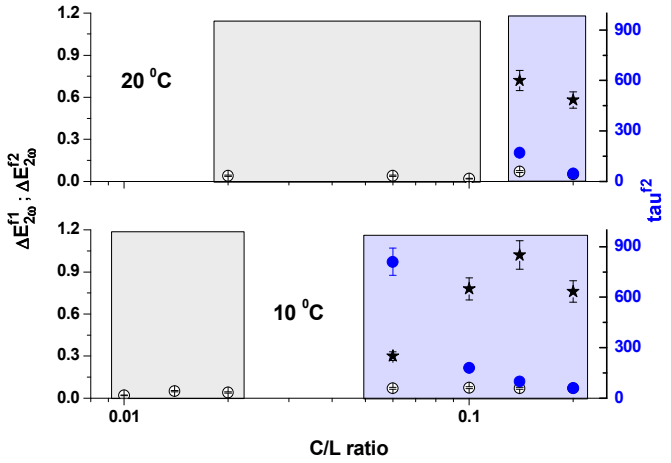

Figure 6.6: *A plot similar to Figure 6.4, except here only 1:1 POPG:DPPG liposome was used at two temperatures, 10 and 20 °C, to see the change in the various parameters ($\Delta E^{f1}{}_{2\omega}$: open black circles, $\Delta E^{f2}{}_{2\omega}$: black stars, and tau^{f2}: blue circles) with increasing C/L ratio.*

Table 6.2*: Fitting parameters for the kinetic characteristics of the $E_{2\omega}$ (LDS^{+}) signal following curcumin addition at t = 400 second for POPG:DPPG (1:1) liposome at two different temperature with increasing C/L ratio.*

C/L	10 °C					
	$\Delta E^{f1}{}_{2\omega}$	Decay	$\Delta E^{f2}{}_{2\omega}$ (tau^{f2})	Decay	$\Delta E^{f12}{}_{2\omega}$	Decay
0.002						
0.006						
0.010					0.02±0.01	
0.014					0.05±0.02	
0.020					0.04±0.02	
0.060	0.07±0.01	7±2	0.3±0.09 (810±90)			
0.100	0.08±0.02	5±1	0.78±0.09 (180±20)	3000±500		
0.140	0.07±0.01	6±2	1.02±0.11 (100±13)	2400±300		
0.200	0.07±0.01	4±1	0.76±0.08 (60±8)	2660±290		
C/L	**20 °C**					
	$\Delta E^{f1}{}_{2\omega}$	Decay	$\Delta E^{f2}{}_{2\omega}$ ($\Delta E^{g1}{}_{2\omega}$)	Decay	$\Delta E^{f12}{}_{2\omega}$	Decay
0.002					0.03±0.01	
0.006					0.03±0.01	
0.010					0.02±0.01	
0.014					0.03±0.01	
0.020					0.04±0.02	
0.060					0.04±0.02	
0.100					0.02±0.01	
0.140	0.07±0.01	11±3	0.72±0.10 (170±25)			
0.200	0.05±0.01	5±2	0.58±0.08 (50±12)	740±80		

Error bars represent standard deviation of three experiments performed with freshly prepared liposomes.

The observed trends in the $E_{2\omega}$ (LDS^+ ions) signal following curcumin addition for each sets of liposome are seen to be sensitive to the lipid S/U ratio. In particular, the presence of three distinct kinetic signatures (K_{POPG}, K_{DPPG} & K_{mix}) in the $E_{2\omega}$ (LDS^+ ions) signal suggests that interaction of curcumin with PG bilayer is happening in at least three different ways. Since following curcumin addition the kinetic features of the $E_{2\omega}$ (LDS^+ ions) signal are basically similar, (i.e. it increases and then decreases or starts to decrease) it is reasonable to assume that in all the cases curcumin is disrupting the Na^+-lipid head-group complex by binding itself at the PG head group region. At this point it is pertinent to examine carefully how the $E_{2\omega}$ (LDS^+ ions) signal is affected by the partitioning of curcumin from the aqueous phase to the bilayer. As suggested in previous studies [35-36] and confirmed by our earlier work [17], a two state model for curcumin partitioning into a POPG bilayer was proposed where the drug at low concentration adsorbs on the aqueous-bilayer region releasing the Na^+ counter ions and at high concentration intercalates into the hydrophobic region of the bilayer. We would also like to note that solid state NMR studies performed earlier suggests that curcumin is intercalated in the hydrophobic region of liposomes through hydrogen bond interaction with terminal phosphate groups which also marginally lowers the phase transition temperatures [47]. In addition, cationic molecules like ionic liquids were also shown to influence the phase transition temperature of liposomes in the presence of curcumin [48-49].

The surface bound drug is responsible for the increase in the $E_{2\omega}$ (LDS^+ ions) signal and the bilayer intercalated state of the drug is responsible for the faster transport of LDS^+ ions, i.e. rapid decay of the $E_{2\omega}$ (LDS^+ ions) signal [17]. Therefore the parameters: $\Delta E^{f1}{}_{2\omega}$, $\Delta E^{f2}{}_{2\omega}$ and $\Delta E^{f12}{}_{2\omega}$; associated with the K_{POPG}, K_{DPPG} and K_{mix} regime would be related to the curcumin molecules which are located at the interfacial region of the bilayer. While the changes in $\Delta E^{f1}{}_{2\omega}$ and $\Delta E^{f12}{}_{2\omega}$ occurs instantaneously (< 1 second) the changes in $\Delta E^{f2}{}_{2\omega}$ were observed to take place at a much slower rate indicating that in the K_{DPPG} regime the Na^+-lipid head-

group complex is much stronger compared to K_{POPG}, and K_{mix} regime. In addition, since the $E_{2\omega}$ (LDS^+ ions) signal decays faster in K_{POPG}, and K_{mix} regime it indicates that in these regimes a certain fraction of the drug molecules is also in the bilayer intercalated state, whereas in the K_{DPPG} regime the population of the drug molecules remains largely associated at the bilayer surface.

We now attempt to present a possible explanation of the results obtained in this study as follows:

1) Curcumin induced changes in the $E_{2\omega}$ (LDS^+ ions) signal in presence of DPPG liposomes can be observed only in a narrow temperature range (27.5 to 37.5 °C): There are at least two factors which is responsible. The first one is the binding strength of curcumin with the DPPG bilayer and the second one is the pre-transition melting of the DPPG bilayers [33], i.e. the ripple phase present between the gel and the LC phase [37]. We note that the temperature range where it is observed coincides with the existence of the ripple phase state of the DPPG bilayers [33], and therefore we propose that in this phase state, curcumin is able to slowly disrupt the Na^+-DPPG complex thereby causing a slow increase in the $E_{2\omega}$ (LDS^+ ions) signal. The disappearance of this effect at higher temperatures is most likely due to the reduced binding of curcumin with DPPG liposomes. This is consistent with a previous study [34] where it has been reported that the binding constant of the drug (with saturated PC liposomes) reduces by three times as the temperature is increased from 25 to 50 °C.
2) Observation of both K_{POPG} and K_{DPPG} type kinetics in liposomes made from a mixture of POPG and DPPG lipids (except 5:1) suggests that in these lipid mixtures both Na^+-POPG and Na^+-DPPG complex are formed, their relative abundance being directed by the S/U ratio. Since, compared to the LC state, the gel state of these liposomes was

observed to favor the formation of both the counter-ion lipid complexes we propose that *in the gel state individual domains of POPG and DPPG lipids are formed*. It is pertinent to note that in an earlier study, domain separation was observed in GUVs prepared from a mixture of DOPG and DPPG lipids by confocal microscopy [38]. The phase separation into individual POPG and DDPG domains were ascribed to the differential interactions between the acyl chains of the lipid. The differential interaction arises due to the differences in the cross-sectional area of the individual acyl chains of POPG (~67 $^{o}A^{2}$ at 30 °C) and DPPG (~48 $^{o}A^{2}$ at 20 °C) lipids. Due to this the counter-ion concentrations were near the vicinity of the DPPG head group was calculated to be higher than that for POPG lipids. This further supports our contention that Na^{+}-DPPG interaction is stronger than Na^{+}-POPG interaction.

3) It is interesting to note that in the POPG domain, the Na^{+}-POPG complexes are weaker than that formed in pure POPG liposomes and partitioning of curcumin from the aqueous phase to this domain is efficient as suggested by the instantaneous rise followed by the very fast decay of the $E_{2\omega}$ (LDS^{+} ions) signal (Table 6.2 and Figure 6.4). In addition, results obtained from C/L variation experiments using liposomes having 1:1 S/U ratio (Figure 6.6) clearly indicates that at lower C/L ratio, curcumin interacts preferentially with the POPG domains whereas at higher C/L ratio it is able to interact with the DPPG domain. Consistent with the fact that increasing temperature should induce more disordering in the lipid acyl chains, thereby weakening the Na^{+}-DPPG interaction, the values of $\Delta E^{f2}_{2\omega}$ and tau^{f2} (associated with the DPPG domain) decreases with increasing temperature and in some cases the $E_{2\omega}$ (LDS^{+} ions) signal following the completion of tau^{f2} was observed to decay implying that in some cases, curcumin is able to intercalate in bilayer associated with the DPPG domain. With further increase in temperature, for a particular S/U ratio, as more

disorder is introduced in the bilayer, our results indicate that the individual POPG and DPPG domains starts to mix to form a single domain where POPG and DPPG lipids are randomly distributed. It is in this domain the K_{mix} kinetics are observed where the kinetic feature of curcumin induced disruption of the Na^{+}-lipid head-group complex is quite similar to K_{POPG}. However it must also be noted that increase in temperature also decreases the association of curcumin with the lipid bilayer and therefore at higher temperatures the effects of curcumin start to decrease substantially.

Finally, the results obtained by us are summarized in a cartoon (Figure 6.7) where the existence of pure POPG, pure DPPG and mixed POPG-DPPG domains in a bilayer are shown. The effect of curcumin on these individual domains resulting in the differet type of kinetic charecteristics of the LDS+ ions is also shown.

6.4 Summary and conclusions

The role of metal ions (especially Na^{+} and Ca^{+2}) binding to biological membranes is of interest as it affects the structure, dynamics, and stability of lipids, which in turn affect folding, binding, and insertion of proteins. Ion interaction with phospholipids is driven mainly by Coulombic forces near the headgroup region and is therefore more pronounced for anionic lipids [39]. There are several reports of individual domain formation or phase separation in heterogeneous lipid bilayers prepared from a mixture of lipids, especially using a zwitterionic (PC) and an anionic (PS, PI PG etc) with or without cholesterol [40-43]. The formation of individual domains, especially which are anionic in nature is especially important from the view point of protein adsorption and their functioning [39], as well as pore formation induced by charged bio-macromolecules [28-31]. It is important to note that first step in this phase separation involves some electrostatic interaction between the negatively charged lipids and positively charged ions or macromolecules. In this context, the

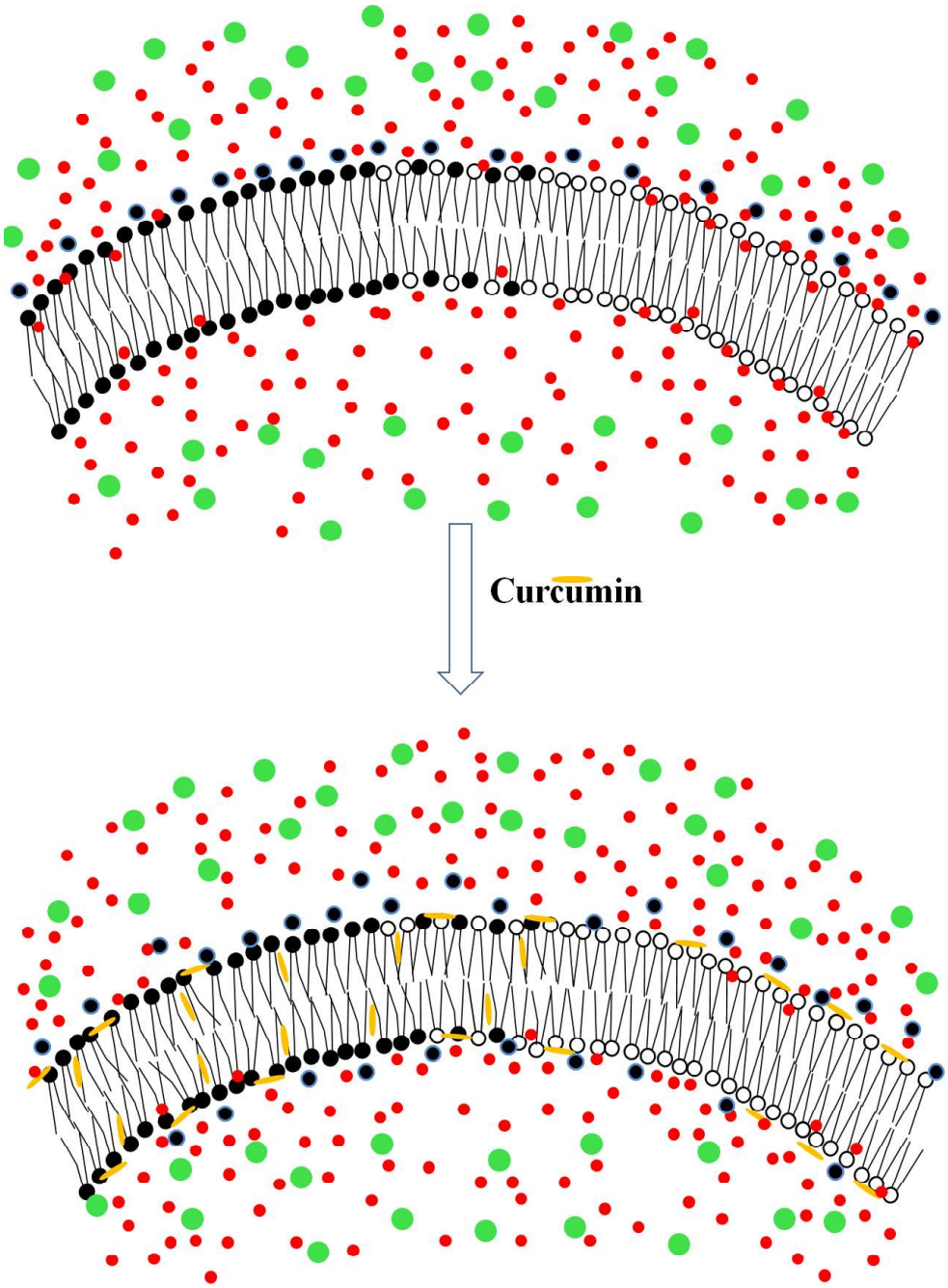

Figure 6.7: *Cartoon showing how formation of individual and mixed domains of POPG (solid head group) and DPPG (hollow head group) lipids modulates the curcumin induced modifications of the bilayer and its effect on the adsorption and transport characteristics of the* LDS^{+} *ions.*

results obtained in this study (and earlier [38]) is of importance as it has suggested that domain formation in lipid mixtures having same head groups is also possible due to the differential packing tendency of the saturated and unsaturated acyl chains of the lipids. In addition, this study further demonstrates the ability of curcumin to change the properties of lipid bilayer which has been postulated as a major cause for the various biological activities of this drug [44-45]. It must be mentioned that in this work, and also in our earlier work [17], we have emphasized only on the counter-ion lipid head group interactions. However, the role of interfacial water molecules must be also acknowledged and investigated. In fact, using the heterodyne detected electronic SFG spectroscopic technique the importance of interfacial water has been summarized recently [5]. In addition MD studies also showed that formation of the Na^+-lipid complexes becomes energetically more stable when a water molecule is shared between them [19,30-31,46]. Therefore it is important to investigate the role of interfacial water on the curcumin induced disordering in the PG bilayer. One way to examine the role of water is by using deuterated water (D_2O) as solvent. This work is presented in the next chapter.

References

1. Eisenthal, K. B.*Chem. Rev*. **2006**, *106*, 1462−1477.
2. Yan, E. C. Y.; Fu, L.; Wang, Z.; Liu, W. *Chem. Rev*. **2014**, *114*, 8471−8498.
3. Johnson, C. M. *Chem. Rev*.**2014**, *114*, 8416−8446.
4. Roy, S.; Covert, P. A.; FitzGerald, W. R.; Hore, D. K. *Chem. Rev*.**2014**, *114*, 8388−8415.
5. Nihonyanagi, S.; Yamaguchi, S.; Tahara, T. *Chem. Rev*. **2017**, *117*, 10665−10693
6. Srivastava, A.; Eisenthal, K. B. *Chem. Phys. Lett*. **1998**, *292*, 345−351.
7. Liu, Y.; Yan, E. C. Y.; Eisenthal, K. B. *Biophys. J*. **2001**, *80*, 1004−1012.
8. Liu, J.; Subir, M.; Nguyen, K.; Eisenthal, K. B. *J. Phys. Chem. B* **2008**, *112*, 15263−15266.
9. Gh., M. S.; Wilhelm, M. J.; Dai, H-L. *J. Phys. Chem. Lett*. **2016**, *7*, 3406−3411.
10. Wilhelm, M. J.; Gh., M. S.; Dai, H-L.*Biochemistry* **2015**, *54*, 4427−4430.
11. Wilhelm, M. J.; Sheffield, J. B.; Gh., M. S.; Wu, Y.; Spahr, C.; Gonella, G.; Xu, B.; Dai, H-L. *ACS Chem. Biol.* **2015**, *10*, 1711−1717.
12. Zeng. J.; Eckenrode, H. M.; Dounce, S. M.; Dai, H-L. *Biophys. J*. **2013**, *104*, 139−145.
13. Kim, J. H.; Kim, M. W. *Eur. Phys. J. E*, **2007**, *23*, 313−317.
14. Kim, J. H.; Yim, S-Y.; Oh, M-K,; Phanb, M. D.; Shin, K. *Soft Matter* **2012**, *8*, 6504−6511.
15. Saini, R. K.; Dube, A.; Gupta, P. K.; Das, K. *J. Phys. Chem. B* **2012**, *116*, 4199−4205.
16. Varshney, G. K.; Saini, R. K.; Gupta, P. K.; Das, K.*Langmuir* **2013**, *29*, 2912−2918.
17. Varshney, G. K.; Kintali, S. R.; Gupta, P. K.; Das, K. *Langmuir* **2016**, *32*, 10415−10421.
18. Kintali, S. R.; Varshney, G. K.; Das, K.*Chem. Phys. Lett*. **2017**, *684*, 267−272.
19. Zhao, W.; Rog, T.; Gurtovenko, A. A.; Vattulainen, I.; Karttunen, M. *Biophys. J*. **2007**, *92*, 1114−1124.
20. Pan, J.; Heberle, F. A.; Tristram-Nagle, S.; Szymanski, M.; Koepfinger, M.; Katsaras, J.; Kučerka, N.*Biochim. et Biophys. Acta* **2012**, *1818*, 2135−2148.

21. Klasczyk, B.; Knecht, V. *J. Phys. Chem. A* **2011**, *115*, 10587−10595.

22. Pandit, S. A.; Berkowitz, M. L. *Biophys. J.* **2002**, *82*, 1818−1827.

23. Bockmann, R. A.; Hacy, A.; Heimburgy, T.; Grubmuller, H. Bilayer. *Biophys. J.* **2003**, *85*, 1647−1655.

24. Gurtovenko, A. A.; Vattulainen, I. *J. Phys. Chem. B* **2008**, *112*, 1953−1962.

25. Broemstrup, T.; Reuter, N. *Biophys. J.* **2010**, *99*, 825−833.

26. Rønnest, A. K.; Peters, G. H.; Hansen, F. Y.; Taub, H.; Miskowiec A. *J. Chem. Phys*. **2016**, *144*, 144904.

27. Qiao, B. F.; Cruz, M. O. *J. Phys. Chem. B* **2013**, *117*, 5073−5080.

28. Harries, D.; May, S.; Ben-Shaul, A. *Soft Matter* **2013**, *9*, 9268−9284.

29. Kostritskii, A. Y.; Kondinskaia, D. A.; Nesterenko, A. M.; Gurtovenko, A. A. *Langmuir* **2016**, *32*, 10402−10414.

30. Tolokh, I. S.; Vivcharuk, V.; Tomberli, B.; Gray, C. G. *Phys. Rev. E* **2009**, *80*, 031911.

31. Von Deuster, C. I.; Knecht, V. *Biochim. Biophys. Acta Biomembr*. **2011**, *1808*, 2867−2876.

32. Lentz, B. R. *Chem Phys Lipids* **1993**, *64*, 99−116.

33. Riske, K. A.; Barroso, R. P.; Vequi-Suplicy, C. C.; Germano, R.; Henriques, V. B.; Lamy, M. T. *Biochim. et Biophys. Acta* **2009**, *1788*, 954−963.

34. Bhattarai, R.;Roy, B.; Guha, P.; Bista, A.; Bhadra, A.; Karmakar, G.; Nahak, P.; Chettri,P.; Panda, A. K. *J. Surface Sci. Technol*. **2015**, *31*, 77−85.

35. Hung, W. C.; Chen, F. Y.; Lee, C. C.; Sun, Y.; Lee, M. T.; Huang, H. W. *Biophys. J.* **2008**, *94*, 4331−4338.

36. Sun, Y.; Lee, C-C.; Hung, W-C.; Chen, F-Y.; Lee, M-T.; Huang, H. W. *Biophys. J.* **2008**, *95*, 2318−2324.

37. Koynova, R.; Tenchov, B. *O A Biochemistry* **2013**, *1*, 9.

38. Himeno, H.; Shimokawa, N.; Komura, S.; Andelman, D.; Hamada, T.; Takagia, M. *Soft Matter* **2014**, *10*, 7959−7967.

39. Binder, H.; Zschörnig, O. *Chem. Phys. Lipids* **2002**, *115*, 39−61.

40. Ganesan, S. J.; Xu, H.; Matysiak, S. *J. Phys. Chem. B* **2017**, *121*, 787−799.

41. Broemstrup, T.; Reuter, N. *Biophys. J*. **2010**, *99*, 825−833.

42. Slochower, D. R.; Wang, Y-H.; Tourdot, R. W.; Radhakrishnan, R.; Janmey, P. A. *Adv. Coll. & Interf. Sc*. **2014**, *208*, 177−188.

43. Epand, R. M.; Epand, R. F. *Mol. Bio Syst*. **2009**, *5*, 580−587.

44. Bilmen, J. G.; Khan, S. Z.; Javed, M. U. H.; Michelangeli, F. *Eur. J. Biochem* **2001**, *268*, 6318−6327.

45. Ingolfsson, H. I.; Koeppe, R. E.; Andersen, O. S. *Biochemistry* **2007,** *46,* 10384−10391.

46. Zhao, W.; Rog, T.; Gurtovenko, A. A.; Vattulainen, I.; Karttunen, M. *Biochimie* **2008**, *90*, 930−938.

47. Barry, J.; Fritz, M.; Brender, J. R.; Smith, P. E. S.; Lee, D-K.; Ramamoorthy, A. *J. Am. Chem. Soc*. **2009**, *131*, 4490−4498.

48. Patra, D.; El Khoury, E.; Ahmadieh, D.; Darwish, S.; Tafech, R. M. *Photochem. Photobiol*. **2012**, *88*, 317−327.

49. El Khoury, E. D.; Patra, D.*J. Phys. Chem. B* **2013**, *117*, 9699−9708

Chapter 7

Deuterium Isotope effect on curcumin induced adsorption & transport properties of a cationic dye across POPG liposomes

7.1 Introduction

The medicinal pigment curcumin has been extensively studied because of its broad spectrum biological activities [1-5]. Curcumin has a great affinity for biological membranes and has been shown to alter their properties. The results of earlier studies suggest that curcumin can regulate various structurally-unrelated membrane proteins by altering the properties of the surrounding lipid bilayer [6-9]. Consequently, several studies have been performed in model membrane systems to understand how curcumin affects the bilayer properties by different bio-physical techniques [10-17]. One way to probe the curcumin induced changes in the membrane bilayer properties is to monitor the adsorption and transport of other molecules across a bilayer in presence of curcumin. The adsorption and transport kinetics of several organic ions across a lipid bilayer has already been monitored by the interface specific second harmonic generation (SHG) spectroscopic technique [18-28] and the underlying principle behind this has been already discussed in detail [18-19]. Using this technique we have investigated the curcumin induced changes in the permeability of a cationic hemicyanine dye, LDS^+ ions across a negatively charged POPG (1-palmitoyl-2-oleoyl-sn-glycero-3-phospho-(1'-rac-glycerol) liposome bilayer [14, 16-17]. When POPG liposomes were incubated with curcumin the transport of LDS^+ ions across the bilayer was observed to be significantly faster [14]. Further we have also showed that curcumin increases the adsorption and transport of LDS^+ ions, while partitioning from the aqueous to the bilayer phase [16-17]. In order to explain the curcumin induced increase in the adsorption of LDS^+ ions on the outer POPG

bilayer we have proposed that curcumin disrupts the counter ion (e.g. Na^+) – lipid interactions near the head group region of POPG lipids. According to several Molecular Dynamics simulations, these interactions which occur via formation of ion-lipid and lipid-ion-lipid complexes were responsible for stabilizing the bilayer by reducing the lipid-lipid repulsion arising due to similar charge of the lipid head groups [29-32]. In addition these studies have also showed that the formation of the Na^+-lipid complexes becomes energetically more stable when a water molecule is shared between them. Several recent studies using the heterodyne detected electronic sum frequency generation technique have shed light upon how the interaction of lipid head groups with water affect the interfacial pH and orientation of interfacial water molecules [33-36]. So far, the studies carried out by us have emphasized only on the effect of curcumin on the counter-ion lipid head group interactions. However, the role of interfacial water molecules on the curcumin induced disordering in the POPG bilayer must also be investigated. One way to examine the role of water is to use POPG liposomes suspended either in H_2O or D_2O and then compare the effect of curcumin on the adsorption and transport of the LDS^+ ion using the SHG technique. Here we report how the effect of curcumin induced disruptions of the counter ion - solvent - lipid interactions changes by isotopic substitution of the solvent. Since our earlier results [16-17] suggests that the enolic hydrogen of curcumin may play a crucial role, we have also compared the effect of replacing them with deuterium.

7.2 Results

The average laser power used in the SHG experiments was 500 mW and the temperature of solutions was kept at 7.5 $^{\circ}$C unless mentioned otherwise. Micro-liter aliquots (< 2 μL) from a concentrated stock solution of $curc_h$ in methanol (or, $curc_d$ in deuterated methanol) were added to the liposome to get the desired curcumin: lipid (C/L) ratio. The amount of methanol

(or deuterated methanol) added to the POPG liposomes did not induce any changes in the liposomes characteristics which was confirmed by measuring their size, zeta potential and also comparing the transport characteristics of the LDS^+ ions across the bilayer. Before investigating the effect of curcumin we have studied the effect of substituting H_2O by D_2O on the transport characteristics of LDS^+ ions across POPG bilayer. Figure 7.1 describes the time dependent changes of the SH electric field ($E_{2\omega}$) generated from a solution of POPG liposomes suspended in pH 5 buffer (or, pD 5 D_2O buffer) to which 5 uM LDS^+ ions were added at t = 100 second. Before addition of LDS^+ ions the observed $E_{2\omega}$ signal arises due to Hyper-Rayleigh scattering from the liposomes [14, 16-17].

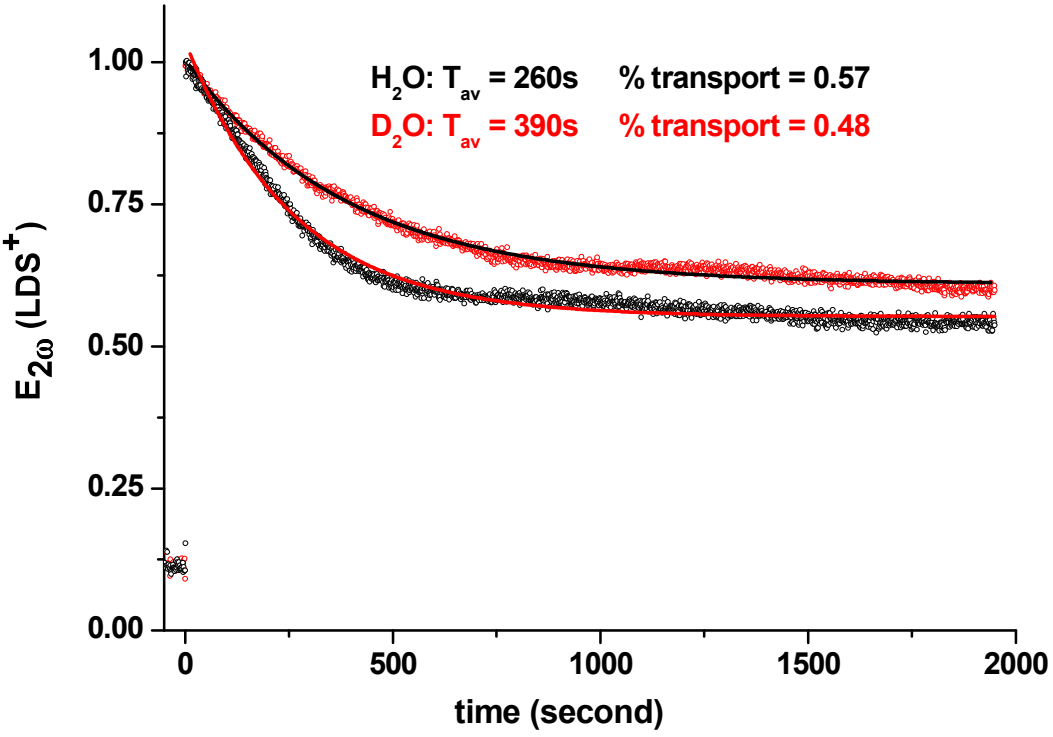

Figure 7.1: *Normalized SH electric field ($E_{2\omega}$) of LDS^+ ions (5 µM) at pH 5.0 (black curve) and pD 5.0 (red curve) at room temperature. LDS^+ ions were added to a solution of POPG liposomes (50 µM) at 0 second time point. The exponential fits for the corresponding curves were shown as lines. The transport time constants (in seconds) and the percentage transport (i.e. ratio of LDS^+ ions adsorbed to the inner and outer bilayer) are also shown in the figure.*

The instantaneous (< 1 second) increase in the $E_{2\omega}$ (at t = 100 second) as soon as LDS^+ ions were added is due to the rapid electrostatic adsorption of the LDS^+ ions on the negatively charged outer bilayer surface of the POPG liposomes as has been demonstrated in numerous studies earlier [18-28]. The SH electric field, after addition of LDS^+ ions, is dominated by the $E_{2\omega}$ signal of LDS^+ ions [$E_{2\omega}(LDS^+)$] which then decreases gradually due to transport of the LDS^+ ions from the outer to inner lipid bilayer [14]. It was observed that the average transport time constant of the LDS^+ ions increases from 260 to 390 second and the percentage transport (i.e. the ratio of the LDS^+ ions residing at the inner and outer bilayer, at equilibrium) also decreases from 57% to 48% when the H_2O is replaced by D_2O.

In order to see the deuterium isotope effect on the curcumin induced changes in the adsorption and transport properties of the LDS^+ ions, we note that in a chemical process, the isotope effect consists of two parts: the solvent isotope effect, where the solvent H_2O is replaced by D_2O and the deuterium isotope effect, where the hydrogen atoms of the molecule (or molecules) of interest is replaced by deuterium. Curcumin being our molecule of interest we have replaced the enolic hydrogen of the molecule by deuterium as described in the experimental section. To investigate the isotope effect, we have carried out the experiment in three different ways by using different combinations of H_2O, D_2O, curcumin (cur_h) and deuterated curcumin ($curc_d$) as follows:

Case I: Control: Here water and $curc_h$ were used and this serves as the control experiment.

Case II: Solvent isotope effect: Here D_2O and $curc_h$ were used and this represents the solvent isotope effect

Case III: Total isotope effect: Here D_2O and $curc_d$ were used and this experiment provides the total isotope effect.

From here on, these three experiments will be referred as control (Case I), solvent (Case II) and total (Case III). It is pertinent to note that in the cross experiment (i.e. case II) there is a

possibility of H/D exchange between $curc_h$ and D_2O during the experimental time window (2000 second). Repeated measurements were made using different batches of samples and the results obtained were consistent which made us to believe that the possibility of H/D exchange during the experimental time window is negligible. Following our earlier work [16] we have kept the pH (or pD) of the liposome solution at 5.0, but since the freezing point of D_2O is ~ 4.0 $^{\circ}$C, we have kept the temperature of the medium at 7.5 $^{\circ}$C. Figure 7.2 describes the time dependent changes of the SH electric field ($E_{2\omega}$) generated from a solution of POPG liposomes for these three experiments where 5 μM LDS^+ ions were added at t = 0 second followed by addition of $curc_h$ (or $curc_d$) at t = 50 second. The curcumin: lipid molar ratio (C/L) was varied from 0.002 to 0.200. For clarity, only some selected traces for each case are shown in Figure 7.2. Consistent with our previous work, it was observed that addition of curcumin resulted in an increase of the $E_{2\omega}$ signal of the LDS^+ ions ($\Delta E_{2\omega}$) which was then followed by a decrease over time. From Figure 7.2, it is obvious that the rate of decrease of the $E_{2\omega}$ signal of the LDS^+ ions with increasing C/L ratio depends upon the experimental conditions, i.e. pertaining to cases I-III. An isotopic substitution of the solvent leads to clearly different trends in the $E_{2\omega}(t)$ signal (following curcumin addition) are especially at higher C/L ratios. In addition, when D_2O is used as the solvent, at higher C/L ratio, the kinetic profiles of the $E_{2\omega}$ signal of the LDS^+ ions (following curcumin addition) was observed to be non-exponential; the decay of the $E_{2\omega}$ signal shows a prominent shoulder.

Following our earlier works, we have estimated the two parameters associated with curcumin induced changes in the $E_{2\omega}$ signal of the LDS^+ ions:

i) The fractional increase of the $E_{2\omega}(t)$ signal immediately after curcumin addition: $\Delta E_{2\omega}$

ii) The decay rate constants of the $E_{2\omega}(t)$ signal following the fractional increase, $\Delta E_{2\omega}$: k_{tr}

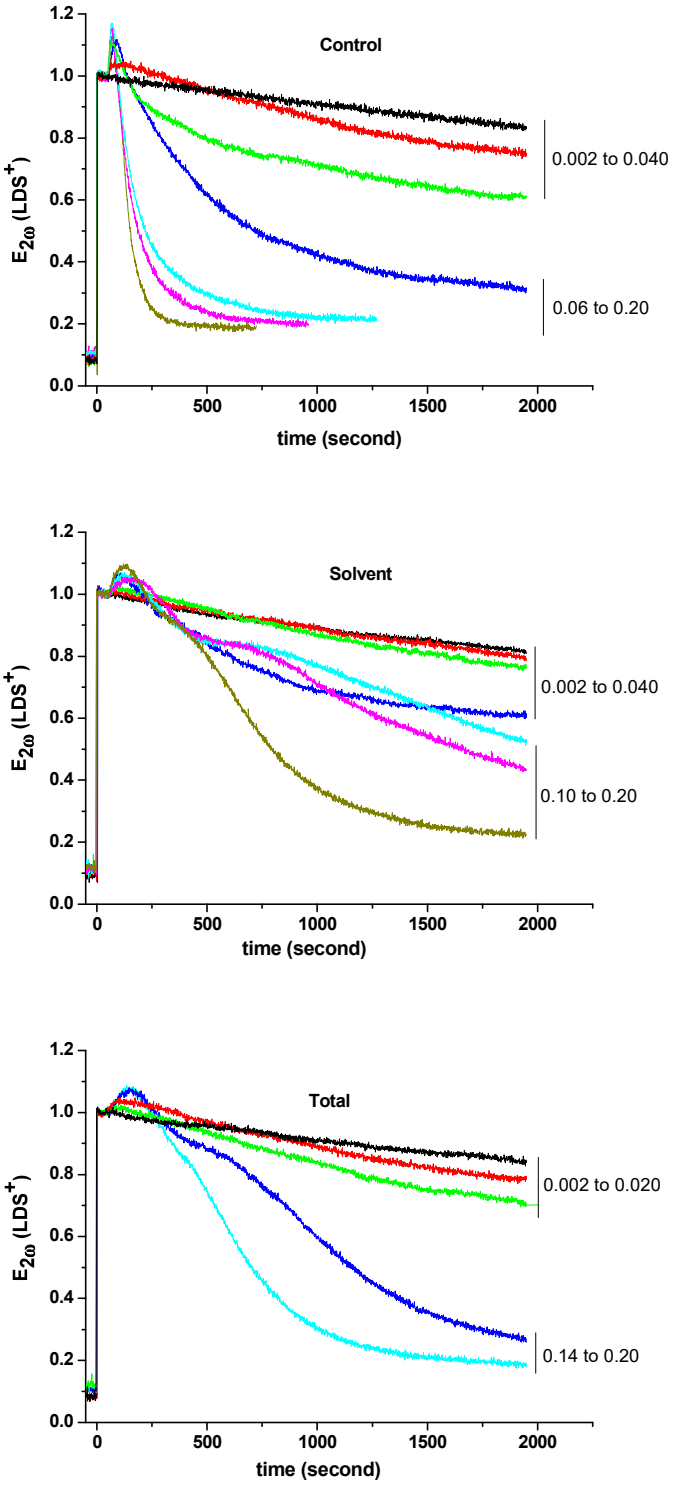

Figure 7.2: *Changes in the $E_{2\omega}$ signal of LDS^+ ions due to the addition of curcumin (added at t = 100 second time point) to a solution containing LDS^+ ions (5 μM) and POPG (50 μM) liposomes. Curcumin:Lipid (C/L) was varied from 1×10^{-3} to 0.2. The temperature of the solution was kept at 7 °C. The three panels represent the cases as described in the text.*

The decay rate constants were estimated by exponential fitting of the $E_{2\omega}(t)$ signal of the LDS^+ ions, from the time point where the fractional increase of the signal following curcumin addition has been completed. For cases, where the $E_{2\omega}(t)$ signal of the LDS^+ ions were observed to be non-exponential, decay rate constants were estimated by exponential fitting of the $E_{2\omega}$ trace after the shoulder formation. It is obvious that the k_{tr} values obtained in this way will not represent the overall kinetics, nevertheless it would give us a rough estimate about the bilayer crossing rate of the LDS^+ ions. Changes in the $\Delta E_{2\omega}$ and k_{tr} values with increasing C/L ratio is presented in Figure 7. 3.

In the control experiment (case I), following curcumin addition, the $\Delta E_{2\omega}$ (or k_{tr}) values were observed to remain similar up to a C/L ratio of 0.02 (or 0.06 in case of k_{tr}), increasing sharply thereafter. In addition, the $\Delta E_{2\omega}$ values were observed to level off at a C/L ratio of 0.10. Although the trend in the $\Delta E_{2\omega}$ and k_{tr} values of LDS^+ ions were slightly different than what We have observed before [14], we note that in these two cases the temperature of the solution is different (2 $^{\circ}$C versus 7.5 $^{\circ}$C) which might affect the curcumin induced alteration of the POPG bilayer.

A significant isotope effect was observed when H_2O is replaced by D_2O for the trending $\Delta E_{2\omega}$ and k_{tr} values with increasing C/L ratio. However, when $curc_h$ is replaced with $curc_d$ no such effects were visible (Cases II and III). Although the trends in the $\Delta E_{2\omega}$ values were observed to be more or less similar for all the three cases, the magnitude of increase in the $\Delta E_{2\omega}$ values (after C/L ratio of 0.02) was seen to decrease considerably (~2x) with respect to the control experiment.

On the other hand, the C/L ratio dependent trends in the k_{tr} values for cases II and III were observed to be quite different from the control case. In particular, when H_2O is replaced by D_2O (solvent and total cases), the increase in the k_{tr} values starts to appear at a higher C/ L ratio (~0.10) and the magnitude of increase was substantially lower (~10x).

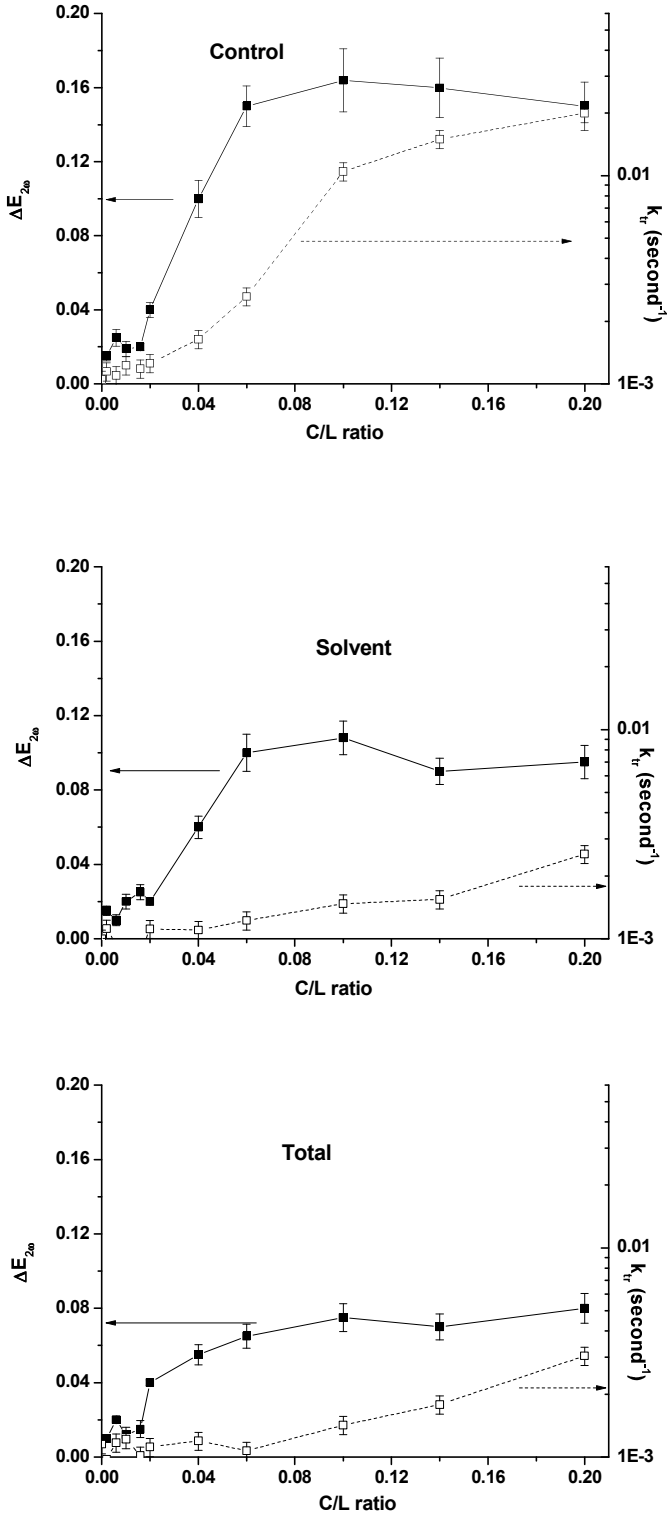

Figure 7.3: *Changes in the $\Delta E_{2\omega}$ (filled squares connected with solid lines) and transport rate constant (k_t) values (hollow squares connected with dashed lines) of LDS^+ ions with C/L values corresponding to the three cases presented in Figure 7.2. The Y-axis representing the k_t values is in logarithmic scale to capture the full variation.*

As stated earlier, the time dependent changes in the $E_{2\omega}$ signal of the LDS^+ ions following curcumin addition were non-exponential in nature at higher C/L ratios when D_2O is used as the solvent. In order to gain further insight about this a temperature variation experiment was performed. The temperature was varied from 7 to 25 $^{\circ}$C and the corresponding $E_{2\omega}$ (t) traces were recorded at a fixed C/L ratio (0.20) for the solvent and total cases and shown in Figure 7.4. From Figure 7.4 it is clear that with increase in temperature the non-exponential characteristics in $E_{2\omega}$ signal of the LDS^+ ions starts to decrease, although it is non-existent for the solvent case, but it is still there for the total case. The corresponding changes in the $\Delta E_{2\omega}$ and k_{tr} values are also shown in the inset of Figure 7.4. While $\Delta E_{2\omega}$ decreases with increasing temperature, the k_{tr} values increases with increasing temperature for the total case. Interestingly, for the solvent case, although the k_{tr} values increases with increasing temperature, the $\Delta E_{2\omega}$ values first increase and then decreases with increasing temperatureThe observed changes in the $E_{2\omega}$ signal of the LDS^+ ions following curcumin addition thus shows a pronounced isotope effect.

To understand the reason behind these changes fluorescence spectroscopic signatures of curcumin ($curc_h$ & $curc_d$) pertaining to all these three cases were also investigated. The fluorescence (steady state and time resolved) properties of $curc_h$ & $curc_d$ under the exact experimental conditions (except LDS^+ ions) pertaining to all the three cases (C/L = 0.10) is presented in Figure 7.5. It can be observed from Figure 7.5 that the fluorescence properties of curcumin can are quite different between the control and the solvent and total case. The fluorescence excitation spectra of curcumin for the control experiment were observed to be slightly blue shifted (~ 2-3 nm) compared to the solvent and total case. Similarly the fluorescence emission spectra of curcumin in the control experiment were observed to have a distinct shoulder on the high energy side (~ 475 nm) compared to the solvent and total case.

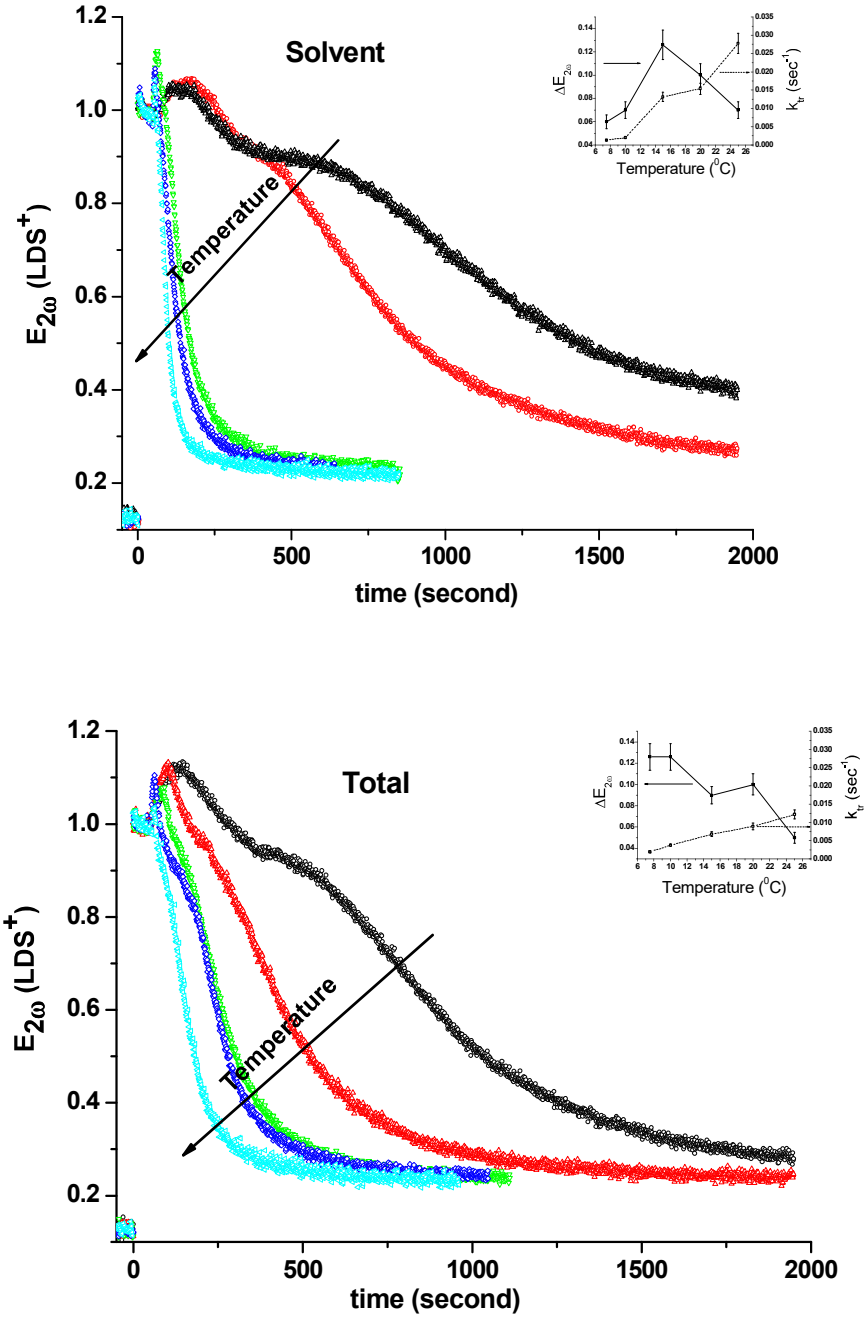

Figure 7.4: *Temperature dependent changes in the $E_{2\omega}$ signal of LDS^+ ions due to the addition of curcumin (added at t = 100 second time point) to a solution containing LDS^+ ions (5 μM) and POPG (50 μM) liposomes for the solvent (top) and total (bottom) cases. Curcumin: lipid (C/L) was kept at 0.2. The temperatures are 7.5, 10, 15, 20 and 25 $^\circ$C. The insets represent the variations in $\Delta E_{2\omega}$ and k_{tr} with temperature.*

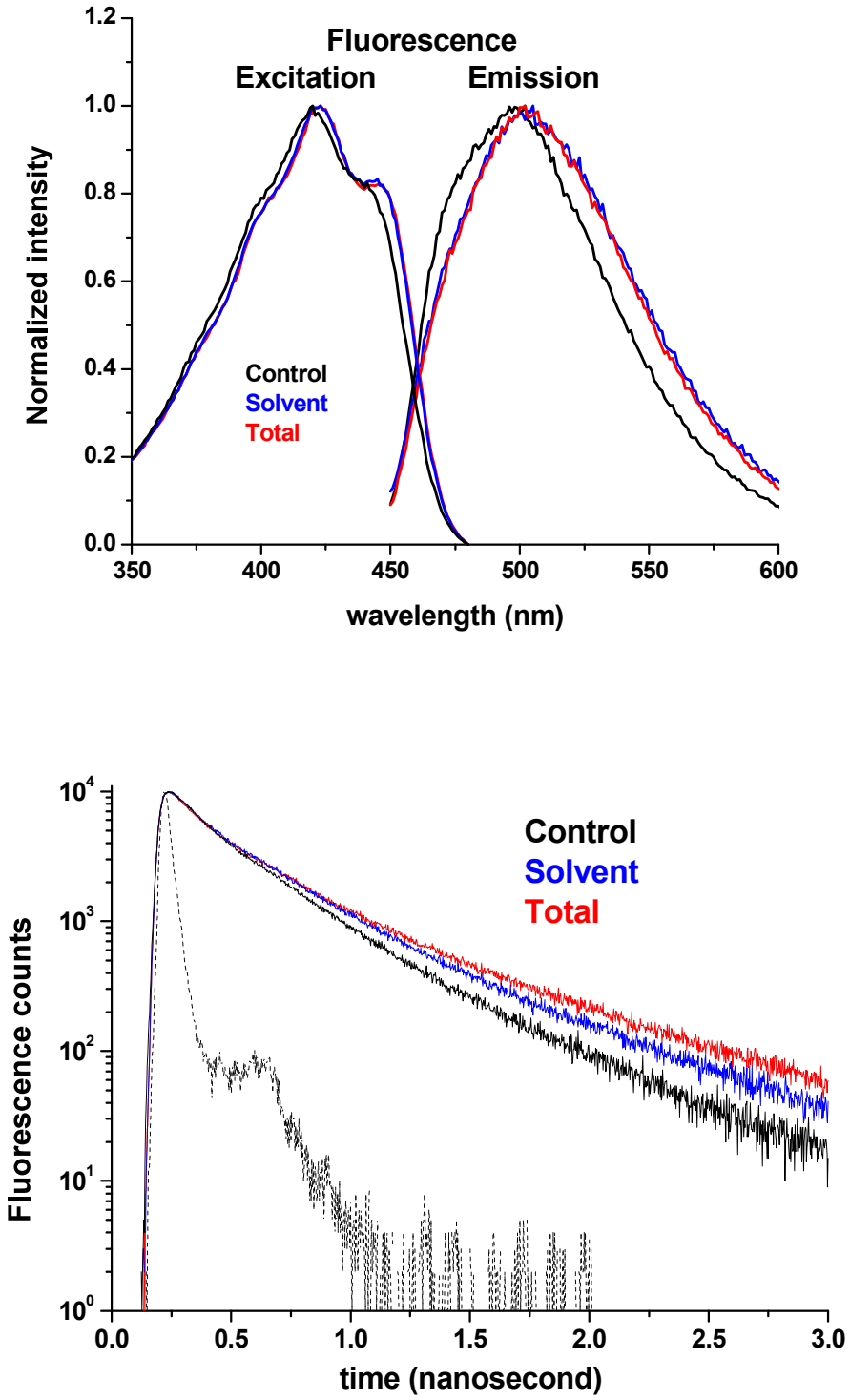

Figure 7.5: *Top: Peak normalized fluoresnce excitation (λ_{em} = 500 nm) and emission spectra (λ_{em} = 420 nm) of curcumin in POPG liposomes (curcumin: lipid = 0.10) Bottom: Corresponding fluorescence lifetimes of curcumin (λ_{em} = 410 nm) for the three cases.The lifetimes are collected over the whole emission band.*

In addition, the average fluorescence lifetimes (presented in Table 7.1) of curcumin in the control experiment is faster compared to the solvent and total case. Although the short component of the lifetime is similar for all the three cases, the long component of the lifetime for the solvent and total case is higher compared to the control experiment indicating the presence of a deuterium isotope effect in the excited state of the curcumin molecule [65].

Table 7.1: F*luorescence lifetime parameters of curcumin corresponding to the data presented in Figure 7.5. The values in parenthesis correspond to the amplitudes of the individual lifetime components. All lifetimes are in picoseconds. The average errors in these values are estimated to be 10%.*

Case	$\tau_1(a_1)$	$\tau_2(a_2)$	τ_{av}
I. Control	160 (0.37)	420 (0.63)	320
II. Solvent	160 (0.31)	490 (0.69)	390
III. Total	180 (0.35)	520 (0.65)	400

7.3 Discussion

The main objective of this work was to investigate the role of the solvent on the curcumin induced changes in the counter ion - solvent - lipid interactions. For this purpose isotopic substitution experiments were carried out to understand, at least qualitatively, the factors which affect the bilayer modification by curcumin.

The physicochemical characteristics of light (H_2O) and heavy (D_2O) water are a little bit different as deuterium is two times heavier than protium [37]. D_2O has higher density, viscosity, as well as melting and boiling points which indicate that its structure is more compact compared to H_2O. Replacement of hydrogen by deuterium within the water molecule was shown to strengthen the covalent [37-39] as well as the non-covalent deuterium bonding [38, 40-41] compared to their respective hydrogen bonding analogs. Intramolecular

deuterium bonds being stronger than hydrogen bonds strengthen the hydrophobic interactions. As a result, the native structures of proteins were observed to be more rigid and increase their tendency to aggregate in D_2O [42-46] and various biological processes are affected when H_2O is replaced with D_2O [47-52]. The effects of D_2O on biological membranes are so far focused on the function of membrane proteins [53-58]. As stated earlier in the introduction section, water molecules penetrate the head group region of the bilayer and forms a hydrogen bonding network connecting the lipid molecules and counter ions (e.g. Na^+) [29-32]. It is expected that replacing H_2O by D_2O should increase the strength of this network resulting in alterations in the properties of the phospholipid bilayers. Results of differential scanning calorimetry (DSC) and electron spin resonance (ESR) studies suggest a stronger packing of lipid hydrocarbon chains and a lateral compression of lipid molecules resulting in bilayer ordering and restricted mobility at the phospholipid head group region when the H_2O is replaced by D_2O [59-61]. A recent molecular dynamics (MD) simulation study reveals that while there is no significant changes in the time averaged properties (e.g. area per lipid, membrane thickness etc) the time-dependent properties were significantly changed when H_2O is replaced by D_2O. The mobility of the heavy water molecules associated with phospholipid head group region becomes substantially slower and the lipid-D_2O and lipid-lipid interactions becomes more stable due to the heavier mass of deuterium and stronger deuterium bonds compared to hydrogen bonds [62].

Our results on the transport characteristics of the LDS^+ ions across a POPG bilayer shows a "solvent" isotope effect when H_2O is replaced by D_2O. A 33% decrease in the transport rate accompanied by a 9% decrease in the overall transport of the LDS^+ ions could be observed when POPG liposomes were suspended in D_2O medium. Overall this reflects the D_2O induced changes in the bilayer properties as discussed above. The magnitude of this "solvent" isotope effect is ~1.3 times if the average transport rate of the LDS^+ ions is considered. At

this point we would like to compare the results of a recent study, where the fluorescence properties of the fluorophore Laurdan incorporated in either DMPC or POPC large unilamellar vesicles were studied in H_2O and D_2O medium [63]. It was observed that for both lipids the fluorescence spectral relaxation becomes slower (14 to 17 %) when H_2O is replaced by D_2O. This has been attributed to the reduced mobility of the hydrated functional groups of the lipid molecules surrounding the fluorophore. The total emission shift of Laurdan was observed to be slightly smaller in case of liposomes suspended in D_2O which is attributed to the lesser degree of hydration in the head group region of the lipids by D_2O. In addition fluorescence anisotropy studies using the fluorophore DPH suggest that the hydrophobic core of the bilayer is slightly stiffer when the bilayer is hydrated by D_2O. Therefore the overall outcome of the "solvent" isotope effect on a lipid bilayer can be summarized as a "stiffening" effect of the bilayer.

Compared to the moderate "solvent" isotope effect discussed above, a significant isotope effect is observed when curcumin is added *in-situ* during the transport of LDS^+ ions across a POPG bilayer. Since the effect of curcumin is quantified by measuring the parameters $\Delta E_{2\omega}$ and k_{tr} it would be relevant to discuss the significance of these two parameters at this point. Results obtained from our earlier work [16] not only supports a two-state binding model of curcumin with POPG bilayer [10, 13] but more importantly indicates that when the drug is localized at the aqueous bilayer interface, it creates extra binding sites for the LDS^+ ions by disrupting the lipid-counter ion (e.g. Na^+) complexes. It should be noted here that the lipid-counter ion complexes are also mediated by solvent (e.g. water) bridges [29-32]. The creation of extra binding sites is a result of the alteration of the bilayer surface charge density by curcumin thereby causing more LDS^+ ions to adsorb on the outer surface of the POPG bilayer which is quantified by the $\Delta E_{2\omega}$ parameter. When the drug is intercalated in the hydrophobic region of the bilayer (corresponding to a higher C/L ratio) the transport rate of the LDS^+ ions

(quantified by the k_{tr} parameter) were observed to increase significantly. This is consistent with the expectation that curcumin being a polar molecule (dipole moment ~10 Debye [64]) will lower the energy barrier (associated within the hydrophobic domain of the bilayer) of the LDS^+ ions to cross the bilayer.

We now attempt to give an explanation for the observed trends in the $\Delta E_{2\omega}$ versus the C/L ratio as described in Figure 7.3. As discussed before, the parameter $\Delta E_{2\omega}$ represents the disruption of the lipid- H_2O / D_2O -Na^+ network by $curc_h$/$curc_d$ molecules. It is reasonable to expect that this process will involve: i) disruption of the hydrogen/deuterium bonds in the lipid- H_2O / D_2O -Na^+ network and ii) formation of hydrogen/deuterium bonds between the polar head groups of the POPG lipids and in particular the enolic hydrogen/deuterium of the $curc_h$/$curc_d$ molecules [16]. Therefore, the observed ~2x decrease in the magnitude of the $\Delta E_{2\omega}$ values compared to the control indicates that the energetic cost to disrupt the lipid- D_2O -Na^+ network by formation of a hydrogen/deuterium bond between $curc_h$/$curc_d$ and the head group of a POPG lipid is quite high and thus the magnitude of increase in the $\Delta E_{2\omega}$ value for the solvent and total case is lower than the control.

The observed trends in the k_{tr} values were quite similar when the solvent is D_2O. Replacement of H_2O by D_2O induces a significant change in the trending k_{tr} values. As discussed before, the k_{tr} parameter signifies the localization of curcumin in the hydrophobic region of the bilayer, and thus when D_2O is used, the trending k_{tr} values suggest that in this case curcumin is not able to localize in the hydrophobic region of the bilayer. We attribute this to the D_2O induced alteration in bilayer properties as discussed earlier [59-61]. Further support for this hypothesis is provided by the fluorescence spectroscopic signatures of the drug presented in Figure 7.5. Since curcumin is a polar molecule, a blue shift in its fluorescence excitation and emission spectra will indicate that the drug is experiencing a nonpolar environment. The blue shifted fluoresnce excitation spectra and appearnece of a

distinct sholder in the blue side of the fluorescence emission spectra for the control experiment suggests that in these cases a certain population of the drug also resides in a hydrophobic region, i.e. the hydrophobic bilayer.

One interesting observation that could not be explained is the appearance of a shoulder in the time dependent $E_{2\omega}$ traces of the LDS+ ions for solvent and total cases. That this is a kinetic controlled process is revelaed by the disappreance of the shoulder with increase in the temperature, but the origin of this is, at present, unknown.

7.4 Summary and conclusions

In summary, we have attempted to investigate the role of solvent water, on the curcumin induced changes in the adsorption and transport properties of the LDS^+ ions across a POPG bilayer by replacing water with its heavier isotope D_2O. The SHG experiments were designed so as to separate the deuterium and the solvent isotope effect by using different combinations of H_2O, D_2O, $curc_h$ and $curc_d$. Results obtained confirmed the important role of solvent at the aqueous-bilayer interface. Significant isotope effects were observed when D_2O and $curc_d$ were used and the results obtained were interpreted as a result of strength of the deuterium bond and D_2O induced alteration in the bilayer properties.

References

1. Shehzad, A.; Qureshi, M.; Anwar, M. N.; Lee, Y. S. *J Food Sci*. **2017** doi: 10.1111/1750-3841.13793.
2. Stanić, Z. *Plant Foods Hum Nutr*. **2017**, *72*, 1−12.
3. Pulido-Moran, M.; Moreno-Fernandez, J.; Ramirez-Tortosa, C.; Ramirez-Tortosa, M. *Molecules* **2016**, *21*, 264.
4. Oliveira, A. S.; Sousa, E.; Vasconcelos, M. H.; Pinto, M. *Curr Med Chem.* **2015**, *22*, 4196−4232.
5. Prasad, S.; Gupta, S. C.; Tyagi, A. K.; Aggarwal, B. B. *Biotechnol Adv.* **2014**, *32*, 1053−64.
6. Ingolfsson, H. I.; Koeppe, R. E.; Andersen, O. S. *Biochemistry* **2007**, *46*, 10384−10391.
7. Jaruga, E.; Salvioli, S.; Dobrucki, J.; Chrul, S.; Bandorowicz-Pikuła, J.; Sikora, E.; Franceschi, C.; Cossarizza, A.; Bartosz, *G. FEBS Lett*. **1998**, *433*, 287−293.
8. Jaruga, E.; Sokala, A.; Chrulb, S.; Bartosza, *G. Exp. Cell Res.* **1998**, *245*, 303−312.
9. Bilmen, J. G.; Khan, S. Z.; Javed, M. U. H.; Michelangeli, F. *Eur. J. Biochem.* **2001**, *268*, 6318−6327.
10. Hung, W. C.; Chen, F. Y.; Lee, C. C.; Sun, Y.; Lee, M. T.; Huang, H. W. *Biophys. J.* **2008**, *94*, 4331−4338.
11. Barry, J.; Fritz, M.; Brender, J. R.; Smith, P. E.; Lee, D. K.; Ramamoorthy, A. *J. Am. Chem. Soc.* **2009**, *131*, 4490−4498.
12. Perez-Lara, A.; Ausili, A.; Aranda, F. J.; Godos, A.; Torrecillas, A.; Corbalan-Garcia, S.; Gomez-Fernandez, J. C. *J. Phys. Chem. B* **2010**, *114*, 9778−9786.
13. Sun, Y.; Lee, C-C.; Hung, W-C.; Chen, F-Y.; Lee, M-T.; Huang, H. W. *Biophys. J.* **2008**, *95*, 2318−2324.
14. Varshney, G. K.; Saini, R. K.; Gupta, P. K.; Das, K. *Langmuir* **2013**, *29*, 2912−2918.

15. Tsukamotoa, M.; Kuroda, K.; Ramamoorthy, A.; Yasuhara, K. *Chem. Comm.* **2014**, *50*, 3427−3430.

16. Varshney, G. K.; Kintali, S. R.; Gupta, P. K.; Das, K. *Langmuir* **2016**, *32*, 10415−10421.

17. Varshney, G. K.; Kintali, S. R.; Das, K. *Langmuir* **2017**, 33, 8302−8310

18. Eisenthal, K. B. *Chem. Rev*. **2006**, *106*, 1462−1477.

19. Srivastava, A.; Eisenthal, K. B. *Chem. Phys. Lett*. **1998**, *292*, 345−351.

20. Liu, Y.; Yan, E. C. Y.; Eisenthal, K. B. *Biophys. J.* **2001**, *80*, 1004−1012.

21. Liu, J.; Subir, M.; Nguyen, K.; Eisenthal, K. B. *J. Phys. Chem. B* **2008**, *112*, 15263−15266.

22. Gh., M. S.; Wilhelm, M. J.; Dai, H-L. *J. Phys. Chem. Lett.* **2016**, *7*, 3406−3411.

23. Wilhelm, M. J.; Gh., M. S.; Dai, H-L. *Biochemistry* **2015**, *54*, 4427−4430.

24. Wilhelm, M. J.; Sheffield, J. B.; Gh., M. S.; Wu, Y.; Spahr, C.; Gonella, G.; Xu, B.; Dai, H-L. *ACS Chem. Biol*. **2015**, *10*, 1711−1717.

25. Zeng. J.; Eckenrode, H. M.; Dounce, S. M.; Dai, H-L. *Biophys. J*. **2013**, *104*, 139−145.

26. Kim, J. H.; Yim, S-Y.; Oh, M-K; Phanb, M. D.; Shin, K. *Soft Matter* **2012**, *8*, 6504−6511.

27. Saini, R. K.; Dube, A.; Gupta, P. K.; Das, K. *J. Phys. Chem. B* **2012**, *116*, 4199−4205.

28. Kintali, S. R.; Varshney, G. K.; Das, K. *Chem. Phys. Lett.* **2017**, *684*, 267−272.

29. Zhao, W.; Rog, T.; Gurtovenko, A. A.; Vattulainen, I.; Karttunen, M. *Biophys. J.* **2007**, *92*, 1114−1124.

30. Zhao, W.; Rog, T.; Gurtovenko, A. A.; Vattulainen, I.; Karttunen, M. *Biochimie* **2008**, *90*, 930−938.

31. Tolokh, I. S.; Vivcharuk, V.; Tomberli, B.; Gray, C. G. *Phys. Rev. E* **2009**, *80*, 031911.

32. Von Deuster, C. I.; Knecht, V. *Biochim. Biophys. Acta Biomembr*. **2011**, *1808*, 2867−2876.

33. Nihonyanagi, S.; Yamaguchi, S.; Tahara, T. *Chem. Rev*. **2017**, *117*, 10665−10693.

34. Mondal, J. A.; Nihonyanagi, S.; Yamaguchi, S.; Tahara, T. *J. Am. Chem. Soc*. **2010**, *132*, 10656−10657.

35. Mondal, J. A.; Nihonyanagi, S.; Yamaguchi, S.; Tahara, T. *J. Am. Chem. Soc*. **2012**, *134*, 7842−7850.

36. Kundu, A.; Yamaguchi, S.; Tahara, T. *J. Phys. Chem. Lett.* **2014**, *5*, 762−766.

37. Nemethy, G.; Scheraga, H. A. *J. Chem. Phys*. **1964**, *41*, 680.

38. Wade, D. *Chem. Biol. Interact*. **1999**, *117*, 191−217.

39. Wiberg, K. B. *Chem. Rev.* **1955**, *55*, 713−743.

40. Benjamin L.; Benson, G. C.; *J. Phys. Chem*. **1963**, *67*, 858−861.

41. Scheiner, S.; Cuma, M. *J. Am. Chem. Soc*. **1996**, *118,* 1511−1521.

42. Cioni, P.; Strambini, G. B. *Biophys. J.* **2002**, *82*, 3246−3253.

43. Kresheck, G. C.; Schneider, H.; Scheraga, H. A. *J. Phys. Chem*. **1965**, *69*, 3132−3144.

44. Parker, M. J.; Clarke, A. R. *Biochemistry* **1997**, *36*, 5786−5794.

45. Sasisanker, P.; Oleinikova, A.; Weingartner, H.; Ravindra, R.; Winter, R. *Phys. Chem. Chem. Phys.* **2004**, *6*, 1899−1905.

46. Kushner, D. J.; Baker, A.; Dunstall, T. G. *Can. J. Physiol. Pharmacol*. **1999**, *77*, 79–88.

47. Hartmann, J.; Bader, Y.; Horvath, Z.; Saiko, P.; Grusch, M.; Illmer, C.; Madlener, S.; Fritzer-Szekeres, M.; Heller, N.; Alken, R. G.; Szekeres, T. *Anticancer Res*. **2005**, *25*, 3407−3411.

48. Pittendrigh, C. S.; Caldarola, P. C.; Cosbey, E. S. *Proc. Natl. Acad. Sci.* U.S.A. **1973**, *70*, 2037−2041.

49. Bruce, V. G.; Pittendrigh, C. S. *J. Cell. Comp. Physiol*. **1960**, *56*, 25−31.

50. Kushner, D. J.; Baker, A.; Dunstall, T. G. *Can. J. Physiol. Pharmacol*. **1999**, *77*, 79−88.

51. Adams, W. H.; Adams, D. G. *J. Pharmacol. Exp. Ther*. **1988**, *244*, 633.

52. Lamprecht, J.; Schroeter, D.; Paweletz, N. *J. Cell Sci*. **1991**, *98*, 463−473.

53. Andjus, P. R.; Kataev, A. A.; Alexandrov, A. A.; Vuceli´c, D.; Berestovsky, G. N. *J. Membr. Biol.* **1994**, *142*, 43−53.

54. Andjus, P. R.; Vucelic, D. *J. Membr. Biol*. **1990**, *115*, 123−127.

55. Elsing, C.; Hirlinger, A.; Renner, E. L.; Lauterburg, B. H.; Meier, P. J.; Reichen J. *Biochem. J.* **1995**, *307*, 175−181.

56. Prod'hom, B.; Pietrobon, D.; Hess, P. *Nature* **1987**, *329*, 243−246.

57. Vasdev, S.; Gupta, I. P.; Sampson, C. A., Longerich, L.; Parai, S. *Can. J. Cardiol*. **1993**, *9*, 802−808.

58. Vasdev, S.; Prabhakaran, V. M.; Whelan, M.; Ford, C. A., Longerich, L.; Parai, S. *Artery* **1994**, *21*, 124.

59. Chen, C. H. *J. Phys. Chem*. **1982**, *86*, 3559-3562.

60. Ma, L. D.; Magin, R. L.; Bacic, G.; Dunn, F. *Biochim. Biophys. Acta* **1989**, *978*, 283−292.

61. Matsuki, H.; Okuno, H.; Sakano, F.; Kusube, M.; Kaneshina, S. *Biochim. Biophys. Acta* **2005**, *1712*, 92−100.

62. Róg, T.; Murzyn, K.; Milhaud, J.; Karttunen, M.; Pasenkiewicz-Gierula, M. *J. Phys. Chem. B* **2009**, *113*, 2378−2387.

63. Beranová, L.; Humpolí˘cková, J.; Sýkora, J.; Benda, A.; Cwiklik, L.; Jurkiewicz, P.; Gröbner, G.; Hof, M. *Phys. Chem. Chem. Phys.* **2012**, *14*, 14516−14522.

64. Shen, L.; Ji, H-F. *Spectrochim. Acta, Part A* **2007**, *67*, 619−623.

Chapter 8

Summary and future prospective

In this thesis the effect of the medicinal pigment curcumin, on the adsorption and transport characteristics of an organic cation across a lipid bilayer has been studied utilizing the interface specific SHG spectroscopic technique.

In order to monitor the curcumin induced changes in liposomes having PG head groups, a hemicyanine dye, LDS-698 has been used. Using ~800 nm femotosecond laser excitation, a detailed spectroscopic characterization of the cationic form of the dye, LDS^+ was done to demonstrate its suitability as a second harmonic probe to monitor the permeability of PG liposomes.

In the first study, it was observed that curcumin significantly enhances the permeability of a model POPG membrane against the LDS^+ ions. Control experiments were carried out using other lipophilic molecules like DPH and Nile Red to compare the membrane permeability properties of these molecules with curcumin and it was observed that the latter molecule is superior in making the POPG membrane more permeable to LDS^+ ion. This study, while demonstrating the increased permeability of liposomal curcumin, in particular against organic cations, raises the speculation that the biological activity of the drug might result from its membrane altering properties. It is possible that the origin of this enhanced membrane permeability may depend upon the interaction of the molecule with the polar head group region of the lipid which prompted to compare the membrane (POPG) permeability property of curcumin with another lipophilic molecule chlorin-*p6* (C*p6*). A pH dependent membrane permeability study revealed that the effect of C*p6* and Curcumin are opposite, while the former significantly enhanced the transport of LDS^+ ions at acidic pH the latter enhanced it at

neutral pH. Supplementary FRET studies were carried out to understand the pH dependent bilayer localization of the drugs and it was concluded that interaction between the various ionic species of the drugs and polar head groups of the lipid is a crucial factor which is responsible for the drug induced membrane permeability. Next, an attempt was made to understand how curcumin alters the POPG bilayer by monitoring the adsorption and transport properties of LDS^+ ions while curcumin partitions into the bilayer. Following addition of Curcumin, the intensity of SH electric field ($E_{2\omega}$) of LDS^+ ions adsorbed on the outer bilayer of the POPG liposome was observed to increase instantaneously (< 1 second). Control experiments confirmed that this increase is not due to curcumin. The fractional increase in the SH electric field ($E^f_{2\omega}$) and the bilayer transport rates (k_T) of LDS^+ ions were then studied with respect to the pH of the solution and also with the curcumin content in the lipid bilayer. It was established that the neutral form of curcumin is more conducive for increasing the $E^f_{2\omega}$ of LDS^+ ions. It was observed that with increasing curcumin content in the lipid bilayer two distinct regimes could be observed in terms of $E^f_{2\omega}$ and k_T values of LDS^+ ions which supports an earlier two-state binding model of curcumin with the POPG bilayer. Additionally, it was further proposed that initially curcumin binds to the surface of the bilayer replacing the counter ions (Na^+) bound to the lipid head groups and at higher concentrations it intercalates within the hydrophobic domain of the bilayer altering its hydrophobicity inducing enhanced transport of the LDS^+ ions. This hypothesis is further tested by manipulating the POPG bilayer rigidity using a several mixtures of saturated DPPG and unsaturated POPG lipids. The observed kinetic trends of the $E_{2\omega}$ (LDS^+ ions) signal following curcumin addition is explained on the basis of the relative strength of the Na^+-POPG and Na^+-DPPG interaction. Higher ordering of the lipid acyl chain region in DPPG liposome makes the Na^+-DPPG interaction much stronger than the Na^+-POPG interaction. Additionally it is proposed that in liposomes made from POPG and DPPG lipids, individual domains of POPG and DPPG lipids

exist depending on the mole-fractions of the individual lipids and the corresponding phase state of the bilayer. A qualitative insight about how bilayer phase separation can be achieved by modulating the hydrophobic interactions between the lipid acyl chains is one interesting outcome of this work. Although studies carried out so far have emphasized only on the counter-ion lipid head group interactions, the role of interfacial water molecules must be also acknowledged and investigated. The role of interfacial water is investigated indirectly by comparing the curcumin induced changes in the adsorption and transport characteristics of LDS^+ ions using POPG liposomes suspended in water and in deuterated water (D_2O). The isotope effect experiments are designed such as to investigate separately the "deuterium isotope effect" (i.e. where there is H/D exchange) and "solvent isotope effect" (where H_2O is replaced by D_2O). Results obtained showed a significant isotope effect on the adsorption and transport properties of LDS^+ ions while curcumin is partitioning into a POPG bilayer. This is largely due to the solvent isotopeeeffect and is attributed to the D_2O induced modification of bilayer properties.

The results obtained in this thesis work demonstrate the ability of curcumin to alter a POPG bilayer by disrupting the network of lipid-counter ion-water complexes. However in order to get a more comprehensive picture, the interaction of Curcumin with the lipid head group needs to be studied in more detail. Firstly, the role of the acidic hydrogens of curcumin needs to be investigated by using different derivatives of curcumin where these will be replaced by some inert group, i.e. methyl. Secondly, the role of interfacial water, and the role of the enolic hydrogen of curcumin needs to be investigated. This can be done by the SFG technique which can monitor the OH stretch of the water and the enolic OH stretch of curcumin which are well separated in frequency. These studies are expected to provide further insights about the molecular mechanism behind the curcumin induced alterations in lipid bilayer.